FINNISH RAIL ADMINISTRATION

RHK • Technical Unit

Publications of
the Finnish Rail Administration

A
10/2000

INSTRUMENTATION AND MODELLING OF TRACK STRUCTURE, 250 kN and 300 kN AXLE LOADS

- **Pauli Kolisoja**
- **Iikka Järvenpää**
- **Erkki Mäkelä**

FINNISH
RAIL
ADMINISTRATION

Helsinki 2000

Publications of
the Finnish Rail Administration A 10/2000

INSTRUMENTATION AND MODELLING OF TRACK STRUCTURE, 250 kN and 300 kN AXLE LOADS

- **Pauli Kolisoja**
- **Iikka Järvenpää**
- **Erkki Mäkelä**

Helsinki 2000

RHK
FINNISH RAIL ADMINISTRATION
KAIVOKATU 6, P.O.Box 185
FIN-00101 HELSINKI

TEL. +358 9 5840 5111
FAX +358 9 5840 5140
E-MAIL: info@rhk.fi

ISBN 952-445-042-9
ISSN 1455-2604

Kolisoja, Pauli – Järvenpää, Iikka – Mäkelä, Erkki: Instrumentation and Modelling of Track Structure, 250 kN and 300 kN axle loads. Finnish Rail Administration, Technical Unit. Helsinki 2000. Publications of Finnish Rail Administration A 10/2000. 99 pages and 4 appendices. ISBN 952-445-042-9, ISSN 1455-2604.

Key words: instrumentation, modelling, track, railway embankment, vibration

SUMMARY

Instrumentation of a track structure on the railway line between Koria and Kouvola in the summer of 1999 and the related modelling of the track behaviour form a part of the Finnish Rail Administration's (RHK) investigation which is aimed at the introduction of 250 kN and 300 kN axle loads. This study is being accomplished in cooperation with the Laboratory of Geotechnical Engineering at the Tampere University of Technology, the Laboratory for Mechanics of Materials and the Laboratory of Highway Engineering at the Helsinki University of Technology.

On the instrumentation site the track structure and the underlying embankment of the northern track of the line between Koria and Kouvola was instrumented at one cross section near to kilometre reading 187+580, with the aim of monitoring the mechanical behaviour of the track components. Furthermore, the intensity of vibrations induced by the passing of trains was recorded at three different distances from the northern line.

During the monitoring period, which lasted for about two days, the responses of the track structure were recorded as a total of 65 normal freight and passenger trains passed the instrumentation site. In addition, the instrumentation site was passed ten times by a special test train possessing four axles having an exact axle load of 250 kN.

The time records of these run-throughs of the test train give a good idea of the deformations and stresses produced by wheel sets in good shape with an axle load of 250 kN on a recently repaired track. Together with the data measured under the normal rail traffic and also utilising the additional factors reported in the literature, it is possible to estimate the stresses in the track structure under higher axle loads. The measured bending deformations of the rail agree with those derived from the classical beam-on-elastic-foundation theory.

Based on the measurements made from the railway embankment, it can be concluded that the vertical stiffness of the embankment can be modelled fairly accurately using a relatively simple structural model consisting of infinite linear elastic layers on top of each other. However, the values of the elastic modulus used in the structural model must be determined using test methods corresponding to the stress and strain level which corresponds to the actual loading conditions.

On the basis of the preliminary analysis of the measurement results performed so far, it is not possible to give a definite answer to the question of what are the safe minimum values of embankment width which correspond to the different axle loads. Nevertheless, even the results of the very heavily simplified finite element simulations indicate quite

clearly that as the axle load increases and the embankment width decreases the deformations developing in the embankment structure will in any case start to increase rapidly at some point. The measurement results obtained also suggest that as the axle load increases tensile strains may develop in certain parts of the embankment. If this occurs repeatedly, it is quite obvious that a gradual accumulation of permanent deformations will take place in the embankment structure.

The results of the vibration records strengthen the generally accepted idea that a rise in axle loads increases vibration, at least in goods traffic. Based on these measurements, one cannot, however, state what kind of influence speed, axle load, or the length of the train have on the origin or propagation of vibration.

Kolisoja, Pauli – Järvenpää, Iikka – Mäkelä, Erkki: Ratarakenteen instrumentointi ja mallinnus, 250 kN:n ja 300 kN:n akselipainot. Ratahallintokeskus, Tekninen yksikkö. Helsinki 2000. Ratahallintokeskuksen julkaisuja A 10/2000. 99 sivua ja 4 liitettä. ISBN 952-445-042-9, ISSN 1455-2604.

Avainsanat: instrumentointi, mallinnus, raide, ratapenger, tärinä

TIIVISTELMÄ

Korian ja Kouvolan välisellä rataosuudella kesällä 1999 toteutettu ratarakenteen instrumentointi ja siihen liittyvät mallinnustarkastelut ovat osa Ratahallintokeskuksen (RHK) 250 kN ja 300 kN akselipainojen käyttöönottoon tähtäävää tutkimusprojektia, joka aloitettiin kesällä 1998. Tutkimus on tehty Tampereen teknillisen korkeakoulun geotekniikan laboratorion (TTKK/GEO), Teknillisen korkeakoulun lujuusopin laboratorion (TTK/LUJ) ja Teknillisen korkeakoulun tielaboratorion (TKK/TIE) yhteistyönä.

Instrumentointikohteessa mainitun rataosuuden pohjoisenpuoleinen raide ja sen alla oleva ratapenger instrumentoitiin yhdestä, suunnilleen kilometrilukeman 187+580 kohdalla sijainneesta, poikkileikkauksesta ratarakenteen osien mekaanista käyttäytymistä rekisteröivillä mittausjärjestelyillä. Lisäksi instrumentointikohteessa mitattiin junaliikenteen aiheuttaman tärinän voimakkuutta kolmella eri etäisyydellä radan pohjoisenpuoleisesta raiteesta.

Noin kaksi vuorokautta kestäneen mittausjakson aikana ratarakenteen vasteita mitattiin kaikkiaan 65 normaalia junaliikennettä edustaneen tavara- ja henkilöjunan kulkiessa instrumentointikohteen yli. Näiden lisäksi mittauskohteen ylitti kymmenen kertaa erityisesti näitä mittauksia varten varustettu koejuna, jonka akseleista neljälle oli asetettu mahdollisimman tarkoin 250 kN suuruinen akselipaino.

Raiteesta saadut mittaustulokset koejunaa koskevilta osin antavat varsin selkeän kuvan siitä, kuinka suuria rasituksia hyväkuntoisin pyöräkerroin varustettu vaunu edellä mainitulla 250 kN akselipainoilla synnyttää raiteen rakenneosiin peruskorjatulla radalla. Täydennettynä normaalista liikenteestä saaduilla mittaustuloksilla sekä kirjallisuudesta löytyvillä erilaisia olosuhteita koskevilla täydentävillä tiedoilla on mahdollista arvioida korotettujen akselipainojen aikaansaamia rasituksia. Kiskoista mitatut taivutus-muodonmuutokset pitävät hyvin yhtä klassillisen, kimmoisalla alustalla olevaa jatkuvaa palkkia koskevan teorian kanssa.

Ratapenkereestä tehtyjen mittausten perusteella voidaan todeta, että ratapenkereen pystysuuntaista jäykkyyttä on mahdollista mallintaa varsin tarkasti suhteellisen yksinkertaisella rakennemallilla, joka koostuu kerroksittain lineaarisesti kimmoista materiaalimallia noudattavista osista. Rakennemallissa käytettävät moduuliarvot on tällöin kuitenkin määritettävä koetavoilla, jotka sekä jännitys- että muodonmuutostason suhteen vastaavat rakenteen todellista kuormitustilannetta.

Kysymykseen siitä, mikä on erilaisia akselipainoja vastaava pengerleveyden turvallinen minimiarvo, ei nyt suoritettujen mittausten ja alustavien mallinnustarkastelujen perusteella ole mahdollista antaa yksikäsitteistä vastausta. Voimakkaasti yksinkertaistetunkin elementtimallinnuksen perusteella näyttäisi kuitenkin varsin ilmeiseltä, että akselipainon kasvaessa ja pengerleveyden pienentyessä ratapenkereeseen syntyvät muodonmuutokset alkavat jossain vaiheessa hyvin voimakkaasti kasvaa. Saadut mittaustulokset antavat myös selvää viitettä siitä, että akselipainon kasvaessa ratapenkereen tiettyihin osiin saattaa muodostua vetojännityksiä, jotka lukuisia kertoja toistuessaan väistämättä aiheuttavat palautumattomien muodonmuutosten vähittäistä kumuloitumista pengerrakenteeseen.

Tärinämittausten osalta tulokset vahvistavat käsityksen säiliöjunien korkeista tärinäarvoista. Yleisesti voidaan todeta, että tulokset eivät kuitenkaan kerro selkeästi esimerkiksi nopeuden, massan tai junan pituuden vaikutuksesta tärinän synnyssä.

FOREWORD

This study on instrumentation and modelling of track structure forms part of the Finnish Rail Administration's investigation which is aimed at the introduction of 250 kN and 300 kN axle loads. The study is being accomplished in cooperation with the Laboratory of Geotechnical Engineering at the Tampere University of Technology, the Laboratory for Mechanics of Materials and Laboratory of Highway Engineering at the Helsinki University of Technology.

The study consists of a summary of the instrumentation and measurements and their practical arrangements carried out at the instrumentation site on the railway line between Koria and Kouvola in the summer of 1999. The results of the preliminary analyses carried out on the measurement results and the related modelling of the mechanical behaviour of track structures are covered in the report. Finally, some suggestions for further studies are presented, with the aim of bringing out the most important issues to be investigated and of outlining the most practical ways of utilising the results obtained from the instrumentation.

Pauli Kolisoja, from the Laboratory of Geotechnical Engineering at the Tampere University of Technology, was responsible for writing chapters 1 – 4, with the exception of the account of the instrumentation of the rail, which has been written by Iikka Järvenpää, from the Laboratory for Mechanics of Materials at the Helsinki University of Technology. In addition, Iikka Järvenpää was responsible for writing chapter 5, while Erkki Mäkelä, from the Laboratory of Geotechnical Engineering at the Tampere University of Technology, wrote chapter 6. The work has been supervised by Pasi Leimi and Kari Ojanperä, Senior Inspectors at the Finnish Rail Administration, Technical Unit.

Helsinki, July 2000

Finnish Rail Administration

Technical Unit

CONTENTS

1. INTRODUCTION

A full scale instrumentation of a track structure was carried out in the summer of 1999. The work constituted a part of the investigation of the feasibility of raising the permitted axle loads designated by the Finnish Rail Administration (RHK) in 1998 – 2000. The instrumentation site is situated on the railway line between Koria and Kouvola, at the kilometre reading of 187 + 580. The northern rail of the track and the embankment beneath was instrumented. The track at the instrumented cross section was straight and had no frost insulation plates.

The aim of the instrumentation was to obtain actual measurement data on how different axle loads affect the following issues:

- Stresses in different parts of the track structure
- Distribution of loads on the railway embankment
- Intensity of vibration propagation to the track environment.

Most of the measurements were made under normal traffic running over the instrumentation site. By this means, measurement data was obtained from both passenger and freight trains. The measured freight traffic included many Russian tank wagons, which cause high vertical forces. Such wagons are used to import oil products from Russia. Apart from normal traffic, measurements were also carried out with a test train running over the instrumented cross section at various speeds. In the test train, all the axle loads in one four-axle wagon had been set as close to 250 kN as possible.

The planning of the measurement arrangements and the implementation was commenced by an order of the RHK in October 1998. The Laboratory for Mechanics of Materials and the Laboratory of Highway Engineering at the Helsinki University of Technology (TKK) and the Laboratory of Geotechnical Engineering at the Tampere University of Technology (TTKK) took part in the planning. The results of the planning have been documented in the RHK's publication A4/1999 "Instrumentation and modelling plan of a track structure, 250 kN and 300 kN axle loads" (Järvenpää et al. 1999). In accordance with its title, the report covers not only a description of the measuring arrangements, but also the preliminary guidelines indicating how the achieved measurement data should be utilised in modelling the mechanical behaviour of the track structure and the track components.

According to the instrumentation and modelling plan, the aim of the modelling, which was scheduled to take place during the latter half of 1999, was to compare the measured behaviour of the track structure in the instrumentation site to the actual behaviour of the track structure and its single components which have been modelled using relatively simple and easily applicable calculation and modelling methods. The following was stated in the plan as the aim of the preliminary modelling: based on the measurement results "*we can estimate the reliability of the measurement data obtained from the instrumentation site, we can get an overview of the mechanical behaviour of the embankment and the different components of it, and the possibilities to apply the*

methods used in the modelling to other corresponding modelling tasks, as well as we can create a basis for more detailed analyses of the measurement results possibly to be performed later on." (Järvenpää et al. 1999).

This report contains a summary of how the instrumentation and measurements were carried out on the railway line between Koria and Kouvola in May – July 1999 and the results of the preliminary modelling made in accordance with the above-mentioned targets. Based on the analyses of the measurement results performed thus far, suggestions for further studies in regard to the modelling of the mechanical behaviour of track structures and their components are presented at the end of the report. Furthermore, some issues, mainly concerning the loading assumptions of track structures, are considered in the same connection. They came up while the test results were being analysed even if they didn't include into the primary aims of the project in the beginning. However, with the help of the modelling work performed thus far these questions could be commented to some extent at least.

2. INSTALLATION OF THE INSTRUMENTATION

2.1 Installation phases

In compliance with the preliminary plan, the measuring instruments were installed in three different phases:

1. Measuring instruments were installed on the two lowest installation levels in the embankment on 26 May 1999. The date was determined so that the sleepers and rails were to be changed at the instrumentation site almost immediately after the installation.

2. The measuring instruments to be placed directly under the cleaning level of the ballast were mounted at night between 27 and 28 May 1999. The ballast cleaning machine was halted precisely at the instrumentation site to make it possible to carry out the instrument installation directly at the desired installation depth under the ballast cleaning machine.

3. Instruments were installed on the rails and sleepers on 21 – 30 June 1999. However, vertical anchoring rods extending to the stiff subgrade layers had been installed previously for fastening the transducers which measure the sleeper displacement. The time for installing the instrumentation in the rails had been chosen so that the track had been exposed to traffic for some time after rail exchange and tamping. Thus, movements in the track structures which were expected to happen immediately after these measures could be assumed to have mainly occurred before installation of the instrumentation.

Before any actual measurements were made, functioning of the measuring arrangements and the data acquisition devices were also tested at the instrumentation site. These preliminary measurements were made from the rails and sleepers in 30 June – 1 July. Regarding the measuring instruments inside the embankment the preliminary test was made on 1 July 1999.

2.2 Phase 1

2.2.1 Installation procedure

The measuring instruments which were placed deep inside the embankment were installed according to the following work phases:

- The track was cut for a distance of about 10 metres and the embankment was excavated from the side (Figure 2.2:1). Until to the mid level of the embankment – at a depth of about 1.3 metres below the track - the excavation extended under both rails, but at a level of 2.0 metres below the track the excavation extended only under the outermost rail.

- While the embankment was being excavated the original density state was measured by means of volumeter tests, using a radiometric density measuring equipment (Troxler) and indirectly by means of measurements made using a portable falling weight deflectometer (Figure 2.2:2).

Figure 2.2:1 Cutting the track and excavating the embankment.

Figure 2.2:2 Measuring the density state of the embankment during the excavation.

- The sensors to be placed at a depth of 2.0 metres below the track were installed and their actual position was recorded.
- The original embankment material was compacted in layers approximately up to the mid height of the embankment.
- Measuring instruments to be installed at a depth of about 1.3 metres below the track were installed and their actual position was recorded (Figure 2.2:3).
- The upper part of the embankment was compacted in layers by using the original materials (Figure 2.2:4).
- The track was mounted temporarily on its place using fish-plated rail joints

Figure 2.2:3 Recording the positions of the measuring instruments.

Figure 2.2:4 Filling the embankment by compacting it in layers.

2.2.2 Installed measuring instruments

A diagram showing how the measuring instruments at the depth of 2.0 metres below the track level were placed in relation to the final position of the northern track is shown in Figure 2.2:5 and correspondingly those at a depth of 1.3 metres in Figure 2.2:6.

As can be seen in Figures 2.2:5 and 2.2:6, the final positions of the measuring instruments vary slightly in relation to the position of sleepers and sleeper spacing. In fact, the mutual gaps of parallel measuring instruments had been chosen to fit a distance of one and a half times the sleeper spacing, keeping in mind that there would be a slight variation in regard to how the transducers are placed in relation to sleepers. On the other hand, by this means one could almost certainly avoid the undesired situation of having the same type of sensors all accidentally placed precisely in the middle of sleeper spacing. The problem when choosing the installation points for the transducers was that the rails and sleepers were to be changed at the instrumentation site just after the measuring instruments were installed, and the final positions of the sleepers were thus unknown at the time of installation.

On the other hand, when taking into account the installation depth of transducers in relation to the deviations from the ideal positions for the transducers, which would be right under the middle line of a sleeper and the sleeper spacing, it can be said that the actual location of transducers does not affect the integrity of the measuring results. Loads transmitted through the sleepers to the ballast and the embankment beneath in any case have time to spread out rather evenly before reaching the level of transducers. Likewise, it can be concluded that the small lateral deviations of the measurement instruments from the vertical planes passing through the middle line of the rails do not have any greater effect on the integrity of the measuring results or their mutual comparability.

Summaries of the number of transducers and their exact positions on the two lowest installation levels are given in Tables 2.2:1 and 2.2:2.

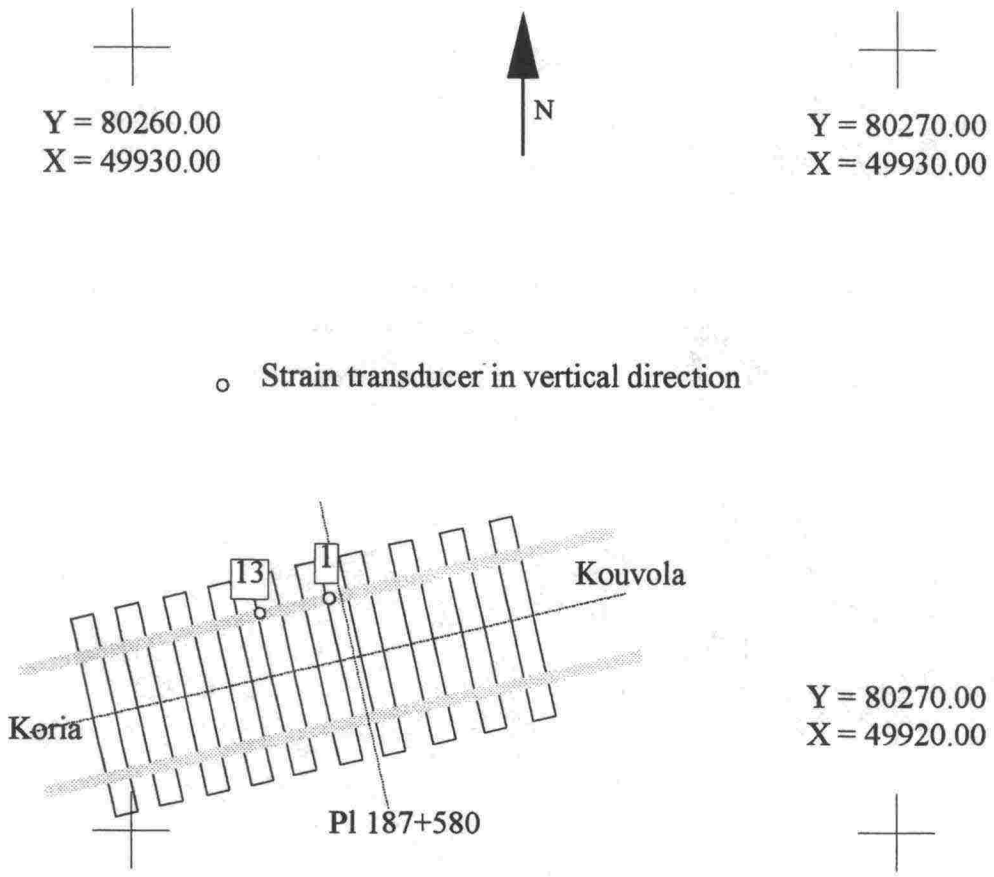

Figure 2.2:5 Positions of the measuring instruments at a depth of 2.0 metres.

Table 2.2:1 Measuring instruments at a depth of 2.0 metres.

Type of measuring instrument	No. of measuring instrument	Installation depth
Strain transducer in vertical direction	1 13	2.00 1.99
Temperature sensor	25	-

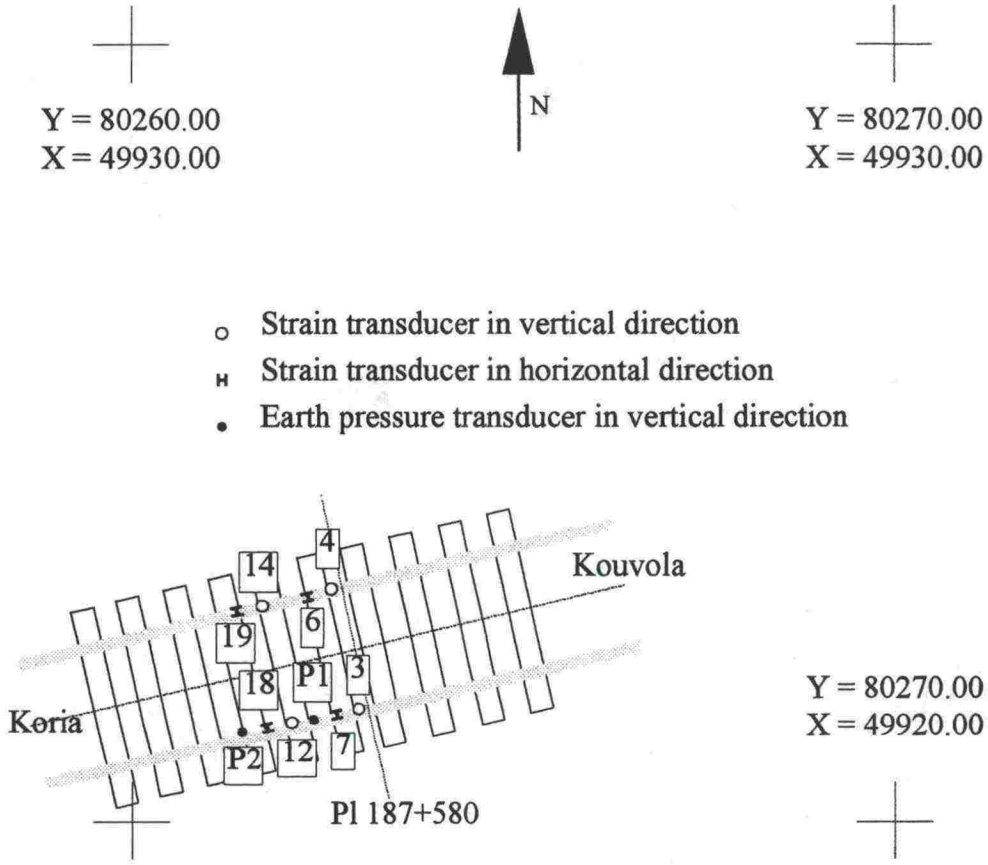

Figure 2.2:6 Positions of measuring instruments at a depth of 1.3 m.

Table 2.2:2 Measuring instruments at a depth of 1.3 m.

Type of measuring instruments	No. of measuring instrument	Installation depth
Strain transducer in vertical direction	3 4 12 14	1.26 1.31 1.23 1.30
Strain transducer in horizontal direction	6 7 18 19	1.31 1.25 1.22 1.30
Earth pressure transducer in vertical direction	P1 P2	1.24 1.22
Temperature sensor	26 27	1.21 1.27
Water content sensor	V1	-

2.2.3 Deviations from the instrumentation plan

With regard to the number and type of installed measuring instruments, the instrumentation was carried out at the two lowest installation levels in accordance with the preliminary plan (Järvenpää et al. 1999). However, the real composition and layer structure of the embankment deviated from the estimates. When the embankment was excavated the thickness of the ballast layer was found to be about 1.2 metres (Figure 2.2:7). Under the ballast there was about 0.8 metres of sand and somewhat coarser grained gravel underneath. The thickness of the gravel layer could not be determied during the excavation, but presumably the layer extended somewhat beneath the original ground level around the embankment.

The apparent cause of the clearly abnormal thickness of the ballast layer is the thick layer of fine grained soil in the subgrade of the instrumentation site. In this layer, the effects of consolidation settlement in relation to the rail position have apparently been eliminated by filling in the ballast layer gradually. At the same time the lowest layers in the embankment have slowly sunk under the original ground level.

With regard to the present railway embankment design and construction instructions, the abnormal order of layers – uniform sand right under the ballast and coarse grained gravel underneath it – can also be considered as the outcome of gradual construction of the embankment and strengthening phases in the long run. It may even be possible that the gravel underneath has sometimes been the original ballast layer. The grading curves of the layer materials will be presented in more detail in chapter 4.

In regard to the installation of measuring instruments, the unexpected embankment structure had not had as much effect on the two lowest installation levels. Measuring instruments at a depth of 2.0 metres were installed in the upper part of the lower coarse grained layer and those at a depth of 1.3 metres correspondingly on the fine sand layer somewhat beneath the bottom of the ballast layer.

At the beginning of the measurements another deviation from the instrumentation plan occurred which was related to the embankment width. The width was not made exactly in accordance with the normal cross section of a double track, but the embankment at the instrumentation site was wider than this. For this reason, the embankment was narrowed for a distance of about 10 metres in the middle of the monitoring period. The principle figures of the embankment cross section before and after narrowing are shown in Figure 2.2:7. The estimated boundaries between the different structural layers have also been outlined in the same figure.

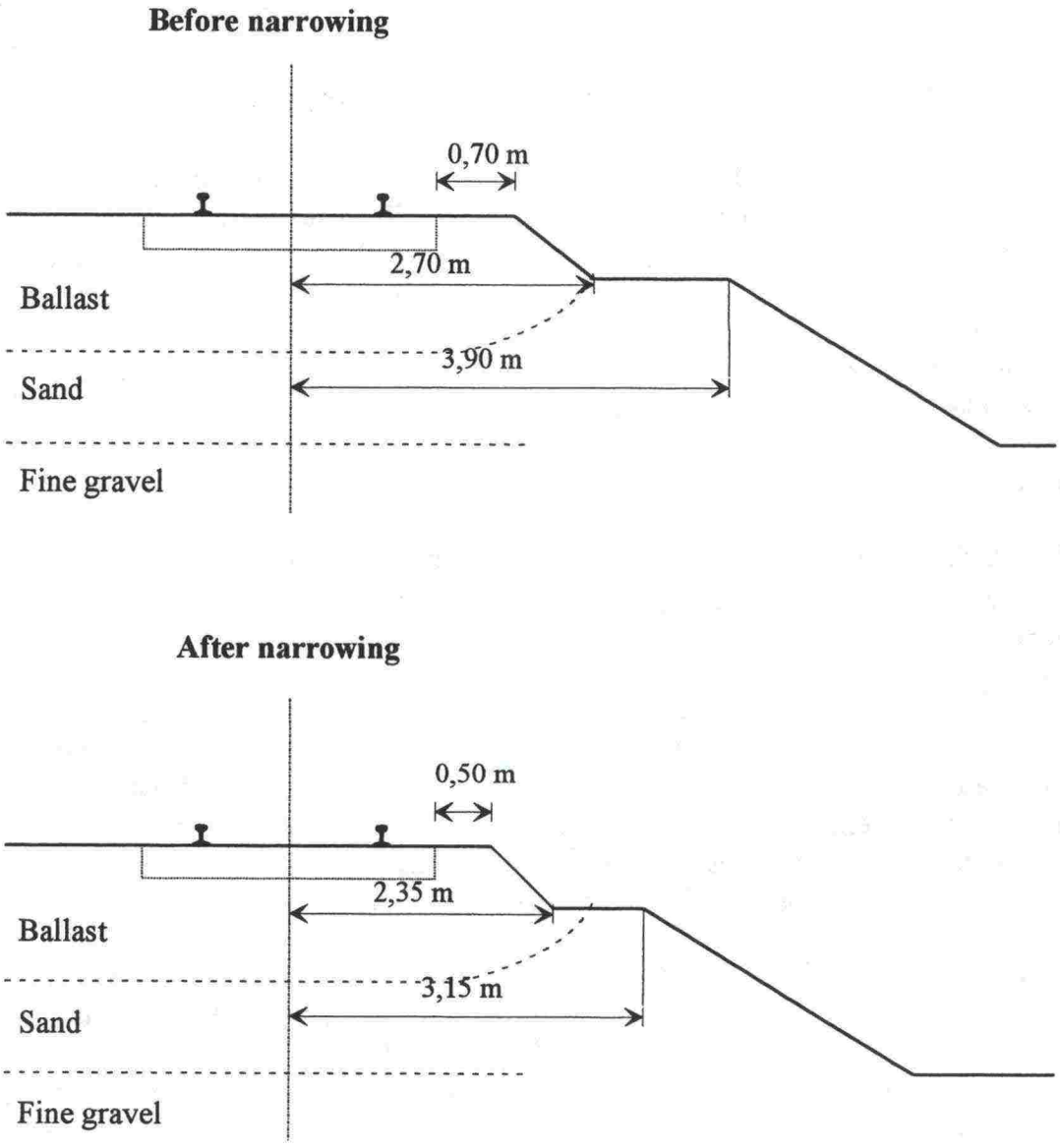

Figure 2.2:7 Shape of the embankment before and after narrowing.

2.2.4 Results of density measurements

As stated above in chapter 2.2.1, the original density in the structural layers of the embankment was measured during the excavation by water volumeter tests and by a radiometric density measuring device. In addition to this, the density was tested indirectly by a portable falling weight deflectometer. While the embankment layers were recompacted in layers the density was controlled by using the two latter measuring methods. The aim was to ensure sufficient density of the layers, so that no harmful post settlements would occur at the instrumentation site.

A summary of the density measurements made in connection with the excavation and the recompaction of the layers is given in Table 2.2:3. Although the measured density at the surface of the compacted layer may be slightly higher than the average density of the corresponding layer, based on the results shown in Table 2.2:3 it appears that the compaction of the layers was sufficiently effective.

Table 2.2:3 Results of the density measurements on embankment layers.

Measurement level	Measurement method and unit of the result	Measurement result	
		During excavation	After compaction
1.3 m below the track level (sand)	Radiometric dry density measurement [kg/m^3]	1719	2111
		1784	1974
		1792	2014
		1766	2060
		1788	2037
		1763	1997
	Modulus value recorded by the Loadman-equipment [MPa]	85	104
		144	96
		116	122
		104	133
2.0 m below the track level (gravel)	Dry density by water volumeter [kg/m^3]	1749	
		1778	
	Radiometric dry density measurement [kg/m^3]	1878	
		1919	
		1867	
		1860	
		1884	
		1856	
	Modulus value recorded by Loadman-equipment [MPa]	89	
		82	
		89	

2.3 Phase 2

2.3.1 Installation procedure

As mentioned in chapter 2.1, the measuring instruments inside the embankment at a level of –0.7 metres were installed when screening of the ballast layer had proceeded until to the instrumentation site. The ballast cleaning machine was stopped exactly on top of the instrumentation site so that installation could be carried out right on to the ballast layer under the cleaning depth. As the installation layer for the instruments did not have to be excavated any more than required for the mounting space, there was no problem with keeping the density state constant. Neither did the density state of the ballast over the mounting level require any special measures to be taken, as the whole track on the layer had to be supported after the screening of the ballast.

2.3.2 Installed measuring instruments

As the position of transducers could now be bound to the position of the new rail over the installation level during phase 2, the actual position was not controlled by geodetic measurements. In fact, this would have been quite difficult because of the prevailing darkness during the installation time.

A summary of the positions of the measuring instruments at a level of –0.7 metres in relation to the northern track is given in Figure 2.3:1. As shown in the figure, half of the vertical strain transducers are placed rather accurately under a sleeper and half of them in a sleeper spacing.

A summary of the number and exact installation depths of transducers at a level of –0.7 metres is shown in Table 2.3:1.

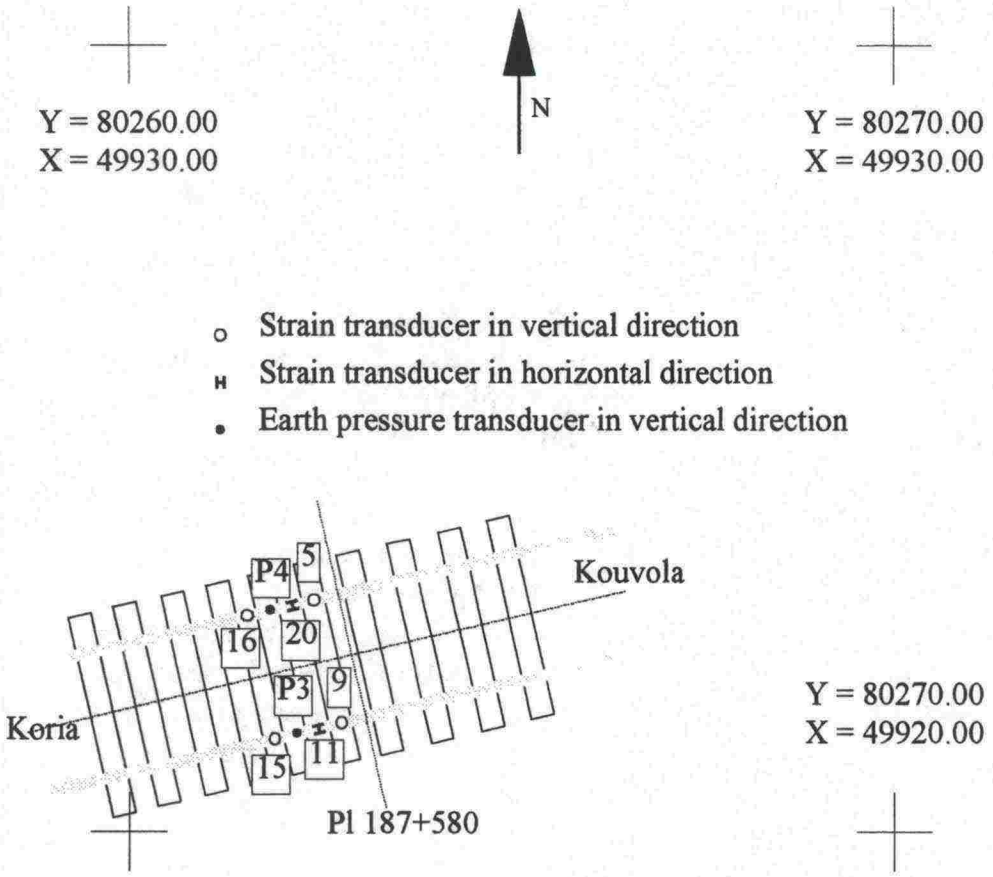

Figure 2.3:1 Position of measuring instrument at a depth of – 0.7 m.

Table 2.3:1 Measuring instruments at a depth of – 0.7 m.

Type of measuring instrument	No. of measuring instrument	Installation depth
Strain transducer in vertical direction	5 9 15 16	0,66 (*
Strain transducer in horizontal direction	11 20	0,66 (*
Earth pressure transducer in vertical direction	P3 P4	0,66 (*
Temperature sensor	28	0,66 (*
Water content sensor	V2	0,66 (*

(* Installation depth determined on the basis of the ballast cleaning level.

2.3.3 Deviations from the instrumentation plan

The most important deviation regarding phase 2 was that the ballast layer was much thicker in the embankment than expected. For this reason, the measuring instruments at the level of –0.7 metres below the track had to be installed inside the ballast although this, owing to the very coarse grained nature of the material, was considered impossible with regard to the reliability of the measurements. However, the required measuring instruments had already been obtained and the chances for checking the modelling of the mechanical behaviour of the embankment would have been considerably weakened in the absence of measuring data from the upper part of the embankment. Consequently, a decision was made to install the measuring instruments at the planned installation depth.

The instrumentation plan was followed with regard to the number of measuring instruments at the level of –0.7 metres, with the exception that one lateral strain sensor was also placed at the referred depth underneath both rails. The aim of these installations was to gain more experience on how suitable the developed sensor type is under different installation and measuring circumstances, although one should regard the success of measurements with this type of material with some reservation.

2.4 Phase 3

2.4.1 Installation procedure

The instrumentation of the superstructure (Figure 2.4:1) was carried out according to the plan. This was facilitated by the fact that the Laboratory for Mechanics of Materials at the Helsinki University of Technology had some experience of similar measurements. Due to the fine weather the time reserved for the mounting was adequate.

The strain gauges (SGs) were installed analogously on both rails in the middle and one third of a sleeper spacing using cyanoacrylate adhesive (Kyowa CC-33A). After wiring the bonded SGs to full-bridge circuits the installations were protected against humidity using Sikaflex compound. Three SGs were bonded on the sleeper, one in the middle of the upper surface and one underneath both rails near the upper edge on the side of the sleeper. The sleeper surface was impregnated several times at the bonding points by the same cyanocrylate adhesive and the surface was roughed off after drying. These SGs were completed to half-bridge circuits by using passive ('dummy') strain gauges.

Steel fixtures for those transducers measuring displacements of rails were bonded to the sleeper by using fast hardening epoxy resin. Deep into the soil rammed vertical steel rods served as attachments for the transducers, which were meant to measure vertical displacements of the sleeper.

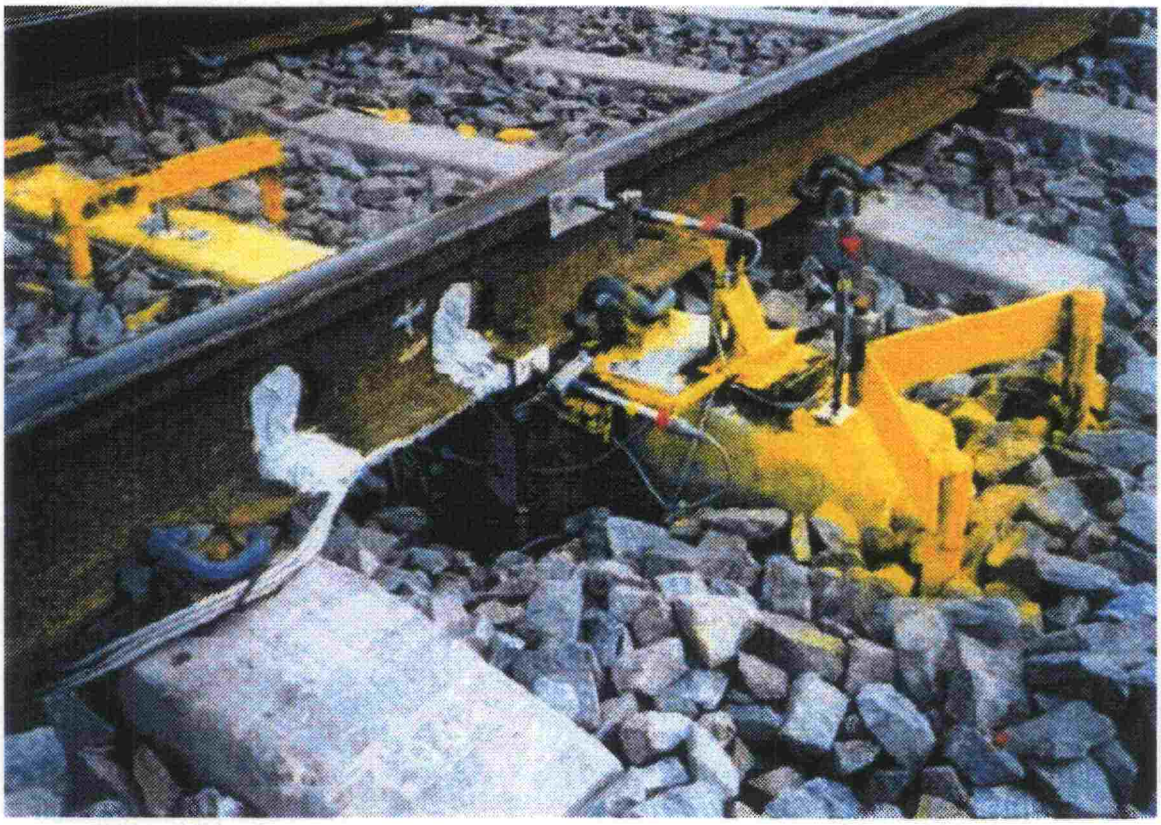

Figure 2.4:1 Completed rail instrumentation.

2.4.2 Measuring instruments

Most of the SGs installed on rails were of type Kyowa KFW-5-120-D16-11L1M2S ('T-type' SG). These have two measuring grids, which are 5 mm long with 90° angle between their measurement directions. Single SGs mounted on the rail web for recording the vertical force were of type KFW-5-120-C1-11L1M2R. A flexible piece of plastic plate to provide basic protection together with a thin plastic covered twin cable to facilitate installation work had been integrated in both types of SGs during production. All the SGs were temperature adjusted for steel. The grid length of Kyowa KC-70-A1-11-type single SGs bonded on the sleeper was 70 mm.

The inductive transducers for measuring rail and sleeper displacements were all of type HBM W10TK which have a spring-return plunger inside their pipe-like body. Based on earlier experiments from similar measurements, the transducers were furnished with auxiliary external spring in order to improve their mechanical frequency response characteristics to follow better those rather rough movements occurring in track structures. Plastic coated 4x0.5mm^2 cable equipped with a braided protective shield was used as cable for the transducers as well as for SGs.

2.4.3 Deviations from the instrumentation plan

There were no actual deviations from the plan concerning the superstructure. It can be noted, however, that the transducers measuring the vertical displacement between the rail foot and the sleeper were fixed under the rail as near to the sleeper as possible in accordance with the second given alternative.

3. PERFORMANCE OF THE MEASUREMENTS

3.1 Measuring dates and measured traffic

Measurements at the instrumentation site on the railway line between Koria and Kouvola were carried out from 14.30 on 6 July 1999 to 12.00 on 8 July 1999. During this time measurements were carried out continuously day and night for all traffic running from east to west, except for the period 16.00 – 18.00 on 7 July 1999, when the embankment was narrowed as described in Chapter 2.2.3 and in Figure 2.2:7.

The traffic which ran over the instrumentation site during the monitoring period is summarised in Table 3.1:1. A test train which was equipped specifically for the measurements was run over the measuring site ten times, as can be seen in Table 3.1:1. The train consisted of a Dv12 2545 diesel locomotive and a 4-axle Rbnqss-wagon 75140-4 (Figure 3.1:1), where the axle load in all axles was set as close to 250 kN as possible. The report on the weighing of the test train, as well as a more detailed description of other traffic running over the measuring site, is given in appendix 1.

Table 3.1:1. Summary of the traffic running over the instrumentation site.

Type of train and direction	Number of measured crossings
Test train with 4 axles of 250 kN (Koria - Kouvola)	5
Test train with 4 axles of 250 kN (Kouvola – Koria)	5
Tank train (Kouvola – Koria)	10
Other freight train (Kouvola – Koria)	20
Express train (Kouvola – Koria)	30
Other passenger train (Kouvola – Koria)	5
Maintenance vehicle (Kouvola – Koria)	1

Figure 3.1:1 Test train with four axle loads of 250 kN.

3.2 Measurement arrangements

3.2.1 Measurements from superstructure

The vertical and lateral component (=Y-force) of the wheel load was measured from both rails by the Laboratory for Mechanics of Materials at the Helsinki University of Technology. The shear strains in rails due to the load in the middle of the sleeper spacing were utilised in the measurements. Strain gauge bridges were calibrated with the aid of a hydraulic cylinder, a load transducer and a load frame mounted on a rail. The calibrated vertical load range was 0 – 170 kN and the lateral one 0 – 70 kN. 200 kN and 100 kN respectively had been chosen for the nominal measuring range of the amplifiers. SGs were also used to measure the strain of the lower surface of the rail foot in both rails in the middle of the sleeper spacing and further the sleeper bending strain at three points.

The vertical displacement of the rail foot and the lateral displacement of the rail foot and head relative to the sleeper were measured from both rails by transducers. For the first-mentioned quantity two transducers were placed near to the edges of the foot of both rails. The vertical displacement of the sleeper relative to the ground was measured by transducers placed in the middle and at the ends of a sleeper.

The SG bridges were connected to HBM3073 and the displacement transducers to HBM MC55-type amplifiers. The signals were balanced before the measurements, so that the output of the amplifiers was zero at no load condition. The outputs were observed between recordings and the detected level offsets were corrected except those for the SGs on the lower surface of the rail foot in the middle of the sleeper spacing. The transducer signals, amplified to suitable volt level, were led to recording equipment, i.e. to a PC with a data acquisition (DAQ) board and two Teac RD-145T DAT-recorders. The sampling frequency of the DAP1200E/6 DAQ-board was set to 10 kHz. Since there was a total of 24 DAQ-channels active, a sample of each signal was received every 2.5 milliseconds. The samples were saved in a train-specific disc file in the PC. Recording was started and stopped manually. The signals were backed up by the above-mentioned 16-channel DAT-recorders. Their sampling frequency was six times higher compared to the DAQ-board.

A summary of the quantities, their polarity and corresponding DAQ channel numbers are presented in Figure 3.2:1 and Table 3.2:1.

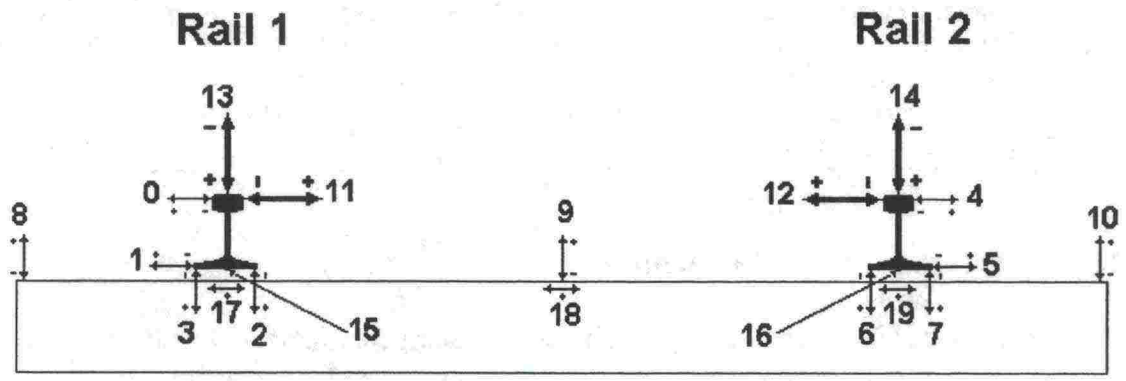

Figure 3.2:1 Quantities measured from the superstructure. The numbers refer to the numbering of channels in data acquisition, given in Table 3.2:1.

Table 3.2:1 DAQ channel numbers of quantities measured from the superstructure.

Channel number	Measured mechanical quantity
0	Horizontal displacement of the head of rail 1 relative to the sleeper
1	Horizontal displacement of the foot of rail 1 relative to the sleeper
2	Vertical displacement of the inner edge of the foot of rail 1 relative to the sleeper
3	Vertical displacement of the outer edge of the foot of rail 1 relative to the sleeper
4	Horizontal displacement of the head of rail 2 relative to the sleeper
5	Horizontal displacement of the foot of rail 2 relative to the sleeper
6	Vertical displacement of the inner edge of the foot of rail 2 relative to the sleeper
7	Vertical displacement of the outer edge of the foot of rail 2 relative to the sleeper
8	Vertical displacement of the sleeper end on the side of rail 1 relative to the ground
9	Vertical displacement of the middle section of the sleeper relative to the ground
10	Vertical displacement of the sleeper end on the side of rail 2 relative to the ground
11	Horizontal component of the wheal load exerted on rail 1
12	Horizontal component of the wheal load exerted on rail 2
13	Vertical component of the wheal load exerted on rail 1
14	Vertical component of the wheal load exerted on rail 2
15	Strain on the lower surface of the foot of rail 1 in the middle of the sleeper spacing
16	Strain on the lower surface of the foot of rail 2 in the middle of the sleeper spacing
17	Strain near the upper edge of the sleeper side underneath rail 1
18	Strain on the upper surface of the sleeper in the middle section
19	Strain near the upper edge of the sleeper side underneath rail 2
20-23	Pressure transducers of TUT

3.2.2 Measurements in rail embankment

The Laboratory of Geotechnical Engineering at the Tampere University of Technology was responsible for the strain measurements made inside the rail embankment at three different depths and earth pressure measurements made at two different depths. Additionally, the reading of the sensors which were measuring the temperature and the water content of the embankment were registered at the beginning and at the end of the monitoring period.

As all the mounted strain gauges, apart from one – i.e. sensor no. 18, which was mounted in lateral direction at a depth of –0.7 metres – seemed in principle to be fit for operation at the beginning of the monitoring period and inside their measuring area, the total number of registered strain transducers was 15. Ten of these recorded the vertical strain, and five the lateral strain, of the embankment. In addition, there was a total of four transducers for vertical earth pressure installed at a depth of –0.7 metres and –1.3 metres, which were registered continuously during the measurements.

The data acquisition equipment used in the registration of strain transducers comprised a 16-channel 12 byte Computerscope A/D-converter board available at the Laboratory of Geotechnical Engineering of the Tampere University of Technology. The highest sampling frequency of the converter board in a one-channel recording is 1 MHz. The sampling frequency during these measurements was, however, only 1 kHz for each measuring channel. Owing to the limited number of measuring channels in the Computerscope data acquisition system, registering of the pressure transducers installed

in the embankment had been connected to the data acquisition system which had been brought to the instrumentation site by the Laboratory of Highway Engineering of the Helsinki University of Technology (see chapter 3.2.1).

The Computerscope data acquisition system uses two data bytes in order to store one measuring observation. Thus, by using a sampling frequency of 1 kHz in the data acquisition from 15 strain transducers, the amount of measuring data per one measuring second was about 30 kilobytes. While taking into account that the measurement was started manually a few seconds before the train arrived at the instrumentation site, the stored amount of measuring data from a single train passage varied between 200 kilobytes and 1.5 megabytes, depending on the train length. The amount of data measured from all strain transducers during the whole monitoring period totalled about 50 megabytes.

4. BASIC DATA OF MODELLING

4.1 Rail characteristics

During upgrading work, the old track structure on the line section between Kouvola and Koria had been renewed completely, using BP89 steel sleepers and 60 E 1 -rail. BP89 sleepers are equipped with Pandrol clip shoulders, on which the rail is placed through Pandrol e 1817 clips. A rubber 10 mm P-rail pad manufactured by Teknikum lies underneath the rail. A P-insulator providing galvanic isolation between the clip shoulders and the rail is included in the structure.

4.2 Embankment characteristics

4.2.1 Embankment dimensions

The deviation from the normal track cross section of the embankment at the instrumentation site, which was detected during the measurements, was already dealt with in chapter 2.2.3. As the embankment width around the instrumentation site was changed during the measurements, the results obtained during the first day correspond to a one-sided embankment width that is 0.75 metres more than the width of the embankment during the second monitoring day (Figure 2.2:7). However, the test train, with its 250 kN axle loads, was run only after the embankment width had been narrowed.

4.2.2 Grain size distribution of embankment materials

The grain size distribution of the embankment materials, which were determined based on samples taken during the installation of the measuring instruments, has been presented for the ballast before cleaning in Figure 4.2:1 and for the sand under ballast and for the gravel beneath it in Figure 4.2:2. According to Figure 4.2:1 the result obtained with the sample taken from the ballast layer can to some extent be considered doubtful, as according to this result the material would have lain clearly under the screening limit, which apparently was not the case.

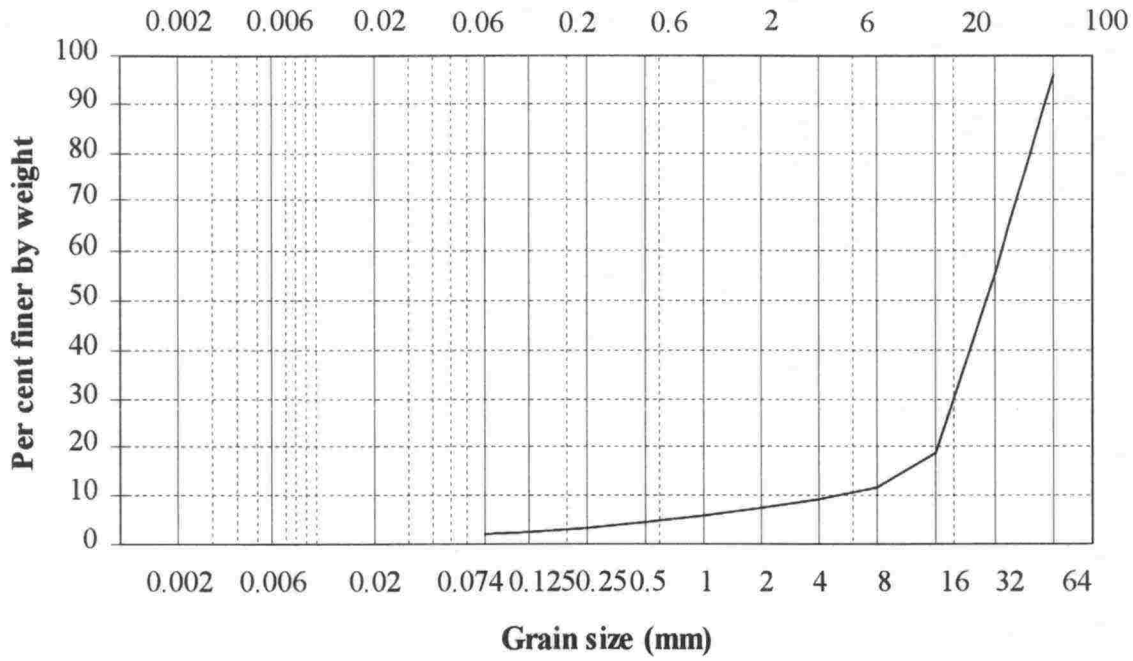

Figure 4.2:1.Grain size distribution of ballast layer before cleaning.

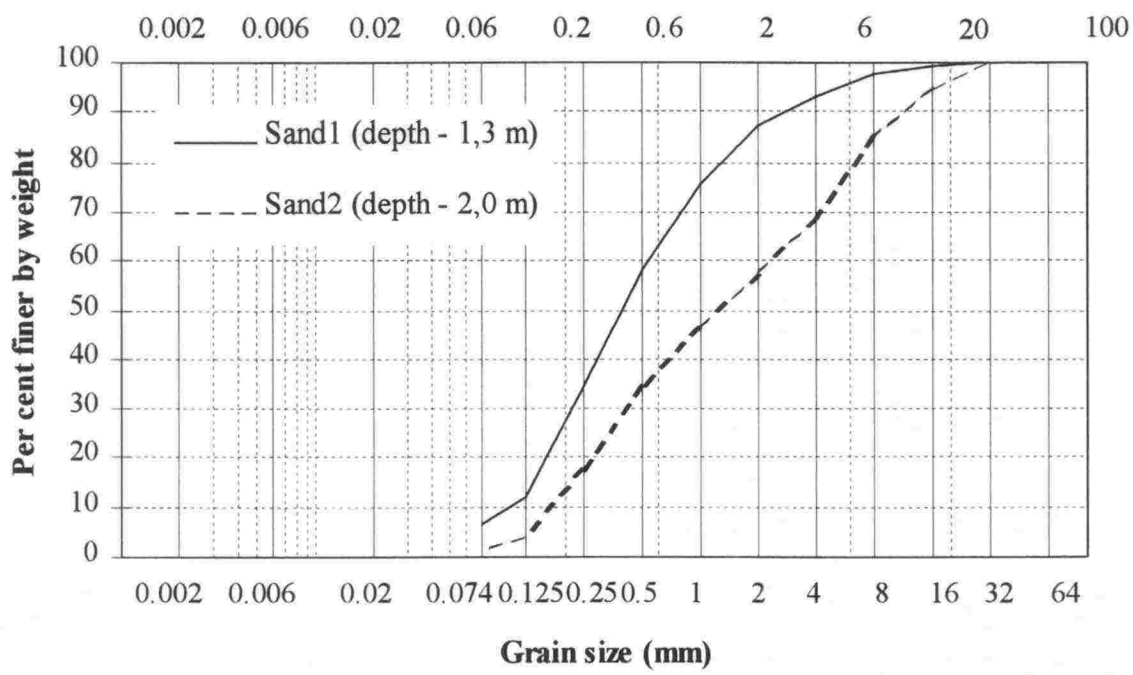

Figure 4.2:2. Grain size distribution of sand and gravel in the embankment.

4.2.3 Mechanical characteristics of embankment materials

In view of the preliminary modelling taking place in autumn 1999, the embankment materials were to be tested for stress level dependent modulus values describing the resilient deformation behaviour of the materials. The cyclic loading triaxial test was the method to be used and the tests were made with the large scale triaxial testing equipment available at the Laboratory of Geotechnical Engineering of the Tampere University of Technology (Figure 4.2:3).

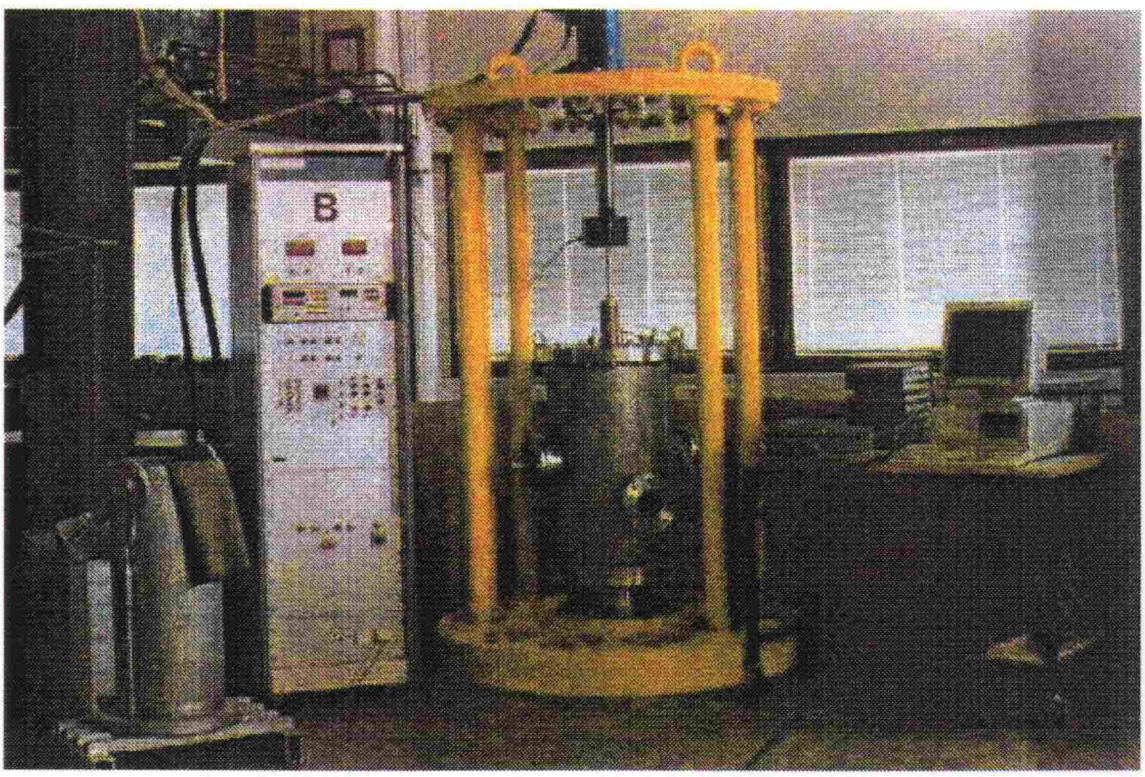

Figure 4.2:3. Large scale cyclic loading triaxial equipment at the Laboratory of Geotechnical Engineering of the Tampere University of Technology.

The test method was the American SHRP (Strategic Highway Research Program) protocol P46 loading procedure (AASHTO T 294-92 I). As this loading procedure consists of 15 different combination of constant confining pressure and cyclic axial load, the result will be 15 different values of the resilient modulus. The values obtained this way for the materials of the sand layer beneath the ballast and the gravel underneath are included in enclosure 2.

In order to take into account the dependency of the modulus values on the stress level in the practical modelling, the measured behaviour of the material should be presented by means of a suitable material model. For the modelling to be performed using a multi layer linear elastic model (chapter 6), the dependency of the modulus values on the stress level has been described here by a so-called $k\theta$-model of formula 4.2:1:

$$M_r = k_1 \theta_0 \left(\frac{\theta}{\theta_0} \right)^{k_2} \qquad (4.2:1)$$

where,

M_r	*is*	*resilient-modulus*
θ	*is*	*sum of the principal stresses with the maximum value of axial load,* $\theta = \sigma_1 + 2\sigma_3$
θ_0	*is*	*reference stress 100 kPa*
k_1	*on*	*material parameter ('modulus value')*
k_2	*on*	*material parameter ('stress exponent')*

When the material parameters k_1 and k_2 of formula 4.2:1 have been adjusted to the actually measured results of appendix 2, the dependency of the modulus values on the stress level is as described by the broken lines in connection with the measured results. The corresponding values of material parameters k_1 and k_2 are given in Table 4.2:1.

Table 4.2:1 Material parameters k_1 and k_2 for the materials at the instrumentation site according to formula 4.2:1.

Material	k_1	k_2
Cleaned ballast	2000	0,50
Uncleaned ballast	1750	0,50
Sand	1635	0,38
Gravel	2265	0,50

The ballast of the instrumentation site was not tested at this stage, but parameter values have been estimated on the basis of tests made earlier on materials which have similar grading properties (Kolisoja 1997). Firstly, this is due to the fact that testing of a single specimen with a material of this type of grading would not give a more reliable result. Secondly, it was desired to save some of the sampled material for special studies which might become necessary during more advanced modelling later on.

Static triaxial tests up to a failure under a confining pressure of 50 kPa were also made with the samples that were first exposed to the cyclic loading triaxial test procedure (enclosure 2). More comprehensive determinations for determining the plastic deformation behaviour of the embankment materials were not, however, included in the tests, either in static, or in repeated cyclic, loading at this stage.

4.3 Subgrade characteristics

4.3.1 Soil conditions at the instrumentation site

Data on the soil conditions at the instrumentation site was limited during the planning of instrumentation to the investigations made in connection with mast positioning of the catenary line in 1975 and a culvert study made on the railway line about 750 m towards Kouvola from the instrumentation site in 1970. Involving Swedish weight soundings, these investigations had not been performed at a depth lower than about 12 metres under the original ground level.

On the basis of the earlier investigations and visual observations made of the landscape it could be presumed that there were fine grained layers present in the area. However, it was not possible to be sure about the thickness of the layers on the basis of the data obtained. Thus, a supplementary soil investigation was scheduled to the instrumentation site, during which two weight soundings reaching to the dense subsoil layers were made. The investigations points and the observed sounding resistances are shown in enclosure 3.

On the basis of the sounding results, the distance of a dense subsoil layer is about 22 metres below the ground surface and at a perpendicular distance of 27.25 metres from the centre line of the northern rail to the south about 18 meters below the ground surface.

Undisturbed soil samples were also taken from two sampling levels at site 1 (enclosure 3). Samples taken from a depth of 2.50 – 2.84 metres represent a somewhat stiffer soil layer in terms of sounding resistance reaching a depth of about 4 metres below the ground surface. The samples taken from a depth of 4.97 – 5.48 metres, on the other hand, represent a soft clay layer with a lower sounding resistance.

The grain size distributions of the soil samples taken from the above mentioned sampling levels are shown in Figure 4.3:1. A summary of the other defined geotechnical properties of the samples is given in Table 4.3:1.

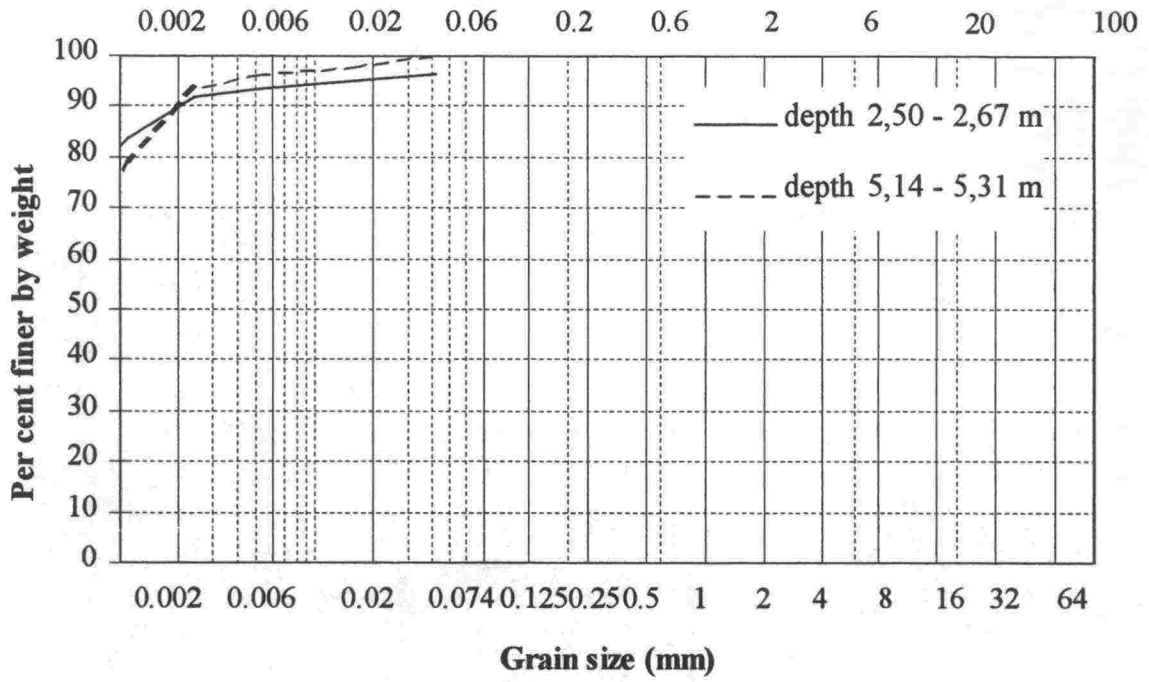

Figure 4.3:1 Grain size distribution of samples taken from the subsoil layers.

Table 4.3:1 Geotechnical properties of the samples taken from the subsoil layers.

Characteristic and measuring unit	Depth 2.50 – 2.67 m	Depth 5.14 – 5.31 m
Soil type	Fat clay	Fat clay
Unit weight [kN/m^3]	15.9	14.2
Water content [%]	66.9	100.4
Organic content [%]	1.78	1.38
Undrained shear strength [kPa]	39.2	21.5
Sensitivity	2.35	15.66
Fines number	114	86

4.3.2 Mechanical characteristics of subsoil layers

Supplementary to the programmed laboratory studies, shear modulus determinations were made on the undisturbed subsoil samples. The determinations were made with the combined Resonant Column and Bender Element (BERC) equipment (Souto et al. 1994) available at the Laboratory of Geotechnical Engineering of the Tampere

University of Technology and shown in Figure 4.3:2. The results are given in appendix 4.

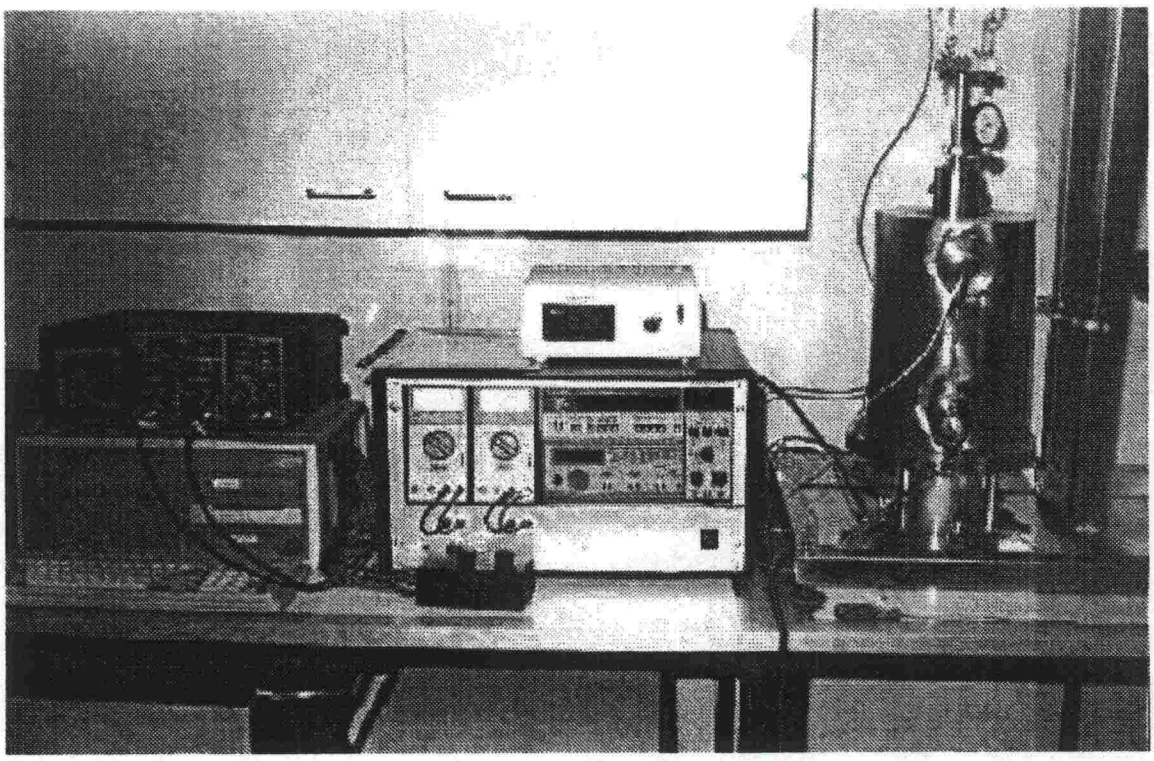

Figure 4.3:2 The combined Resonant Column and Bender Element equipment at the Tampere University of Technology.

As revealed by the measuring results in appendix 4, the values of shear modulus G defined vary, characteristically for subsoil materials, both as a function of the prevailing stress and strain level. For this reason, the choice of modulus values to be used in the modelling requires these factors to be known or assumed. For the multi layer linear elastic model in chapter 6, in particular, the additional problem is that the subsoil is assumed to be a homogenous halfspace, although the stress and strain level is known to change continuously in regard to both depth and lateral distance as the distance from the track increases.

In the multi layer linear elastic model the value of the subgrade shear modulus with the stress and strain level assumptions was estimated as G = 13.3 MPa. On the other hand, when the value of Poisson's ratio with water saturated soil in undrained conditions is known to be $\nu = 0.5$, the Young's modulus of the subgrade E = 40 MPa is obtained in accordance with the basic formulas of the elasticity theory. The validity of this assumption is estimated later in chapter 6 on the basis of a sensitivity analysis to be performed on the subgrade modulus value.

4.4 Choice of representative measurement results

4.4.1 Measurements with 250 kN axle load

From among 10 passages of the test train, measurement no. 64 was chosen for a more detailed study (Figure 3.1:1). During this measurement the test train was run over the instrumentation site at a nominal speed of 50 km/h towards the west, from Kouvola to Koria. This passage was chosen primarily because the speed of the test train was the lowest when the train arrived at the instrumentation site along the straight line from Kouvola. This direction was chosen because normally there were some differences in the average wheel forces between the inner and outer rails when approaching the instrumentation site from the direction of Koria (Table 4.4:1).

Table 4.4:1 The average values of wheel forces and axle loads of the test train during passages of the instrumentation site at different speeds.

Measure-ment No.	Train speed [km/h]	Direction	Wheel force 1 (outer rail) [kN]	Wheel force 2 (inner rail) [kN]	Axle load [kN]
62	41	Eastward	123,3	127,6	251,0
64	47,5	Westward	126,1	127,1	253,2
67	61	Eastward	113,9	132.0	245,9
68	68	Westward	127,8	124,8	252,6
70	80,5	Eastward	109,7	137,1	246,8
73	89	Westward	122,7	124,8	247,1
74	98	Eastward	117,0	129,6	245,6
75	100	Westward	124,3	129,2	253,5
78	90 (braking)	Eastward	113,3	128,0	241.3

As shown in Table 4.4:1, the average axle loads of the test train do not seem to depend on the train speed. The reason for this is most apparently that the rail was renewed at the instrumentation site just before the monitoring period and, moreover, at least by visual estimation, the wheels in the test train seemed to be in very good condition. This similar nondependency on the train speed could also be noted with the other measured quantities.

4.4.2 Measurements with other axle loads

The main emphasis in the measurement data and the related inspections of this report lies, of course, on the measurements carried out by the 250 kN axle loads of the test train. Owing to the great number of measurement data, it was not possible to cover the other results in detail in this report. There is a summary of the measurement events in Table 4.4:2, where the results of other measurements are covered, at least in part. In addition, the results of many other measurements have been handled in different phases, but the measurements in the table represent some typical examples which could be applied as examples of the axle load or distribution in different inspections.

Table 4.4:2 Some measurements additional to the test train selected for a more detailed study.

Measurement no.	Selection criteria or item to be analysed	Chapter
7	Impact of a wheel flat	5.1
11	Short tank train with various axle loads	6.10
40	Tank train with 8-axle wagons	4.5.1
	Distribution of wheel loads and stresses on rail pads	5.1, 5.2
46	Load distribution on consecutive sleepers	5.6
77	Tank train with many high axle loads	5.1, 7.5
85	Maintenance vehicle with smaller axle loads than normal	5.5, 6.10

4.5 Examples of measurement results

4.5.1 Measurements from superstructure

Loads exerted on rails

The vertical wheel load was measured, in accordance with chapter 3.2.1, from the rail in the middle of the sleeper spacing. When the test train arrived at the measurement site from Kouvola for the first time, a static measurement was carried out by running each of the train axles in turn to the middle of the instrumented sleeper spacing and stopping it there momentarily in order to record the measurement values. The results of this static measurement are shown in Table 4.5:1. When taking into account that the value of the acceleration due to gravity is 9.82 m/s^2 on the 60th latitude, the mass of the test train becomes precisely 100,000 kg, i.e. the same as in the weighing. Thus, it can be concluded that the method used for measuring the vertical wheel load works well, at least in static condition.

Table 4.5:1 Static vertical wheel loads recorded from the test train.

Number of axle	Output of amplifier Volts		Load kN		Axle load kN
	Rail 1	Rail 2	Rail 1	Rail 2	
Locomotive:					
1	3,640	4,060	72,8	81,2	154,0
2	3,930	4,110	78,6	82,2	160,8
3	3,940	3,752	78,8	75,0	153,8
4	3,620	4,120	72,4	82,4	154,8
			Weight of the locomotive		623,4
Wagon:					
5	6,020	6,060	120,4	121,2	241,6
6	6,023	6,180	120,5	123,6	244,1
7	6,500	6,280	130,0	125,6	255,6
8	5,710	6,300	114,2	126,0	240,2
			Weight of the wagon		981,5
			Total weight of the train		1604,9

When a train run through the instrumented track section, the signals proportional to wheel loads could be recorded from the rails. As an example, the signals recorded in measurement no. 64 are presented in Figures 4.5:1 and 4.5:2. The test train was running through the measurement site from Kouvola to Koria at a nominal speed of 50 km/h. A peak in the time record of the vertical wheel load occur when a wheel passes the middle of the sleeper spacing. The height of the peak is considered to represent the instantaneous vertical load produced by the wheel at the point in question. The value of the lateral wheel load can be derived from the Y-force signal at the same moment. The direction of impact of the lateral wheel load can be either outwards (negative signal) or inwards (positive). The channel numbers used in Table 3.2:1 and Figure 3.2:1 are referred to in Figures 4.5:1 and 4.5:2.

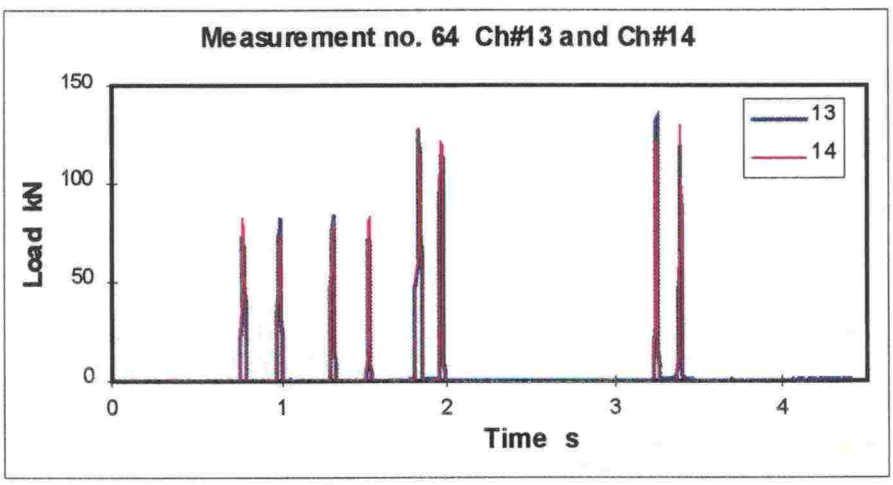

Figure 4.5:1 Example of vertical wheel loads.

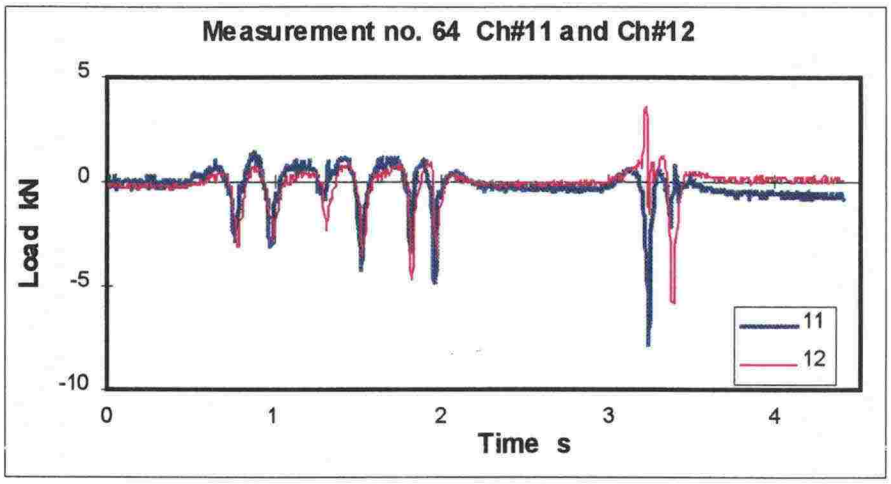

Figure 4.5:2 Time record of the lateral component of wheel loads

Strain on the lower surface of rail

As seen in Figure 4.5:3, the strain signal recorded from the lower surface of the rail foot is very clear, with sharp peaks. The peaks arise when a wheel passes the middle point of the sleeper spacing, where the strain gauges were located. The corresponding deflection of the rail produces tensile stress in the rail foot. The U-shaped valleys are caused by the rail bending upwards at the measuring point while the wheel is on the adjacent sleeper spacing. The corresponding stress is compressive.

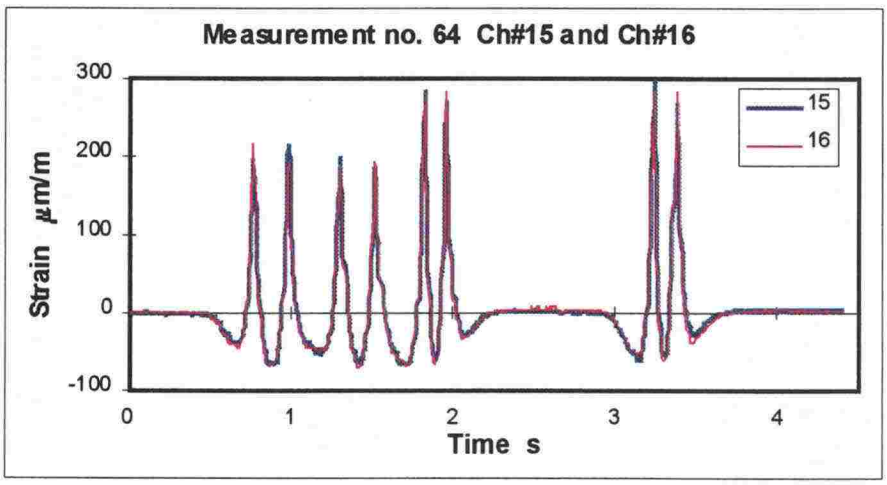

Figure 4.5:3 In this example the highest bending strain of the rail foot was 300 µm/m, corresponding to a stress of about 60 MPa

Rail movement relative to sleeper

The time record of the vertical displacement of the rail foot relative to the sleeper resembles the previous one presenting bending strain, as seen in Figures 4.5:4 and 4.5:5. The effect of each axle can be seen clearly, although the peaks are somewhat more rounded and the valleys are not so deep. The positive direction means a rail displacement towards the sleeper.

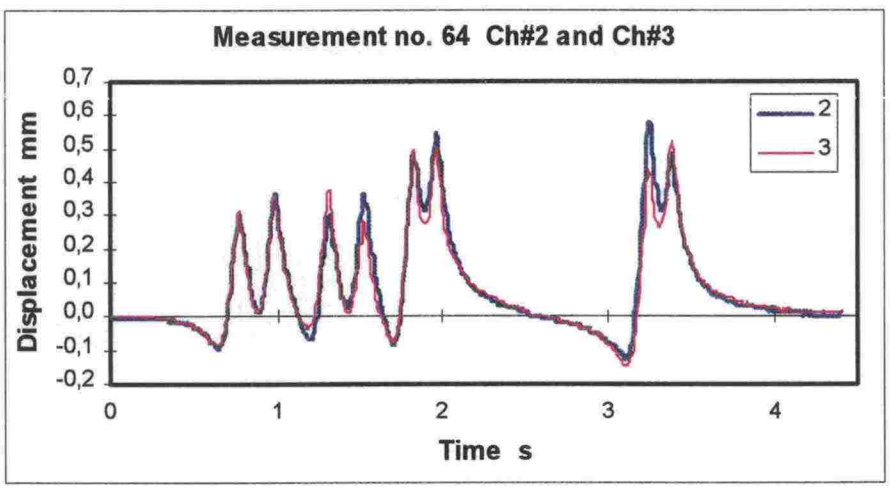

Figure 4.5:4 Vertical displacement of rail 1 in relation to the sleeper.

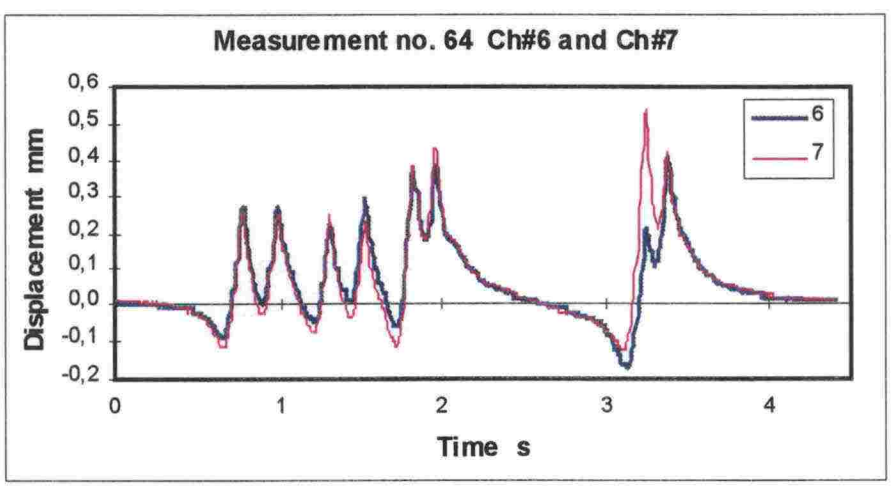

Figure 4.5:5 Vertical displacement of rail 2 in relation to the sleeper.

The lateral displacement of the railhead in Figure 4.5:6 and of the foot in Figure 4.5:7 are presented relative to the sleeper. The lateral movement remained very small, especially in the foot, being restrained by the straight connection to the clip shoulder on the sleeper through the P-insulator. The positive direction of the lateral displacement is outwards from the track. The largest lateral displacement of the railhead in measurement no. 64 occurred in rail 2 and was caused by the front axle of the rearmost bogie of the wagon. By comparing the graphs, it can be seen that the rail is bent inwards.

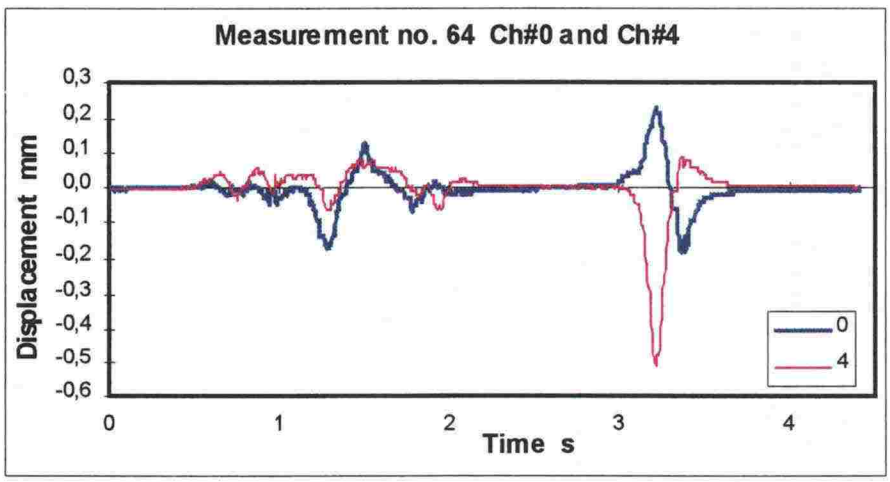

Figure 4.5:6 Example of the lateral displacement of the railhead in rail 1 and 2 relative to the sleeper.

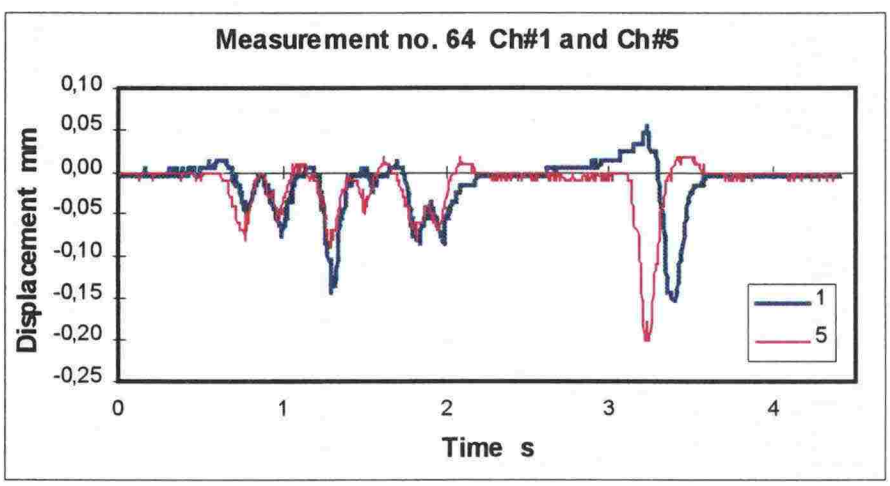

Figure 4.5:7 The lateral displacement of the rail foot in rail 1 and 2 in relation to the sleeper in the example

Vertical displacement of the sleeper

Three transducers measured the vertical displacement of the sleeper relative to the ground. The signals recorded in measurement no. 64 are included in the same Figure 4.5:8. It can be seen from the signals that, among other things, the displacements defer from each other at the ends and in the middle of the sleeper and the impact of the bogies is dominant compared to a single axle. The latter can be seen very clearly in Figure 4.5:9, where is a sample of a recorded vertical wheel load and the corresponding displacement of the sleeper end from measurement no. 40. This applies to 8-axle tank wagons and the displacement, produced by the wagons, is decreased temporarily only while the middle part of the wagon is passing the measurement point.

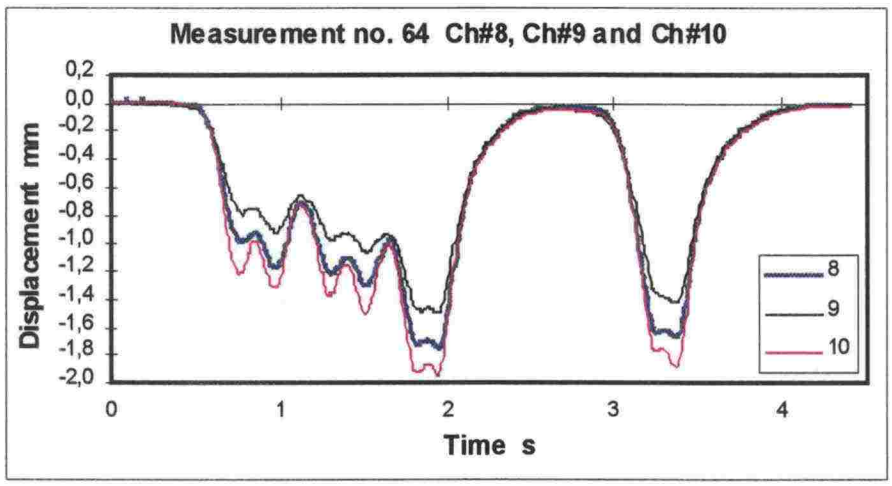

Figure 4.5:8 Sleeper displacements produced by the test train.

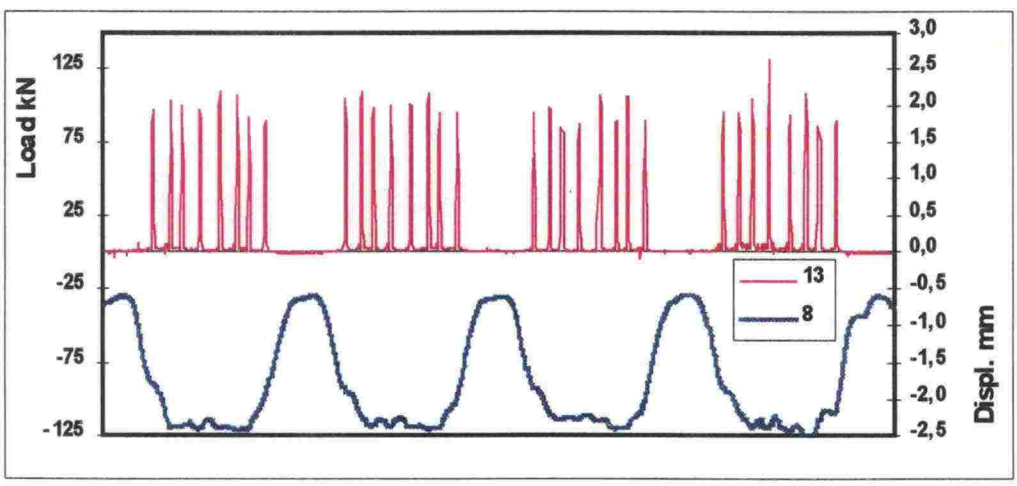

Figure 4.5:9 Vertical displacement of sleeper end under 8-axle tank wagons

When a long train was running through the instrumented site it could be seen that a slowly reversible deformation took place in the soil. The growing trend of displacements shown, for example, in Figure 4.5:10 indicate this. No extended permanent settlement was produced, however. This could have been seen as an offset of the zero level of the measuring amplifiers.

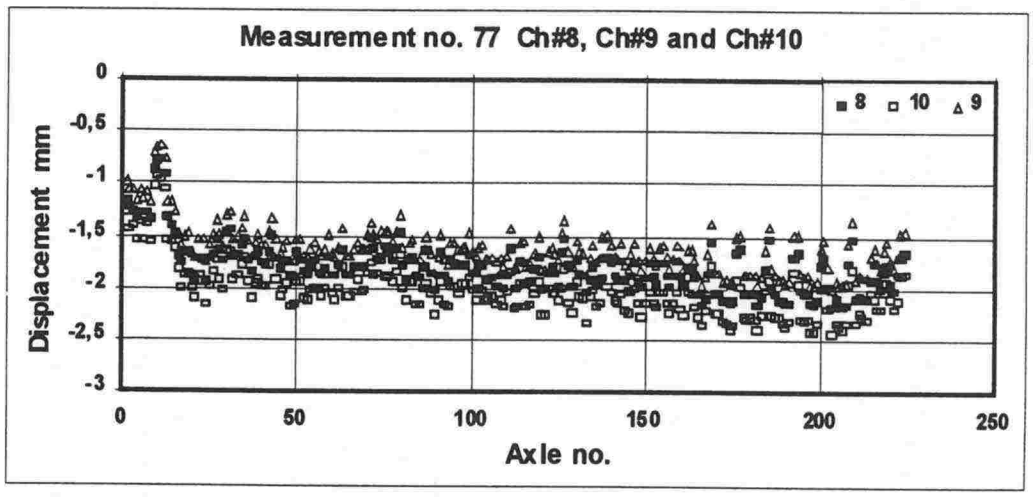

Figure 4.5:10 Example of peak displacements recorded from the sleeper. The tank train consisted of two locomotives and the speed was 59 km/h.

Strains on the sleeper

The signals recorded from the strain gauges installed on the sleeper are shown in Figure 4.5:11. In shape, they mainly resemble the graphs drawn from the sleeper displacements. However, the different bogie axles can be seen more clearly. The highest strain was measured in the middle section of the sleeper.

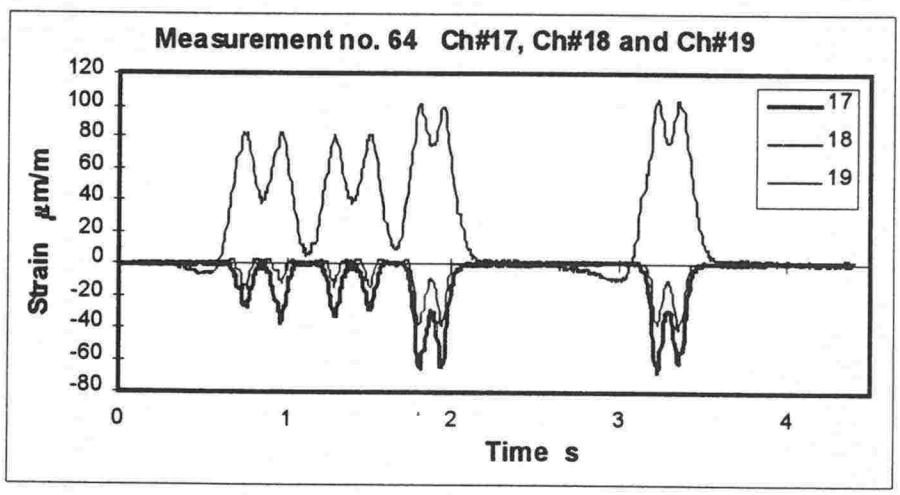

Figure 4.5:11 Example of strains recorded from the sleeper

4.5.2 Measurements from the embankment

Vertical strains

Regarding the embankment the most important task of the analysis work was modelling of the vertical stiffness of the embankment. For this purpose the most important reference quantities were the vertical strains occurring in the structure. These were measured in the embankment at three different depths. There were four parallel strain transducers both on the uppermost and in the intermediate measuring levels, i.e. two under both rails, but on the lowest level there were only two parallel transducers (Figures 2.2:6, 2.2:7 and 2.3:1). The strain signals registered in measurement no. 64 are shown in Figures 4.5:12 – 4.5:14.

With the exception of the ordinary practise in geotechnical engineering, the general rule in all later analyses is that tensile strains and stresses are shown as positive, and compressive strains and stresses are shown as negative. This ensures that the results are compatible with the ones obtained from the rail.

The most consistent results of vertical strain measurements were obtained at a level of -1.3 metres. At the –0.7 metre level one strain transducer has clearly given a smaller strain signal compared to the three others, but owing to the very coarse-grained nature of the material at that installation level – unscreened ballast – the result even in this case should be considered at least satisfactory. At the –2.0 metre level, on the other hand, the signals clearly deviate from each other, although there is no obvious reason for this.

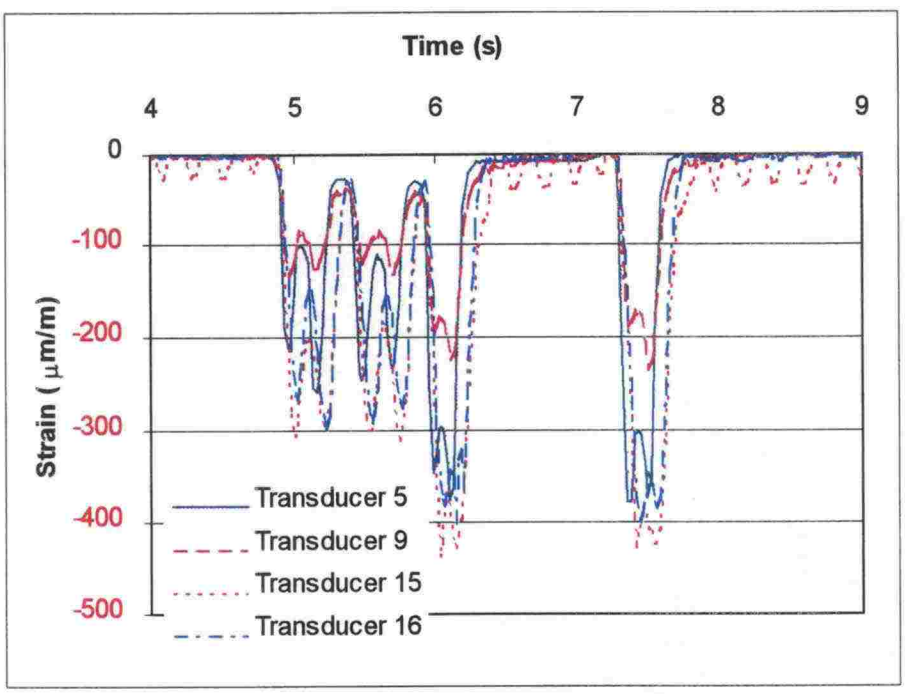

Figure 4.5:12 Vertical strains at the level of – 0.7 m in measurement 64.

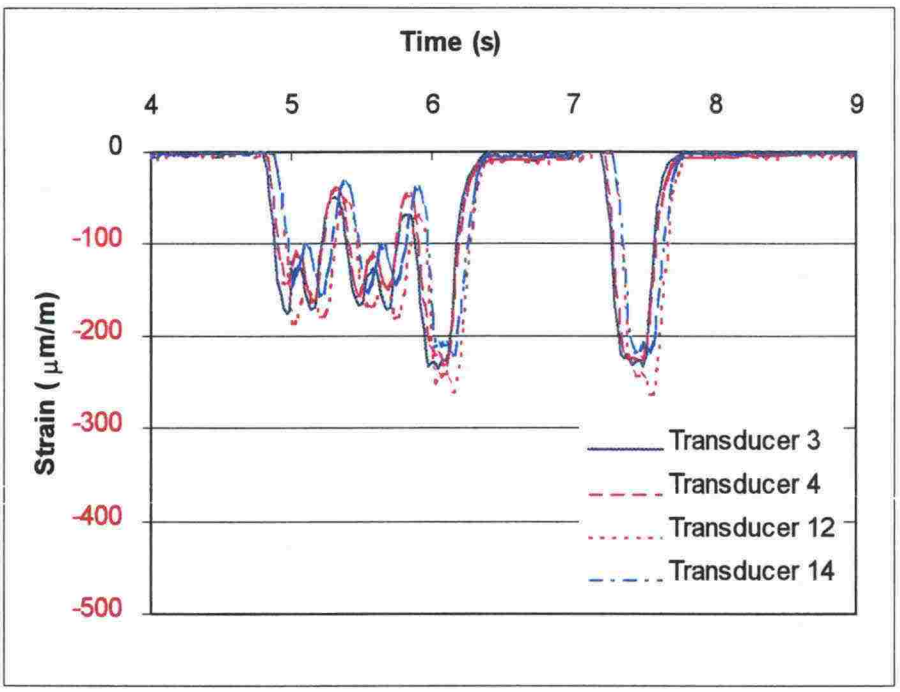

Figure 4.5:13 Vertical strains at the level of – 1.3 m in measurement 64.

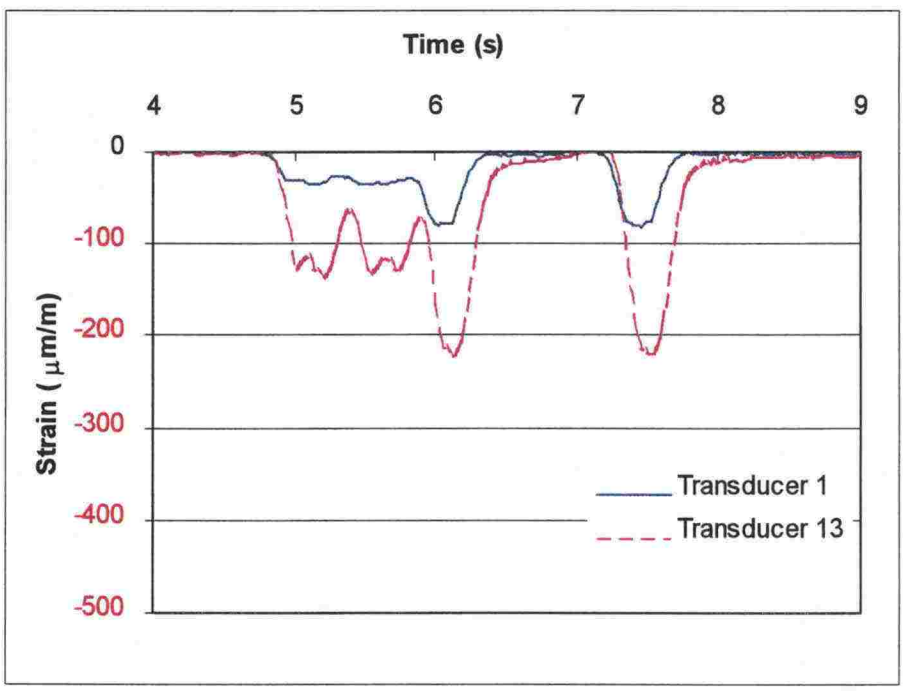

Figure 4.5:14 Vertical strains at the level of – 2.0 m in measurement 64.

Vertical earth pressures

In the modelling of the vertical stiffness of the embankment the measuring transducers for vertical earth pressure had been installed on the two highest instrumentation levels, two on both levels (Figures 2.2:6 ja 2.3:1). They were planned to give supplementary and confirmative information. The earth pressure signals registered in measurement no. 64 are shown in 4.5:15 and 4.5:16.

As can be seen from Figures 4.5:15 and 4.5:16, the measuring instruments installed in the sand layer give a rather similar result. By contrast, the deviation of the parallel measuring instruments installed in ballast is large. The reason for this is most obviously the very coarse grained nature of the material. The largest grains in the ballast are in fact larger than the diameter of the earth pressure transducer.

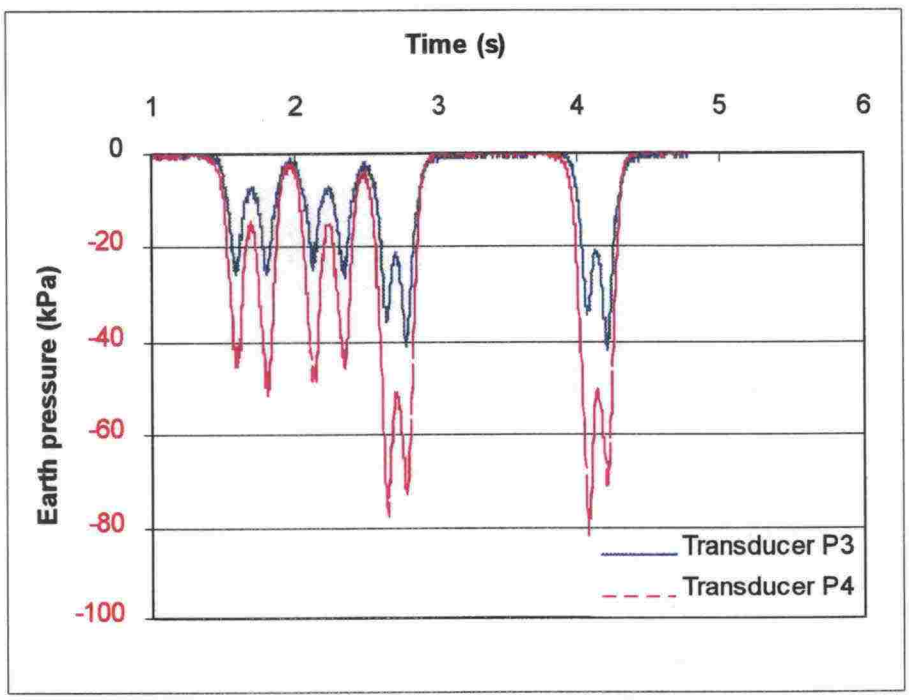

Figure 4.5:15 Vertical earth pressures at the level of – 0.7 m in measurement 64.

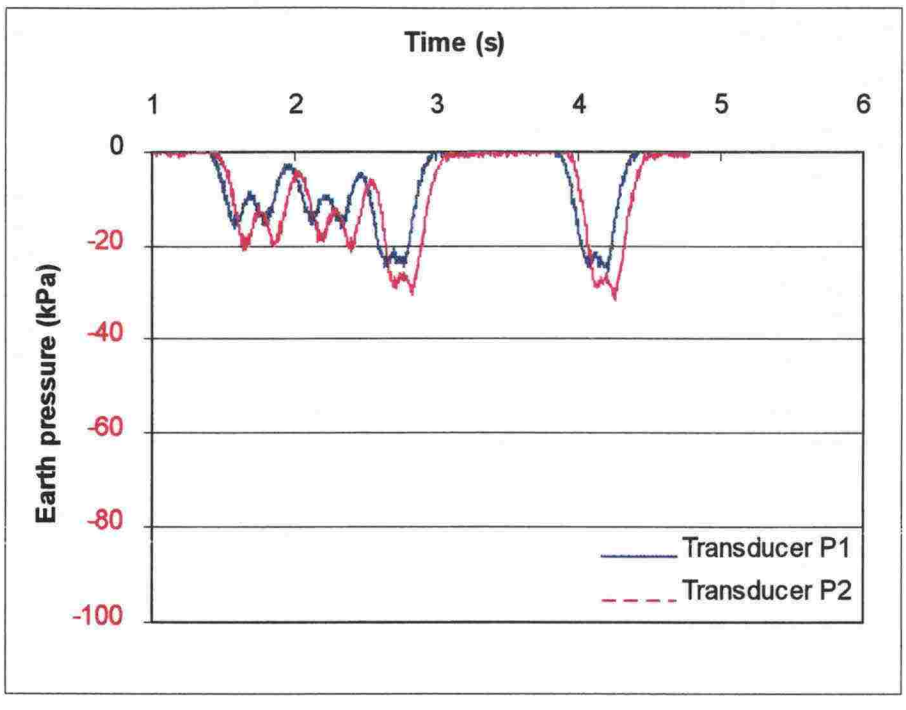

Figure 4.5:16 Vertical earth pressures at the level of – 1.3 m in measurement 64.

Lateral strains

As stated above in chapter 2.3.3, the measuring arrangements for recording of the lateral strains should be considered somewhat experimental. One of the main objectives of these measurements was to obtain experience on the applicability of the instrument type used to the measurement of lateral strain in view of possible later, more detailed, investigations of the adequacy of the embankment width. The measuring signals of the lateral strain transducers in measurement no. 64 are shown in Figures 4.5:17 and 4.5:18.

In regard to the strain transducers installed in the ballast at a level of – 0.7 metres the results of the parallel transducers also in this case are, as was anticipated, rather divergent. The measuring signals of both transducers are characterised by the fact that the measured lateral strains have not recovered between the successive axle passages as much as the vertical strain recorded at the same level (Figure 4.5:12).

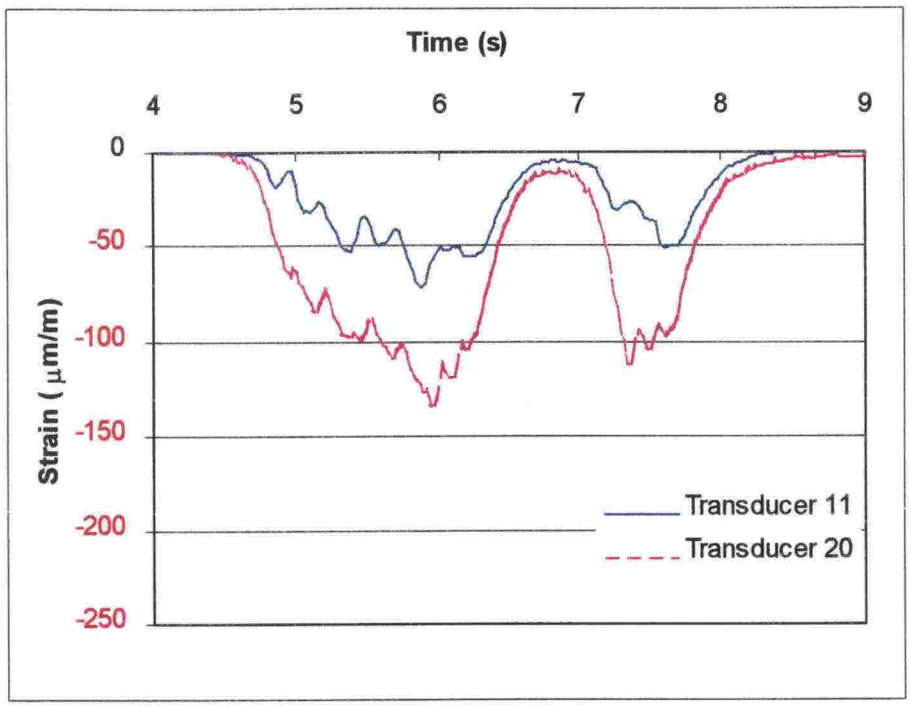

Figure 4.5:17 Lateral strains at a level of – 0.7 m in measurement 64.

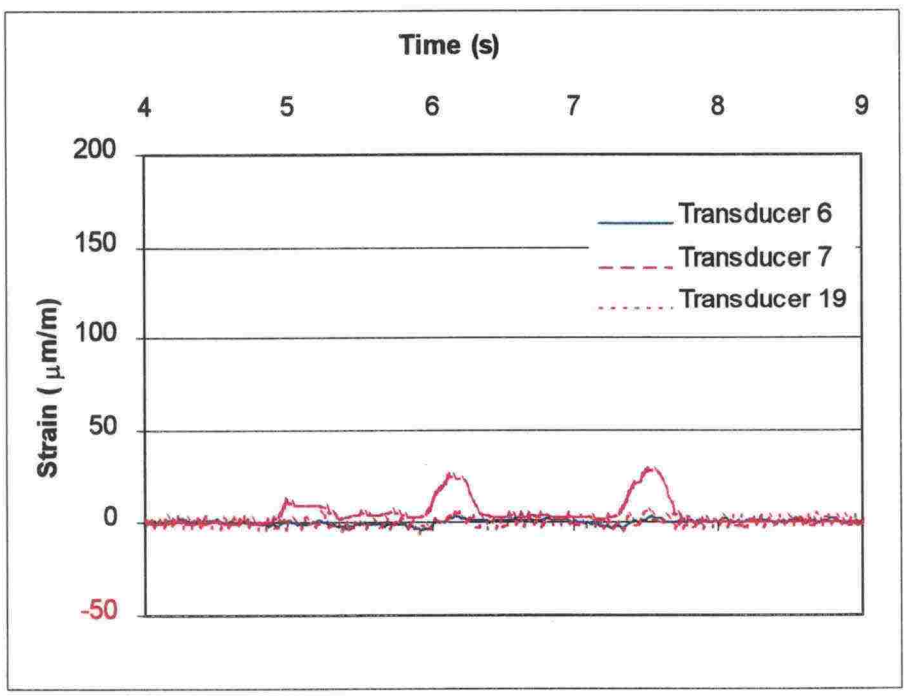

Figure 4.5:18 Lateral strains at a level of – 1.3 m in measurement 64.

The results of the lateral strain measurements at a depth of –1.3 metres appear to clearly depend on under which rail the measurement transducer is placed. With the transducers installed under the outermost rail – transducers no. 6 and 19 – the measured lateral strains seem to be very small, but with the transducer installed under the innermost rail – transducer no. 7 – clearly detectable (Figure 4.5:18).

With the measuring signal registered from the strain transducer under the innermost rail it is especially noteworthy that, unlike with all the other strain measurements, the measured strain is not compressive but an increase in distance of the measuring range of the transducer is observed. In a material which due to its granular nature is not able to tolerate tension, such cyclic tensile strains cause an apparent risk of permanent deformations occurring in the embankment material. As the parallel transducer of the transducers in question – transducers no. 18 in Figure 2.2:6 – had moved outside the measuring range already before the monitoring period owing to the excessive lengthening of the transducer, this observation could also indicate accumulation of a cumulative permanent deformation caused by the effect of repeated tensile strain pulses. In addition to the type of embankment material, the embankment width and the size of the axle load most obviously have a decisive effect on this.

5. MECHANICAL BEHAVIOUR OF SUPERSTRUCTURE

5.1 Rail stresses

One basic idea of the rail instrumentation was that the most dominant stress would be found on the lower surface of the rail foot caused by bending. The strain due to the bending moment was measured from both rails by a strain gauge bridge. Corresponding stress values can be calculated from the measured strains in case the elastic modulus of the rail material is known. Figure 5.1:1 shows some of the stress values calculated from the maximum strains versus the associated vertical wheel load recorded by crossing of different types of trains. It should be noted that usually a minor part of the bending moment comes from wheels of adjacent axles. Figure shows that the bending stresses seem to remain under the level of 80 MPa in case the impacts of wheel flats are ignored. A value of 210,000 MPa for the elastic modulus has been used in the calculations.

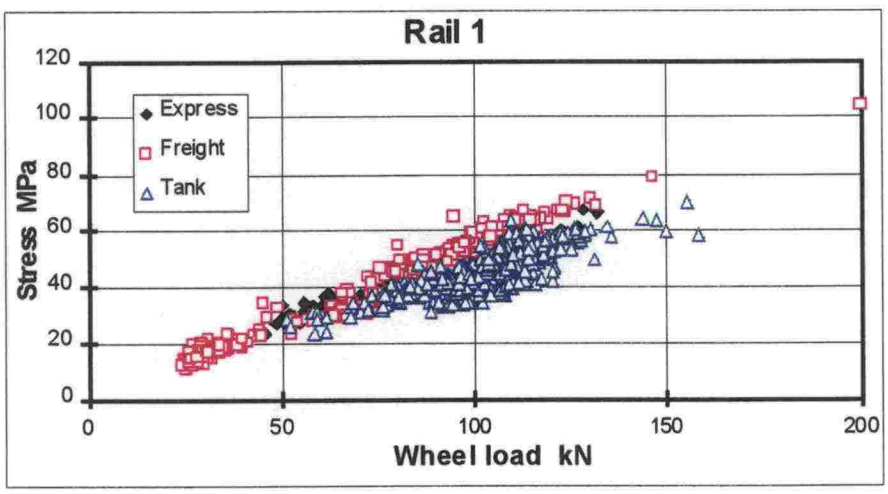

Figure 5.1:1 Maximum values of bending stress on the lower surface of the rail caused by different types of trains.

The wheel sets of the test train appeared to be in good condition and the associated stresses can be considered as a reference case. In this respect, the measurement results in Figure 5.1:2 have been presented as the distribution of peak stresses. The corresponding distribution of vertical dynamic wheel loads is shown in Figure 5.1:3. The average of the measured static wheel loads of the test train came out as 122.7 kN (compare with Table 4.5:1).

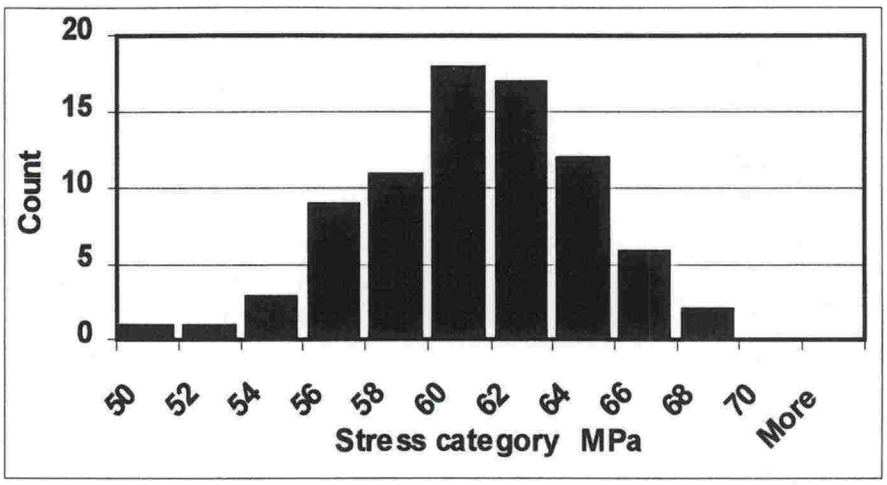

Figure 5.1:2 The distribution of the peak stresses caused by the wagon in the test train. Their average is 59.4 MPa and the standard deviation 6.0%.

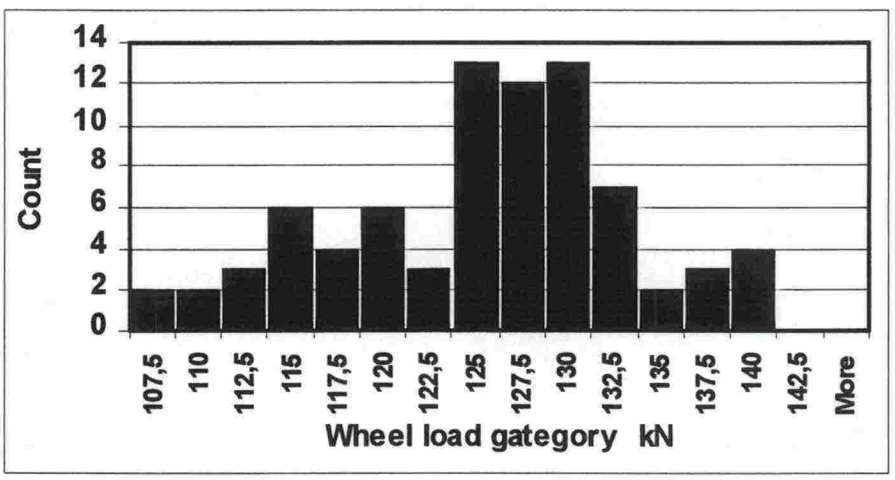

Figure 5.1:3 The distribution of the dynamic vertical wheel loads caused by the wagon in the test train. These were on average 124.3kN and the standard deviation was 6.4%.

A couple of examples of the distribution of vertical wheel loads caused by tank wagons are shown in Figures 5.1:4 and 5.1:5. On the basis of these, the magnitude of the expected maximum loads can be estimated using the valid axle loads.

Based on auditory perception, it can be stated that there were often wheel flats, especially in freight wagons. Although the impact of a wheel flat occurred rather rarely in the middle of the instrumented sleeper spacing, some cases were in fact recorded. This kind of impact can be seen in Figure 5.1:6, where the peak value of 265 kN was recorded for the vertical load. The magnitude of this almost corresponds to the maximum output voltage of the amplifier used in the monitoring, but the peak does not seem to be cut. A peak strain of 484 μm/m was measured from the lower surface of the rail, which gives a calculated stress of 102 MPa. The inertia of the structure has most likely reduced the rail deflection under the impact loading.

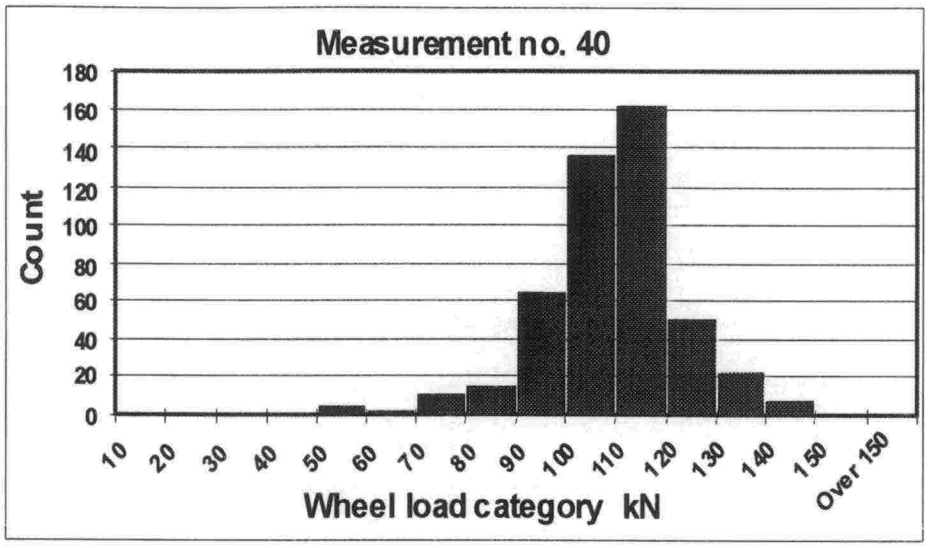

Figure 5.1:4 A distribution of measured wheel loads, with an average of 99.5 kN and a standard deviation of 14.5 kN. Assuming normal distribution, 99.7% of these are expected to be below 143.0 kN, which is their average plus three times the standard deviation.

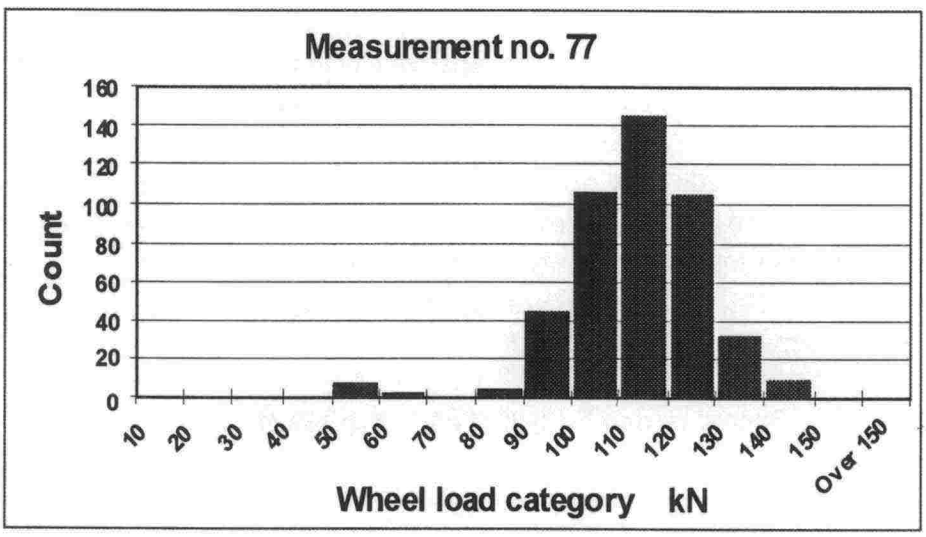

Figure 5.1:5 Assuming normal distribution, 99.7% of the above wheel loads are expected to be below 144.3 kN. The average of these wheel loads is 103.8 kN and the standard deviation 13.5 kN.

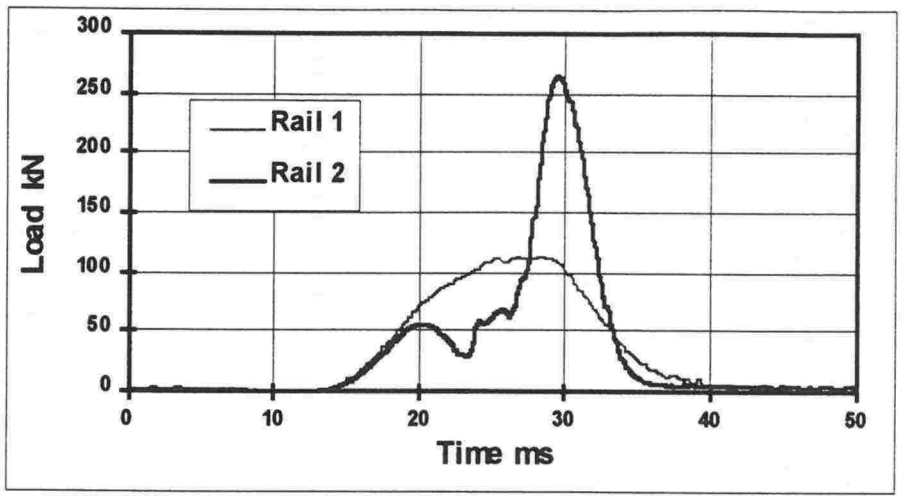

Figure 5.1:6 Impact of a wheel flat in the middle of the instrumented sleeper spacing on rail 2. Since the speed of the freight train was about 15m/s, it would have travelled 0.15 metres in ten milliseconds. The figure also shows the wheel load recorded from the other wheel of the same axle on rail 1.

The strain gauges on the lower surface of the rails were also used in monitoring changes in thermal stresses. Temperature adjusted strain gauges adapted to steel do not indicate strain when mounted on a rail, which is free to expand with temperature. Because the thermal expansion of the rails was restrained, the corresponding changes in thermal stresses could be calculated from the zero level offsets of the strain gauge bridges. The rail temperature was monitored a few times a day by a contact thermometer. The results are shown in Figure 5.1:7. The zero level of the stress is fixed at 17°C, which was said to be the neutral temperature of the track.

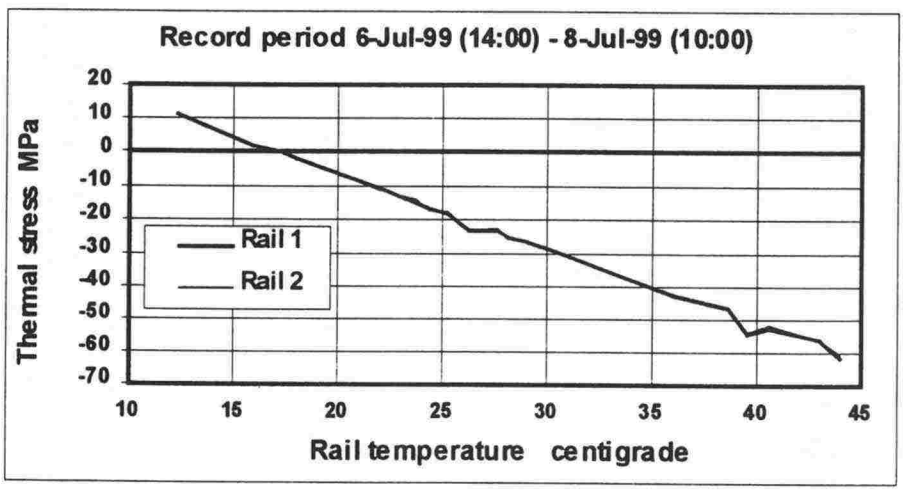

Figure 5.1:7 Thermal stresses calculated from the zero level offsets of the strain gauge bridges as a function of rail temperature. The neutral temperature of the track is assumed to be 17°C.

5.2 Behaviour of rail pads

It is difficult to determine the stresses of rail pads in any other way than by measuring their dynamic compression in terms of the vertical displacement between the rail and the sleeper. The displacement measurement was improved by using two transducers per rail mounted on both sides near the edges of the rail foot. Thus, any possible roll of the rail could also be recorded. The tilt of the rail foot means that the compression of the pad is not evenly distributed. The peak values of the aforementioned displacements recorded in measurement no. 40 are shown in Figure 5.2:1. They are presented as functions of associated vertical wheel loads. The speed of the freight train, consisting mainly of tank wagons, was recorded to vary from 57 to 62 km/h during the measurement. Empty wagons were also included, so that the range of recorded wheel loads is fairly representative in this case. The compression of the rail pad was obviously higher under the inner edge of the feet, so the rails were leaning inwards. Furthermore, the rail pad under rail 1 as a whole was obviously compressed more than the pad under rail 2.

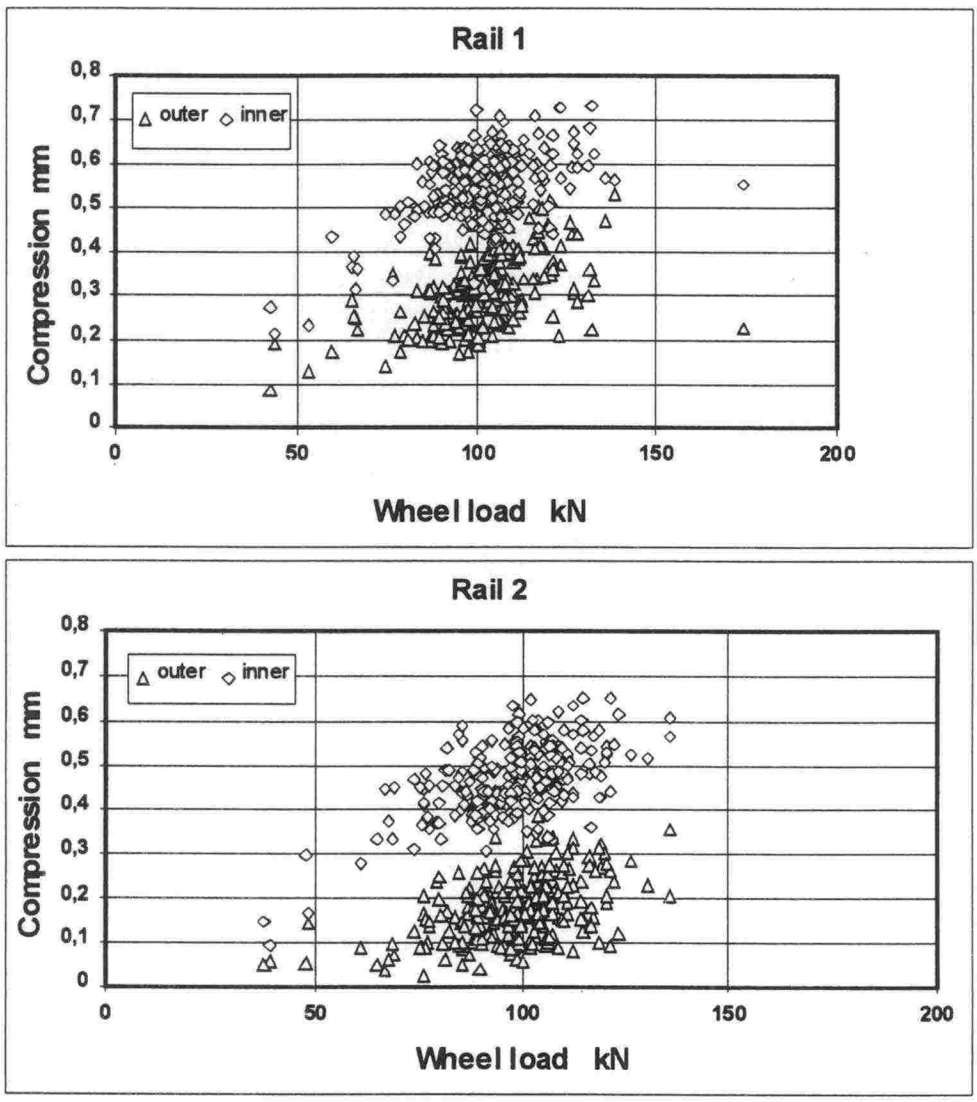

Figure 5.2:1 Peak compressions of the rail pads under the outer and inner edge of the rail foot in measurement no. 40.

5.3 Stresses of rail fastenings

Data on stresses in the rail fastenings was also obtained from these measurements. Steel spring attachments integrated into the sleeper keep the rail in place in the lateral direction through the insulators. They have to carry the lateral component of the wheel loads exerted by the rails. Pair sets of wheel load components recorded for different types of trains are shown in Figure 5.3:1. As the instrumented section was on a straight track, the magnitude of the lateral component, which was stressing rail fastenings, remained lower than those recorded e.g. in curves or switches in some other cases. The positive signal corresponds to an inward load. It can be seen from the figure that the highest lateral loads tend to force the rail outward from the track.

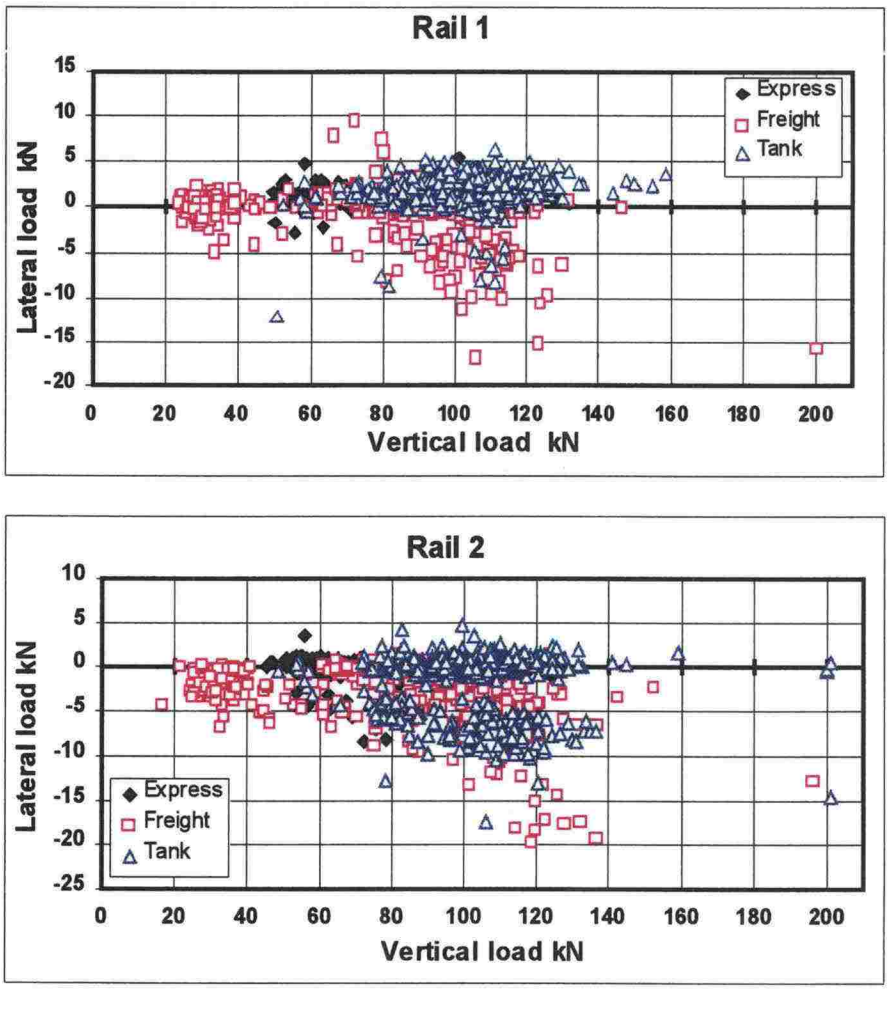

Figure 5.3:1 Pair sets of wheel load components measured for different types of trains.

An idea of the stresses on Pandrol clips is obtained by evaluating the vertical movement of the rail at the edges of the foot. When the rail moves towards the sleeper the spring tension decreases. Likewise, when the rail moves from the rest position in the opposite direction, the tension increases. The magnitude and number of tension ranges occurred is a fundamental factor contributing to spring fatigue. In addition to the compression of a rail pad, the displacements shown in Figure 5.2:1 also represent, with adequate accuracy, the displacement of the clip end from the rest position towards the sleeper. An evaluation of the measurement data showed that the rail foot moved outwards from the sleeper. The maximum displacement was 0.25 mm at the inner edge and 0.20 mm at the outer edge of the foot in both rails. Based on the measurement data of rail 1, the displacement range of the clip end is 1.0 mm on the inner edge and 0.75 mm on the outer edge of the foot. For rail 2, these values are 0.90 mm and 0.55 mm. It should be noted that the above displacement ranges cover even the largest single peak values recorded in these measurements and most of the tension ranges in clips are small. In laboratory tests on rail fastenings, clips have experienced millions of load cycles with a displacement range of 1 – 1.5 mm showing no sign of fatigue.

5.4 Sleeper

The main mechanical input to a sleeper is bending caused by vertical loads and the bearing pressure of the ballast. When the sleeper ends are supported properly underneath, there should not be any bending moment in the middle part of the sleeper. As shown in Figure 4.5:8, the displacements measured at the ends of the sleeper are considerably larger than those in the middle section. This means that the sleeper is bent and there will be tension on the upper surface of the middle part. Strain measurement results agree with this conclusion, as can be seen in Figure 5.4:1. Furthermore, as seen in the figure, freight trains stress the sleeper most. Markers representing tank wagons and express trains are located on a level of their own not to mention wheel flat axles, which jump out. Considerably smaller values are obtained from the strain gauges placed near the upper edge of the sleeper side underneath the rails. These gauges indicated compression. Roughly generalised, the strain level under rail 1 was one half and under rail 2 one third of that in the middle of the sleeper.

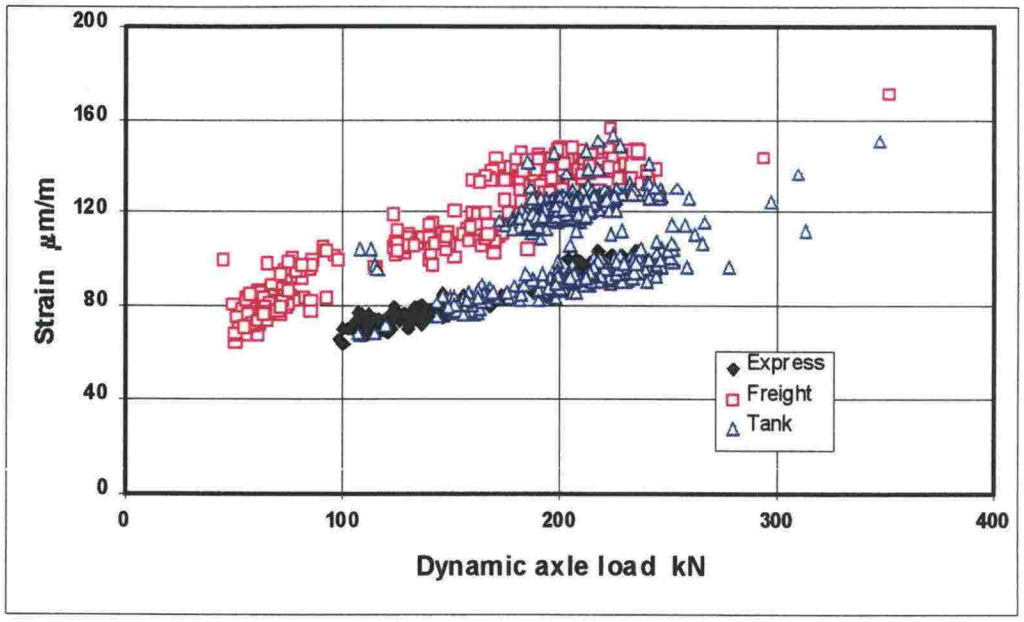

Figure 5.4:1 Maximum strain values in the middle section of the instrumented sleeper due to different types of trains.

5.5 Characteristic length of the track

The deflection and the bending moment of a rail can be calculated with the aid of influence lines. This method was applied first by Zimmermann at the end of the 19th century. A couple of decades earlier Winkler had presented a simplified assumption that the displacement z of an elastic foundation is everywhere directly proportional to the acting pressure load p as follows:

$$p = C z, \tag{5.5.1}$$

where the coefficient C is called the modulus of foundation, bearing coefficient or track modulus depending upon the context. Zimmermann reduced the rail structure to a continuous beam resting on an elastic foundation loaded by a single force. For example, in a certain point of the beam the magnitude of a bending moment produced by an arbitrary wheel load combination can be calculated following the principle of superposition using an influence line derived for the case. Usually influence line is presented as a function of a dimensionless distance from the point under consideration, which serves as the origin. Most of the bending moment is produced by the wheel load applied at the point of origin, where the function of influence line reaches a value of one. The wheel loads of the adjacent axles exert their own effect, which can increase or decrease the moment, and the magnitude depends on how far the wheel is from the point of origin. The distance is made dimensionless by dividing the metric value by the so-called characteristic length of the track. The length depends on the characteristics of all the structural components underlying the rail (rail pad, sleeper, ballast, etc.). The

bending moment of the rail was not directly among the recorded quantities in these measurements. It was replaced by the strain on the lower surface of the rail. By utilising the known relations between the strain, stress and rail cross-section, the following formula is obtained

$$L = 4 E W \varepsilon / \Sigma Q_i \mu(\xi_i), \qquad (5.5:2)$$

which connects the characteristic length L and the strain ε. The following symbols have been used in the formula:

E = elastic modulus of the rail material

W = moment of resistance with respect to the rail foot

Q_i = wheel load i

$\mu(\xi_i)$ = value of the function of influence line at distance ξ_i

$\xi_i = x_i / L$ = dimensionless distance of wheel load Q_i from the origin

x_i = metric distance of wheel load Q_i from the origin

The function of the influence line is of the form

$$\mu(\xi) = (\pm \sin \xi + \cos \xi)/e^{\pm \xi} \qquad (5.5:3)$$

In Figure 5.5:1 there are shown values of the characteristic length, which have been obtained by using each vertical wheel load and associated strain value due to the test train running at different speeds. L-values have been calculated with the aid of an iterative procedure, taking into account the effect of the nearest adjacent wheel. No specific dependency on speed is in evidence. The characteristic length at the instrumented track section seems to be about 0.85 metres. By means of the characteristic length, the beam on an elastic foundation loaded by a single force can be reduced to a simple supported beam with two bearings having the span L and the force acting in the middle. The maximum bending stress is equal in both cases.

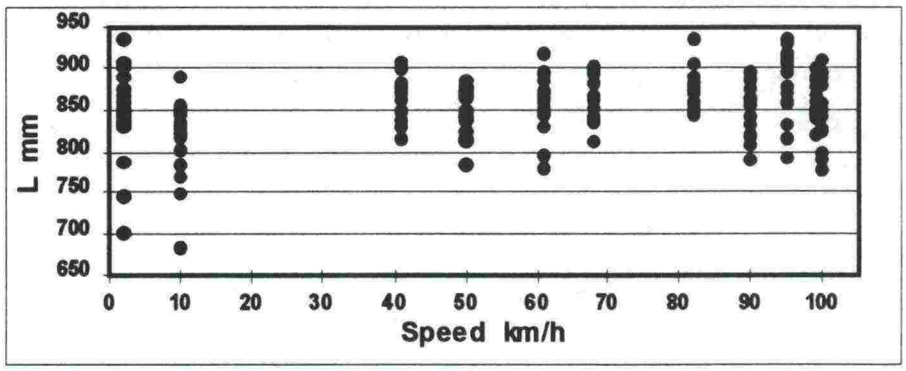

Figure 5.5:1 Calculated values for the characteristic length L of the track represented as a function of the speed of the test train.

Strain measurement results agree well with the strains calculated by the above simple mathematical model. Figure 5.5:2 shows the recorded strain values of rail 1 in measurement no. 64 and the strain graphs calculated with the aid of the measured wheel loads and influence line functions while the characteristic length is the parameter. The influence line of strain for each wheel has been first created into its own local co-ordinate system. Then they have been combined by superposition, so that each wheel is placed at the appropriate distance from the origin of an axis, whose original argument, time, has been multiplied by the speed of the test train. It can be seen that too high strains arise when the value of parameter L is 1.0 m and too small ones with a value of 0.7 m. Using a value of 0.85 m for the characteristic length leads much closer to the measured values.

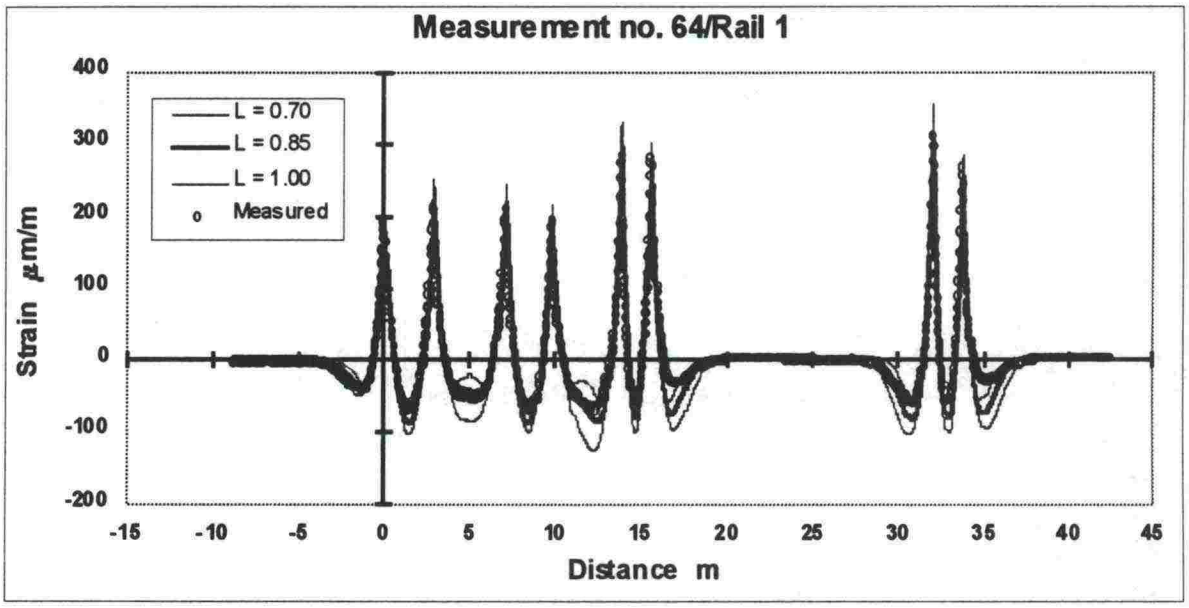

Figure 5.5:2 Example of measured strains compared to theoretical ones.

Presuming that the value of the characteristic length is e.g. 0.85 m, a same kind of comparison can be made between calculated and measured values of the vertical displacement of rails. The function of the corresponding influence line takes the form of

$$\eta(\xi) = -(\pm \sin \xi + \cos \xi) / e^{\pm \xi}. \qquad (5.5:4)$$

The displacement graph can be composed in the same way as above for the strain. The contribution of each wheel z_i to the displacement is obtained using the formula

$$z_i(\xi) = Q_i \, \eta(\xi) / (2bC_R L). \qquad (5.5:5)$$

In the formula, the coefficient C_R is a reduced track modulus, including the elasticity of the rail pad. Assuming that the ballast pressure is distributed over the whole surface of the sleeper-bottom, the width b is obtained by dividing half of this area by the sleeper spacing.

In Figure 5.5:3, the measured values of the rail displacement have been obtained by summarising the compression of the rail pad and the average of the vertical displacement of the middle section of the sleeper and the sleeper end in the side of rail 2. This is assumed to represent with sufficient accuracy the vertical displacement of the half of the sleeper under rail 2. The portion of the rail pad in the total displacement was 10 – 15 % in this case. The graphs have been constructed with the aid of the influence line functions calculated by using measured wheel load values and the reduced track modulus as the parameter. The graph obtained with a value of 0.075 for the parameter appears to agree best with the measured displacements.

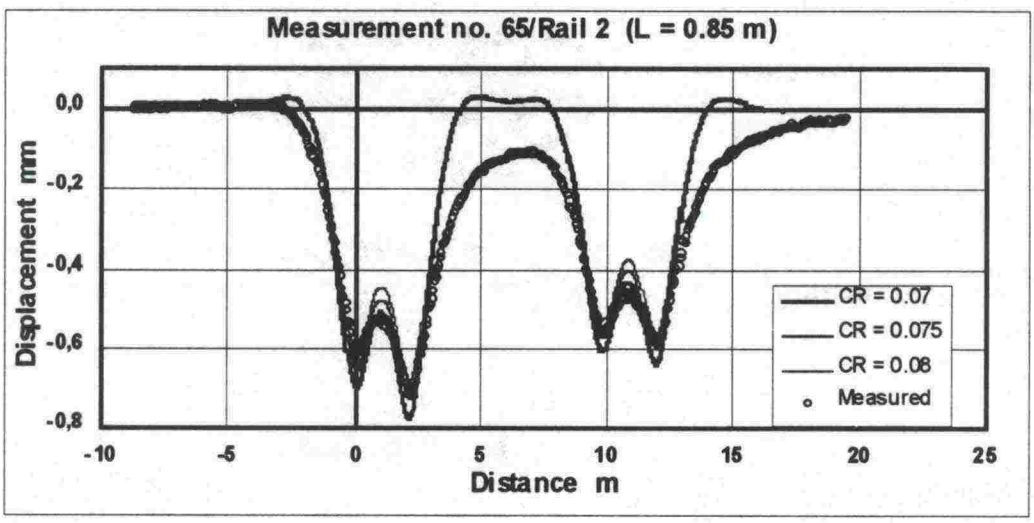

Figure 5.5:3 Example of measured and theoretical vertical displacements of a rail. The measured values were obtained under a TTV 16-type maintenance vehicle crossing the instrumented section at a speed of 84.3 km/h.

5.6 Distribution of load on consecutive sleepers

The distribution of a single wheel load on adjacent sleepers cannot be seen directly from the measurement data. For example, the compression of the rail pad could in theory be used as a load indicator. This is, however, complicated by the fact that in practice the load always originates from more than just one wheel. When searching a case closest to the condition of a single wheel load, comes to mind a 2-axle wagon at the end of a train. In Figure 5.6:1, there is an example of such a case where the vertical displacement between the rail and the sleeper has been recorded. The time axis has been changed to distance as above by multiplying the values of the argument by the train speed. In unloaded condition before the train arrived, the signals have been on the zero level. It can be seen from the graphs that the average compression of the rail pad has been about 0.45 mm when the axle has been on the spot. At a distance of one sleeper spacing it has decreased by about 50 %, but at a distance of two times sleeper spacing there is still 20 % left, after which it finally returns to a standstill at -0.05 mm. This behaviour might be explained by the non-linearity and viscoelasticity in the characteristics of the rail pad and also the soil, which complicates the interpretation of measurement data.

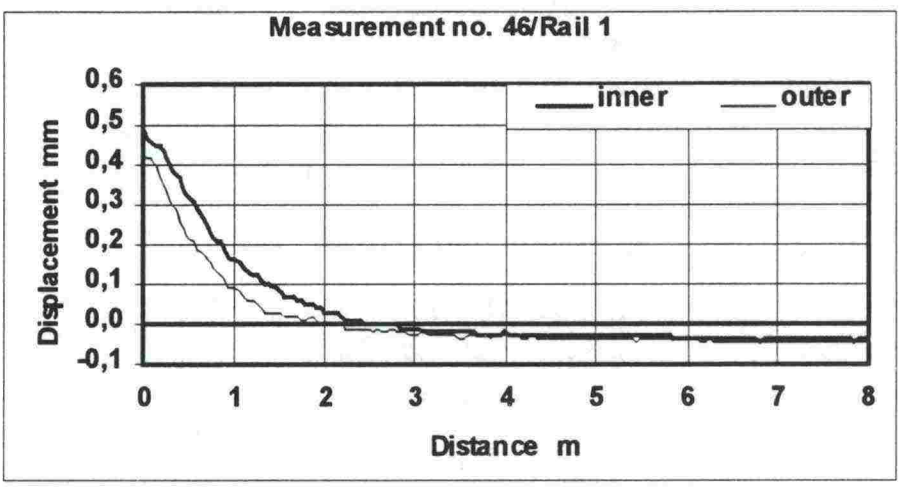

Figure 5.6:1 Example of the reversion of displacement between rail and sleeper after the last axle of the train.

6. MODELLING OF RAILWAY EMBANKMENT USING A MULTI LAYER LINEAR ELASTIC PROGRAM

6.1 Introduction

The modelling of railway embankment using multi layer linear elastic programs has given good results elsewhere in the world (Selig & Waters 1994). The use of these programs requires almost fully elastic behaviour of the embankment under repeated loads. In some earlier studies it has been observed that even a few hundreds of loading cycles is enough to bring about a situation where the embankment materials are behaving almost fully elastically. On the other hand, to reach a constant value of resilient modulus in a cyclic loading requires a few thousand load repetitions (Selig & Waters 1994). Repeated loading of embankment materials and determination of the resilient modulus have been covered more closely in the literature part of this study (Kolisoja et al. 1999).

A few multi layer liner elastic programs have been developed, some of which are intended especially for the modelling of a railway embankment and others correspondingly for the modelling of a road embankment. The greatest difference is how commercial the programs are. Programs for the modelling of railway embankments are usually non-commercial, being developed for the researchers' own use, whereas some of the programs for the modelling of road embankments are commercial and quite easily accessible. These programs share one feature, however, i.e. the assumed behaviour of soil layers to be modelled is in accordance with the linear elastic theory. Bousinessq presented the stress distribution of a spot loading in an elastic half space in 1885. Many of the design programs for road structures use Bousinessq's stress distribution on a circular loading, while the programs for railway embankments use Love's (1928) stress distribution. Love's stress distribution theory has been further developed from Bousinessq's theory and it can take a quadrangular loading into account. The shape of the loaded area is, however, only of practical importance for the ballast, because deeper in the embankment the loads become in any case more evenly distributed.

The commercial program known as BISAR for analysing road pavement structures has been used in this study. It is a multi layer linear elastic program developed by the oil company SHELL. The reliability of the program was checked with another multi layer linear elastic program (NOAH) and in applicable parts also by analytic solutions and numerical analyses (FEM). If the load is similar, a soil material behaves the same way irrespective of the use of the embankment. This enables us to use a program developed for analysing road structures in the analysis of track structures.

6.2 Coordinates of the linear elastic layer model

Multi layer linear elastic programs are based on the assumption of a semi-infinite elastic soil mass, where a rotation symmetrical loading is placed on the ground surface (Figure

6.2:1). Idealising the railway embankment in the lateral direction to extremely extensive layers does not take into account the existence of the embankment edge.

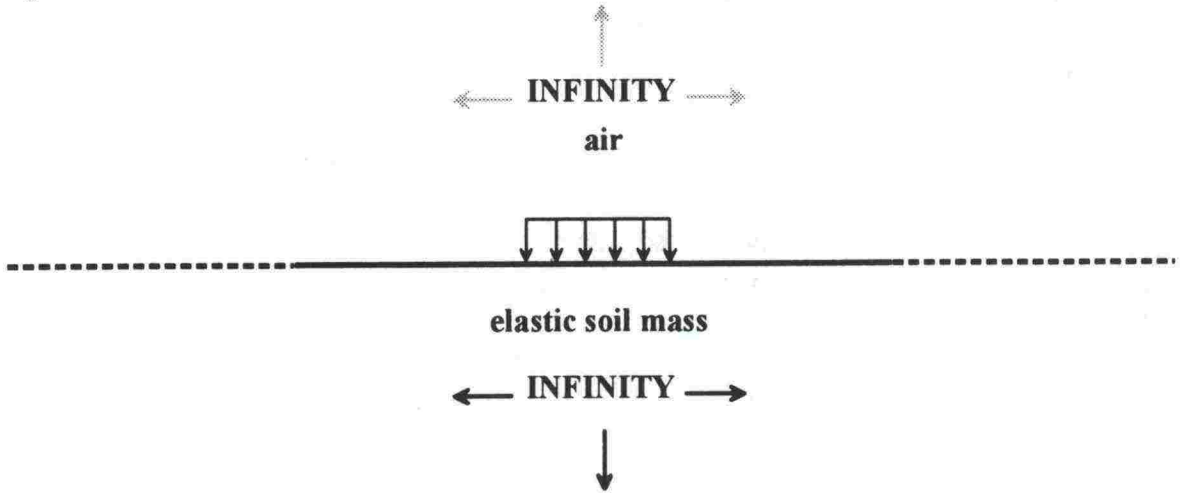

Figure 6.2:1 Elastic semi-infinity with a circular loading.

A cylinder coordinate system (Figure 6.2:2b) is used as the local calculation coordinate system. Hence, the loading should be given as a circular load. For the user, BISAR is shown in a Cartesian coordinate system (Figure 6.2:2a).

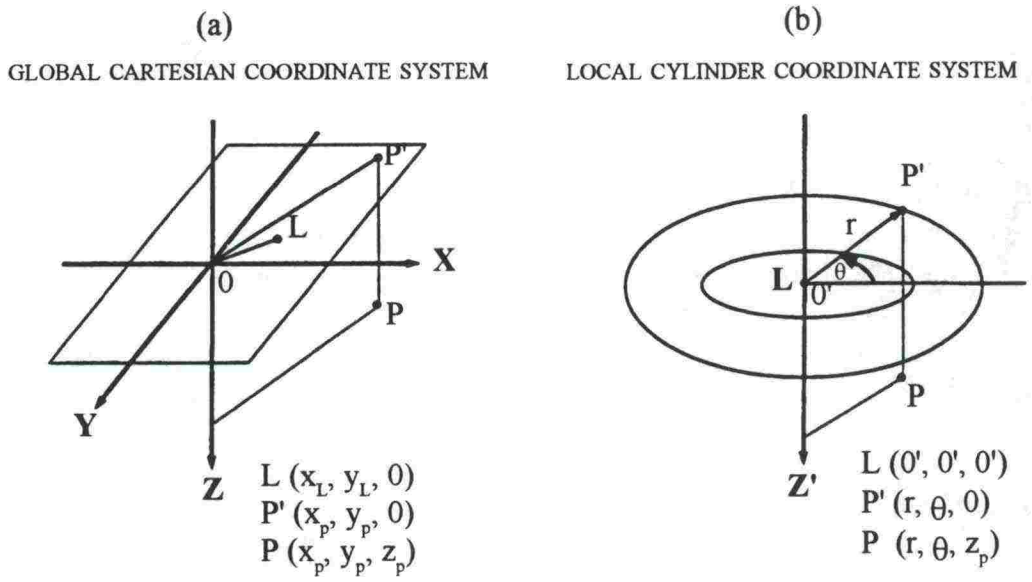

Figure 6.2:2 The connection of (a) global cartesian and (b) local cylinder coordinate system (BISAR 1995).

The place is defined in a cartesian coordinate system by the values of x, y and z. Correspondingly, the place in a cylinder coordinate system is defined by z, θ and r. The explanations of the notations are given in Figure 6.2:2. The connection between the cartesian and cylinder coordinate systems is depicted by equations 6.2:1 – 6.2:3.

$$x = r\cos\theta \tag{6.2:1}$$

$$y = r\sin\theta \tag{6.2:2}$$

$$z = z \tag{6.2:3}$$

Equations 6.2:1 and 6.2:2 assume that the zero point of the local cylinder coordinate system is located at the global origin. In another case, the transfer terms x_L and y_L (Figure 6.2:3) from the local coordinate system have to be added to the global coordinate system. In Figure 6.2:2, L stands for the centre of circular loading, P and P' are the coordinates of the studied points, and 0 and 0' are the origins of the global and local coordinate systems. In Figure 6.2:3, the connection of the global and local coordinate systems is presented for the global coordinate system on the X-Y plane and the directions of the tangent and radius for the local cylinder coordinate system.

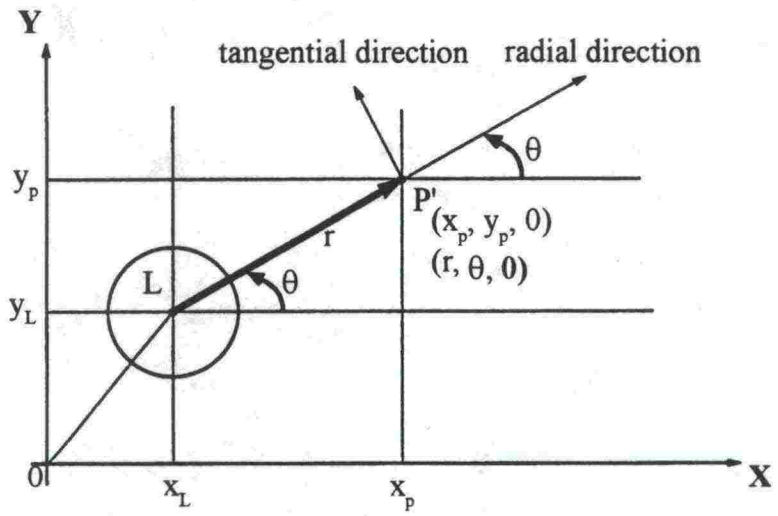

Figure 6.2:3 The connection of the global and local coordinate systems and the direction of the tangent and radius of the local coordinate system (BISAR 1995).

The above-mentioned global and local coordinate systems are independent of a multi layer linear elastic program. However, the positive directions of the global coordinate system used may vary from one program to another.

6.3 The applied theory

Multi layer linear elastic programs assume the soil mass of the layer to be homogenous and in most cases isotropic. In some programs, such as NOAH, the isotropic layer of the subsoil, i.e. the last layer, can be changed into an anisotropic one. The basic equation of multi layer linear elastic programs can be considered to be the strain function (equation 6.3:1) developed by Burmister in 1943, by means of which the stresses and displacements in the i^{th} isotropic layer in a multilayered structure can be calculated. In this case the loading on top of the uppermost layer is a circular load with a radius of a.

$$\phi_i = pa\int_0^\infty \frac{J_0(mr)J_1(ma)}{m}\left[A_i e^{mz} - B_i e^{-mz} + zC_i e^{mz} - zD_i e^{-mz}\right]dm \qquad (6.3:1)$$

The vertical, radial and tangential normal stresses can be defined from the cylinder coordinate system by equations 6.3:2, 6.3:3 and 6.3:4.

$$\sigma_z = pa\int_0^\infty J_0(mr)J_1(ma)[A_i m^2 e^{mz} + B_i m^2 e^{-mz} - C_i m(1-2\nu_i - mz)e^{mz} +$$

$$D_i m(1-2\nu_i + mz)e^{-mz}]dm \qquad (6.3:2)$$

and

$$\sigma_r = -pa\int_0^\infty J_0(mr)J_1(ma)[A_i m^2 e^{mz} + B_i m^2 e^{-mz} + C_i m(1+2\nu_i - mz)e^{mz}$$

$$- D_i m(1+2\nu_i - mz)e^{-mz}]dm + pa\int_0^\infty \frac{J_1(mr)J_1(ma)}{mr}[A_i m^2 e^{mz} +$$

$$B_i m^2 e^{-mz} + C_i m(1+mz)e^{mz} - D_i m(1-mz)e^{-mz}]dm \qquad (6.3:3)$$

as well as

$$\sigma_\theta = -pa\int_0^\infty J_0(mr)J_1(ma)[C_i m e^{mz} - D_i m e^{-mz}]2\nu_i dm$$

$$- pa\int_0^\infty \frac{J_1(mr)J_1(ma)}{mr}[A_i m^2 e^{mz} + B_i m^2 e^{-mz} + C_i m(1+mz)e^{mz}$$

$$- D_i m(1-mz)e^{-mz}]dm \qquad (6.3:4)$$

Shear stress on a curved plane θz in the direction z is defined by equation 6.3:5.

$$\tau_{rz} = -pa\int_0^\infty J_1(mr)J_1(ma)[A_i m^2 e^{mz} - B_i m^2 e^{-mz} - C_i m(2-4\nu_i - mz)e^{mz}$$

$$- D_i m(2-4\nu_i + mz)e^{-mz}]dm \qquad (6.3:5)$$

Displacements can be calculated from equations 6.3:6 and 6.3:7. In this case the vertical displacement is indicated by w

$$w = \frac{1+\nu_i}{E_i} pa\int_0^\infty \frac{J_0(mr)J_1(ma)}{m}[A_i m^2 e^{mz} - B_i m^2 e^{-mz} - C_i m(2-4\nu_i - mz)e^{mz}$$

$$- D_i m(2-4\nu_i + mz)e^{-mz}]dm \qquad (6.3:6)$$

and the displacement in the direction of the radius correspondingly by u.

$$u = -\frac{1+\nu_i}{E_i} pa\int_0^\infty \frac{J_1(mr)J_1(ma)}{m}[A_i m^2 e^{mz} + B_i m^2 e^{-mz} + C_i m(1+mz)e^{mz}$$

$$- D_i m(1-mz)e^{-mz}]dm \qquad (6.3:7)$$

Explanations for the notations in equations 6.3:1 – 6.3:7 are:

a	=	radius of the evenly distributed circular load
p	=	value of vertical stress
r	=	distance in the direction of the radius in the cylinder coordinate system
z	=	depth
σ_z	=	vertical normal stress
σ_r	=	normal stress in the direction of the radius
σ_θ	=	tangential normal stress
τ_{rz}	=	shear stress on the curved plane θz in direction z
w	=	vertical displacement
u	=	displacement in the direction of the radius
E_i	=	Young's modulus of the i^{th} layer
ν_i	=	Poisson's ratio of the i^{th} layer
$A_i \ldots D_i$	=	unknown parameters defined by boundary conditions
J_0	=	Bessels's function of the zeroth degree
J_1	=	Bessels's function of the first degree
m	=	integration parameter

6.4 Definition of loading in the calculation model

The calculation model in the BISAR program does not take into account anything else in the track structure apart from the substructure and the ballast. Loading is given as an evenly distributed pressure affecting on a specified area at the bottom level of the sleeper or correspondingly as a force and an area. Consequently, the bottom of the sleeper is the zero level of the calculation, i.e. the zero level of the calculation lies 225 mm downwards from the height line of the track. Thus, the calculation does not take into account that part of the ballast lying above the bottom of the sleeper.

The effective area of the sleeper end is defined for the BISAR calculation by equation 6.4:1.

$$A_b = (l - m)b / 2 \qquad (6.4:1)$$

where

A_b	=	effective area of the sleeper end

b = width of the sleeper

l = length of the sleeper

m = length of the area in the middle part of the sleeper where no contact pressure is assumed to exist between the bottom of the sleeper and the ballast

In this study, the distance m in equation 6.4:1 is assumed to be 500 mm. Thus, the width of the sleeper multiplied by 500 mm has been reduced from the total area of the sleeper. In many cases m has been assumed to be 600 mm, but the difference between these assumptions with regard to the distribution of stresses and strains deeper inside the embankment is very small.

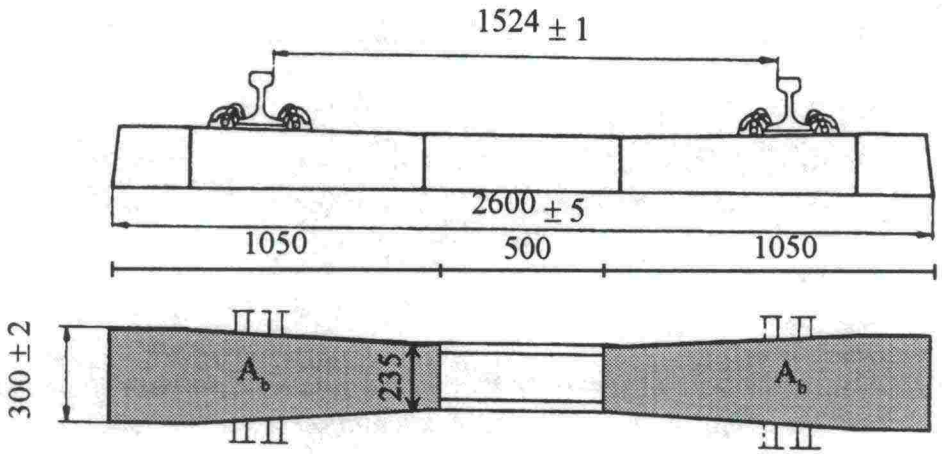

Figure 6.4:1 The effective area of a BP 89 sleeper (Puikkonen 1989 and Gåsemyr 1996).

The loading in the BISAR program is given as a circular load. It is possible to enter a maximum of 10 simultaneous circular loads. The linear elastic theory enables a superposition of the stresses and strains to be made. Consequently, the use of a larger number of circular loads is also possible by summing up of the results e.g. in a spreadsheet program. In the modelling exercise of the present project a decision was made to use two circular loads to correspond to an effective area of one sleeper end A_b (Figure 6.4:2).

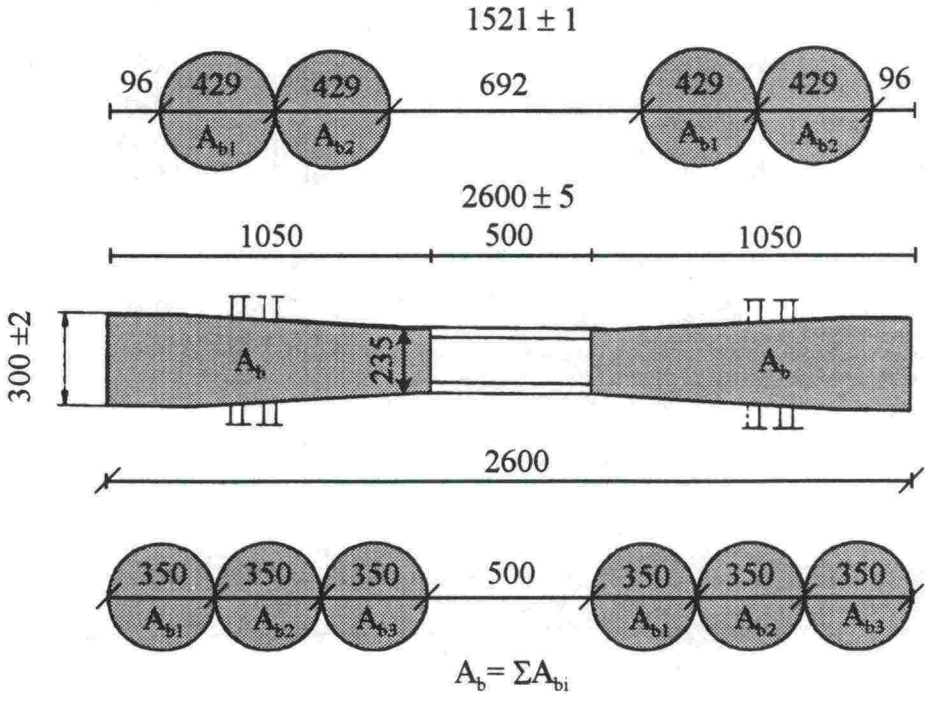

Figure 6.4:2 Modelling of the effective area of a sleeper by different amounts of circular loads and the configuration used in the calculation (the upper one).

At the beginning of the calculation, the circular load configurations were varied. The result obtained with two circular loads proved out to be in practice the same at the depth of the first strain gauges as the results obtained with three circular loads.

According to Riessberger (1998), the wheel load can be assumed to be distributed over consecutive sleepers in the longitudinal direction of the track, as shown in Figure 6.4:3. In Figure 6.4:3, the wheel load is located over the middle sleeper.

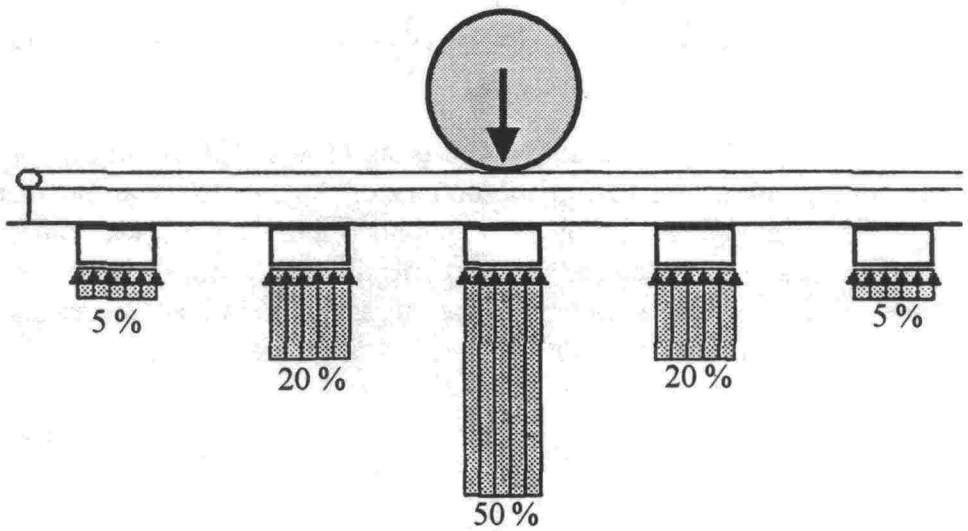

Figure 6.4:3 The assumed distribution of wheel load in the longitudinal direction by Riesberger (1998).

According to Raymond (1985), the longitudinal distribution of a wheel load can be simplified in accordance with Figure 6.4:4. Which of the assumptions is nearer to reality naturally depends on the characteristic length of the rail, which is affected, among other things, by the sleeper spacing, the bending stiffness of the rail and the stiffness of the embankment beneath.

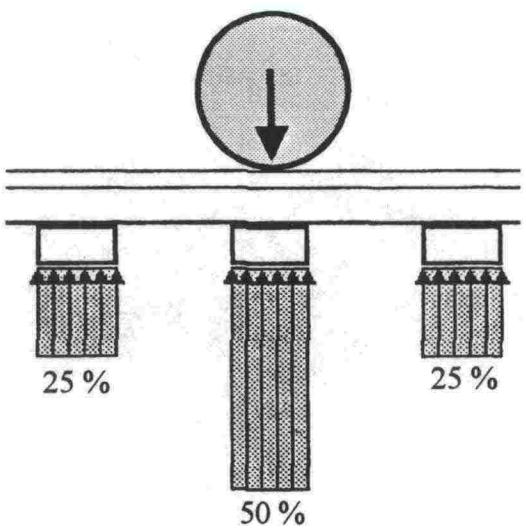

Figure 6.4:4 Simplified assumption of the distribution of a wheel load in the longitudinal direction of the rail (Raymond 1985)

In the assumptions shown in Figures 6.4:3 and 6.4:4, the combined effects of the consecutive axles in the distribution of wheel load is not taken into account. According to the examinations made in Chapter 5.6, the assumption of the separate effect of successive axles holds true rather well in the upper and middle part of the railway embankment of the instrumentation site. However, in reality the effect of successive axles is summing up to some extent in the lower part of the embankment and in the subgrade.

Based on what has been presented above, the basis of the BISAR modelling is the circular load configuration affecting at the bottom of the sleeper in accordance with Figure 6.4:5. The axle load, according to Raymond (Figure 6.4.4), is assumed to be distributed to successive sleepers and at the same time only one axle is taken into account in the calculation. The axle load is the quasistatic axle load corresponding to the measured dynamic wheel loads. The calculation of stresses and strains is made at the point under the rail as shown in Figure 6.4:5.

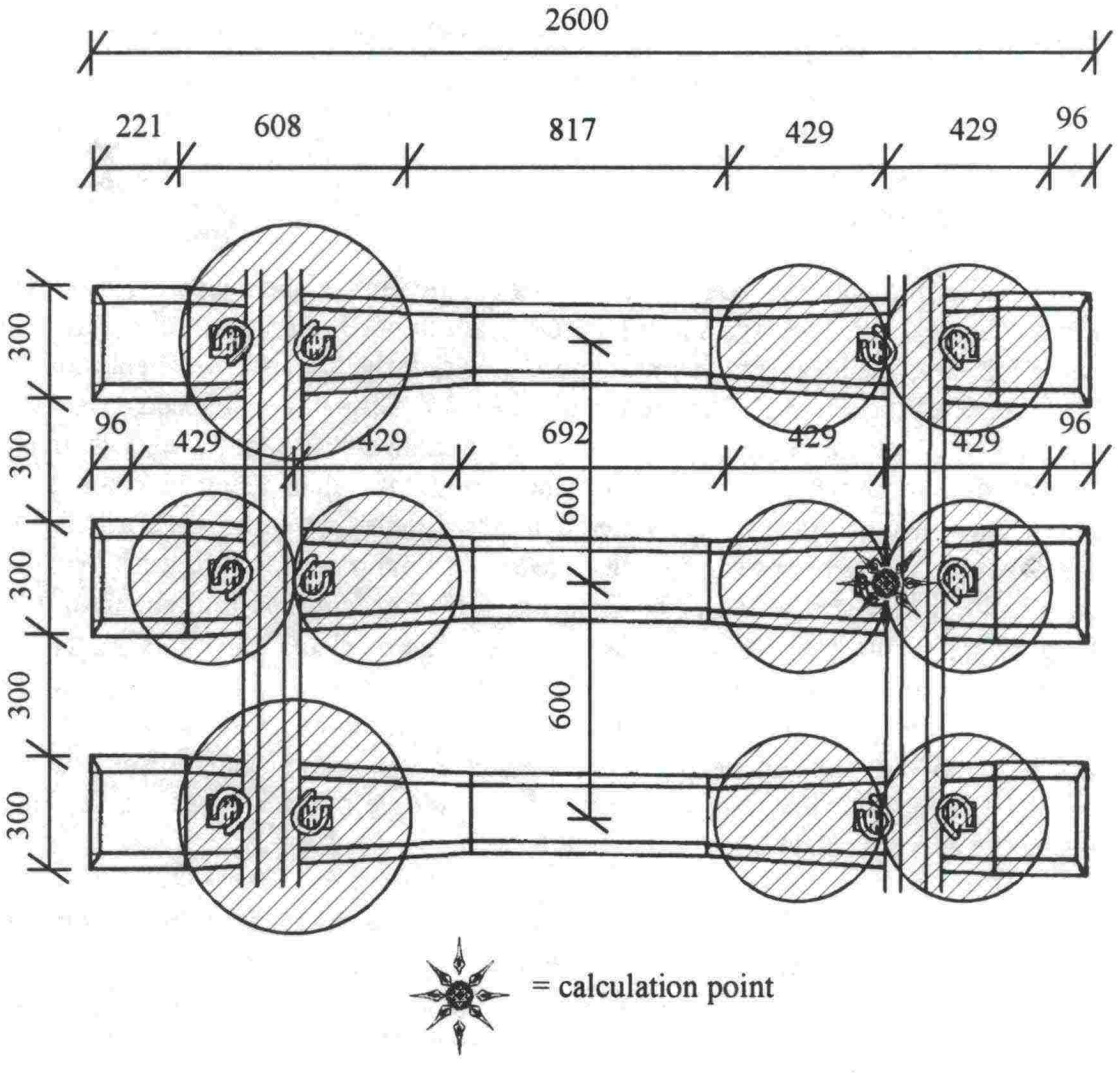

Figure 6.4:5 Circular load configuration and the position of the calculation point.

6.5 Thickness of the calculation layers and the applied modulus values with an axle load of 250 kN

The layers in the instrumented embankment can roughly be divided from the top to down as follows:

- Ballast
- Sand
- Gravel
- Subgrade (clay)

The layers and thicknesses in the embankment are not unambiguous (see Chapters 2.2.3 and 4.2), so they have to be simplified in the calculation. In Figure 6.5:1, there is a schematic embankment where the settlement of gravel and possible mixing with the subgrade is shown.

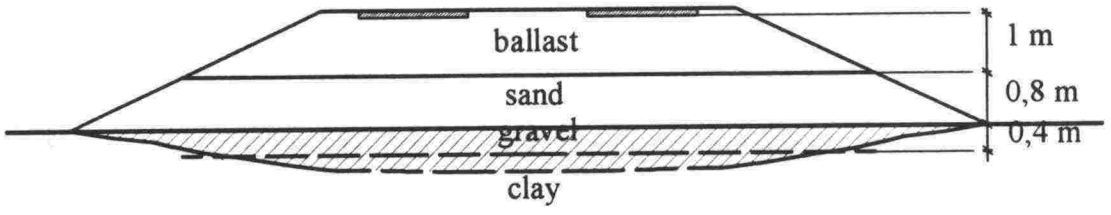

Figure 6.5:1 Schematic embankment.

The calculation model corresponding to the schematic embankment in Figure 6.5:1 is shown in Figure 6.5:2. The layers in Figure 6.5:1 are divided into so-called sublayers in Figure 6.5:2. This enables us to estimate more precisely the values of resilient modulus of the layers in Figure 6.5:1. The modulus values are estimated using equation 4.2:1. The modulus values are obtained by iterating the present stress condition. A change in the stress condition enables us to calculate new modulus values using equation 4.2:1. The new modulus values are then entered in the calculation program (BISAR), by means of which new stresses can be calculated. The final modulus values are obtained when substitution of stresses obtained from the BISAR calculation into equation 4.2:1 no longer appreciably changes the modulus values. Three calculations were enough for the iteration, so the convergence was excellent. Both the axle load and the self weight of the layers are taken into account in the calculation of modulus values. The contributions of the rails and sleepers are estimated in the rounding off of the modulus values. The modulus values are calculated in the middle of each layers so that they represent the average modulus value of each layer.

The modulus value of clay (Figure 6.5:2) was estimated as 40 MPa on the basis of the Resonant Column and Bender Element measurements (Chapter 4.3.2). The modulus value of the layer on top of a layer with low stiffness according to Sweer (1990) is 1.5 – 7.5 times the modulus value of the layer underneath. Thus, the modulus value of the gravel layer in the calculation was limited to $4 \times E_{clay}$ i.e. 160 MPa, although according to equation 4.2:1 one could obtain somewhat higher values for the resilient modulus of that layer. When defining the modulus values the Poisson's ratio of 0.30 was used on all layers, except for the subgrade, where the undrained value of 0.5 has been used.

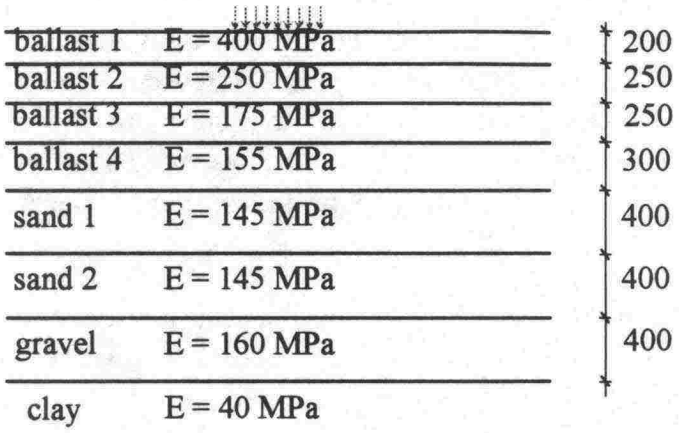

Figure 6.5:2 Layer thicknesses and the applied modulus values in the calculation model.

6.6 Comparison of the calculated and measured values with 250 kN axle load

The values of vertical strain calculated by the BISAR program and those measured at the instrumentation site are shown in Figure 6.6:1. In the calculation of Figure 6.6:1, the modulus values of Figure 6.5:2 are used as the parameters of the embankment layers and the subgrade.

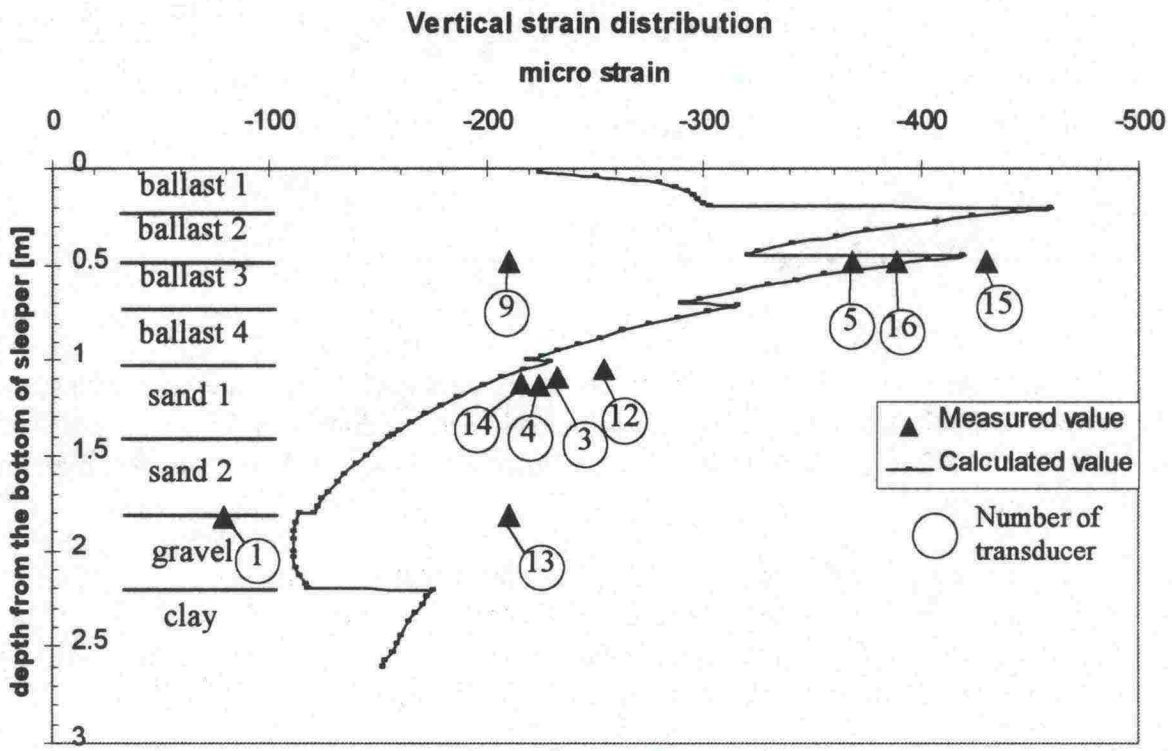

Figure 6.6:1 Measured and calculated values of the vertical strain. The numbers of the transducers has been circled. The parameter values of Figure 6.5:2 have been used in the calculation.

It can be seen from Figure 6.6:1 that the congruency of the measured and calculated values is fairly good. The strain value given by transducer no. 9 does not, however, correspond to the values given by the other transducers on the same level. In view of this calculation, it cannot be estimated which transducer, no. 1 or 13 inside the gravel layer, gives a more reliable result. The positions of the transducers are described in Chapter 2.2.2.

The displacement of bottom of the sleeper at the calculation point of the BISAR calculation (Figure 6.4:5) is as shown in Table 6.6:1. The values of the vertical sleeper displacement are measured at both sleeper ends and in the middle. The measured maximum values are shown in Table 6.6:1, as well as the value corresponding to the BISAR calculation point, which has been interpolated linearly from the values of the sleeper edge and to the middle of the sleeper.

Table 6.6:1 Calculated and measured vertical displacement of the sleeper.

	Measured value (max.)			Calculated value (max.)	
	Outer sleeper end	Middle of the sleeper	Inner sleeper end	Linear interpolation	BISAR calculation
Maximum vertical displacement of the sleeper [mm]	-1.746	-1.489	-1.935	outer-middle -1.642 inner-middle -1.755	-1.32

The differences between the measured and calculated vertical displacements of a sleeper shown in Table 6.6:1 are at least partly explained by Figure 4.5:8. This shows the cumulative effect of successive axle crossings due to soft subgrade in the measured sleeper movement.

Not only strains, but also stresses at different depth levels are obtained from the BISAR calculation. Comparisons between the measured and calculated values at different depths are shown in Figure 6.6:2. The excellent coherence of the calculated and measured values, except for transducer P3, can be seen in the figure.

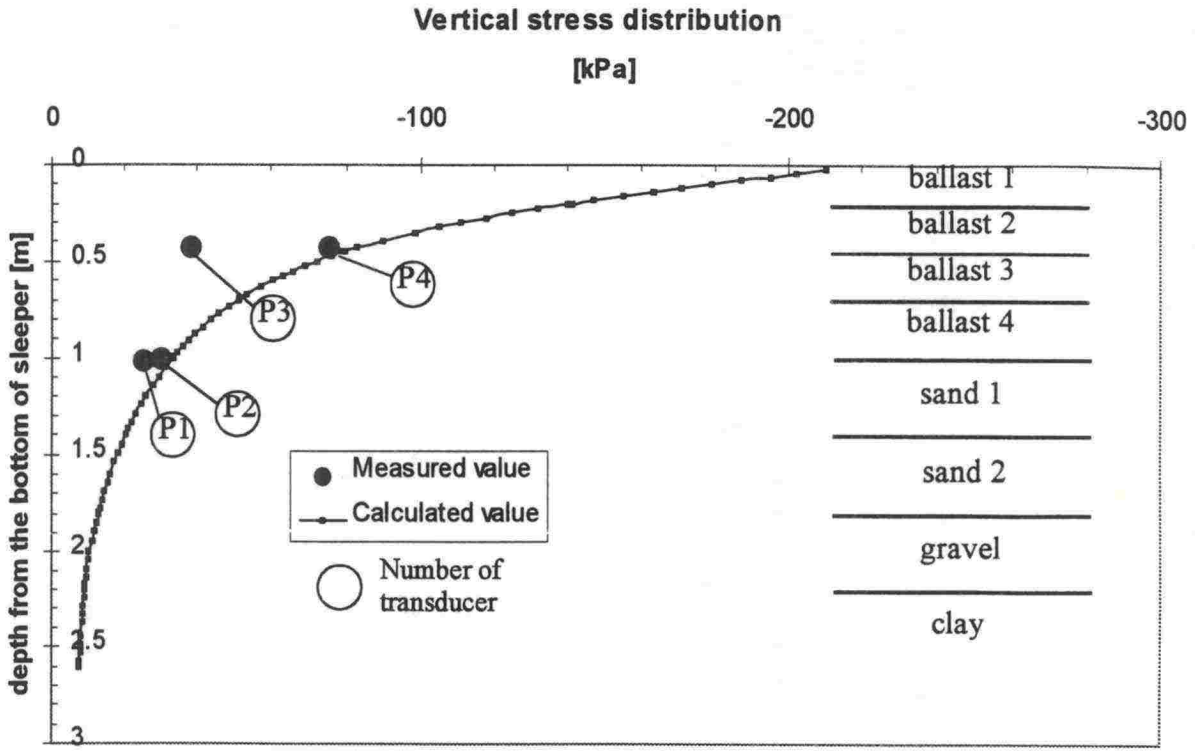

Figure 6.6:2 Comparison between calculated and measured vertical stresses with an axle load of 250 kN.

6.7 Sensitivity of the calculation result to Poisson's ratio with an axle load of 250 kN

The sensitivity of the modulus values used in the calculation for possible errors which could have occurred in the estimation of the value of the Poisson's ratio is checked in Figure 6.7:1. The Poisson's ratio is assumed to range between 0.2 and 0.4. However, the Poisson's ratio for the subsoil clay is assumed to remain at 0.5. The modulus values as shown in Figure 6.7:1 are now obtained.

ballast 1	E = 384 MPa	E = 411 MPa	200
ballast 2	E = 234 MPa	E = 261 MPa	250
ballast 3	E = 159 MPa	E = 184 MPa	250
ballast 4	E = 142 MPa	E = 165 MPa	300
sand 1	E = 135 MPa	E = 151 MPa	400
sand 2	E = 135 MPa	E = 154 MPa	400
gravel	E = 160 MPa	E = 160 MPa	400
clay	E = 40 MPa	E = 40 MPa	
	$\upsilon = 0,2$ except clay $\upsilon = 0,5$	$\upsilon = 0,4$ except clay $\upsilon = 0,5$	

Figure 6.7:1 Modulus values corresponding to values of Poisson's ratio 0.2 and 0.4.

The variation of Poisson's ratio according to Figure 6.7:1 is responsible for the variation in the calculated vertical strains shown in Figure 6.7:2.

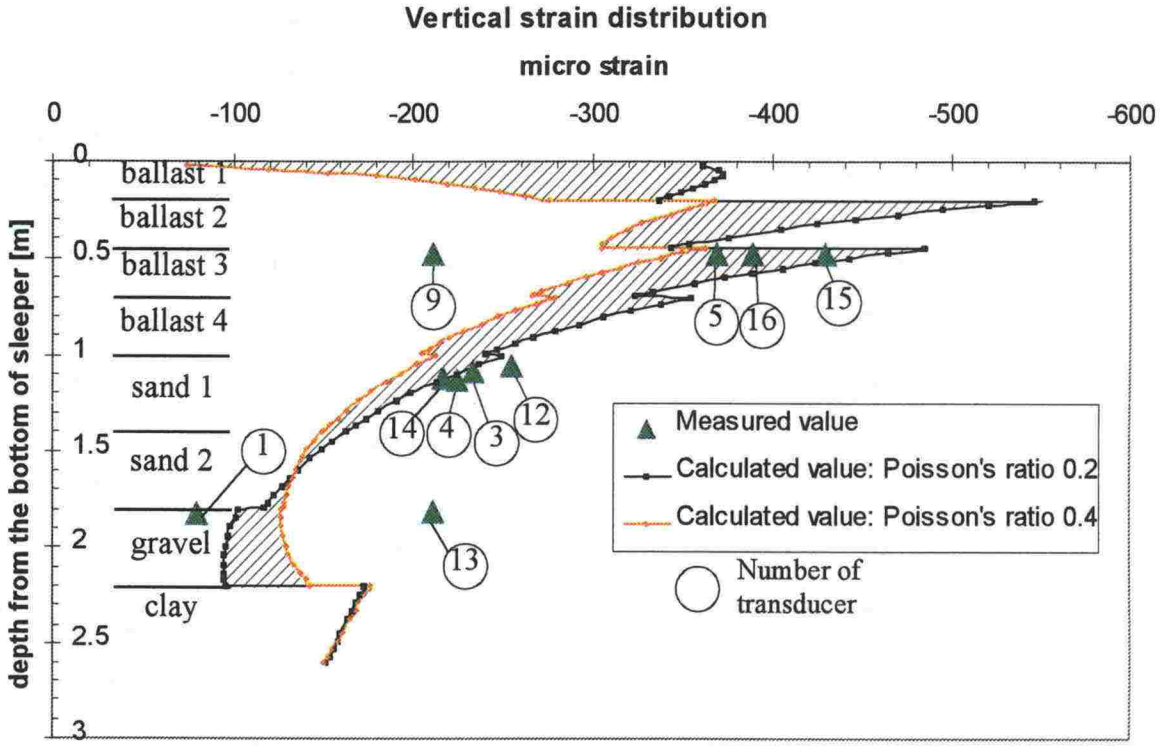

Figure 6.7:2. The range of vertical strain when the Poisson's ratio varies between 0.2 and 0.4.

The effect of variation of the Poisson's ratio of the structural layers appears to be greatest in the uppermost layers of the embankment.

The vertical movement of a sleeper now receives the values shown in Table 6.7:1.

Table 6.7:1 Calculated and measured vertical displacement of the sleeper.

	Measured value (max.)			Calculated value (max.)		
	Outer sleeper end	Middle of the sleeper	Inner sleeper end	Linear interpolation	BISAR calculation	
Maximum vertical displacement of the sleeper [mm]	-1.746	-1.489	-1.935	outer-middle -1.642 inner-middle -1.755	ν=0.2 -1.38	ν=0.4 -1.27

The stresses in the structural model also depend slightly on the Poisson's ratio (Equation 6.3:2). The stress distributions with Poisson's ratios of 0.2 and 0.4 are shown in Figure 6.7:3.

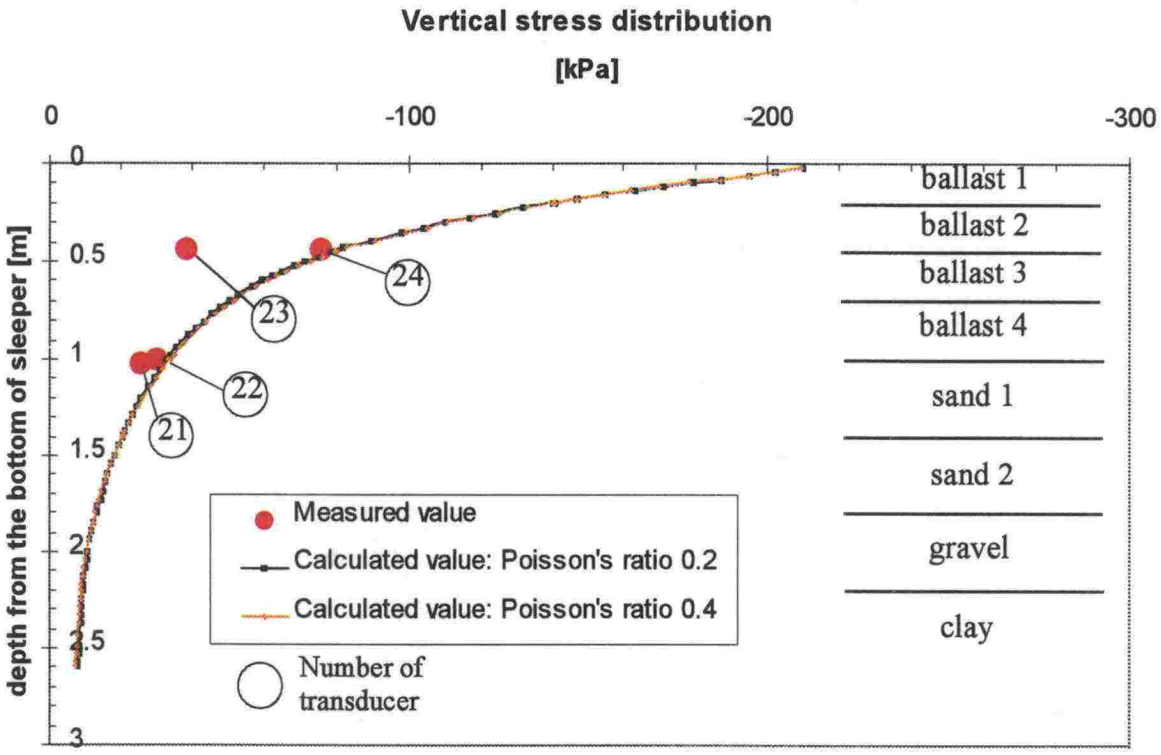

Figure 6.7:3. The effect of variation in the Poisson's ratio on the calculated stresses.

It can be seen from Figure 6.7:3 that the Poisson's ratio has only a minor effect on the stress distribution.

6.8 Sensitivity of the calculation result on the modulus value of the subgrade with an axle load of 250 kN

On the basis of the test results, the possible range of the subgrade modulus value was assumed to be 30 - 50 MPa. According to the assumption made in Chapter 6.5 the change in the subgrade modulus value also affects the modulus values in the gravel ($E_{gravel} = 4 \times E_{clay}$). Figure 6.8:1 shows the effect of the variation of the modulus values in the subgrade and gravel on the vertical strains. The Poisson's ratio is again 0.3 in all layers, except for the subgrade, where it is 0.5.

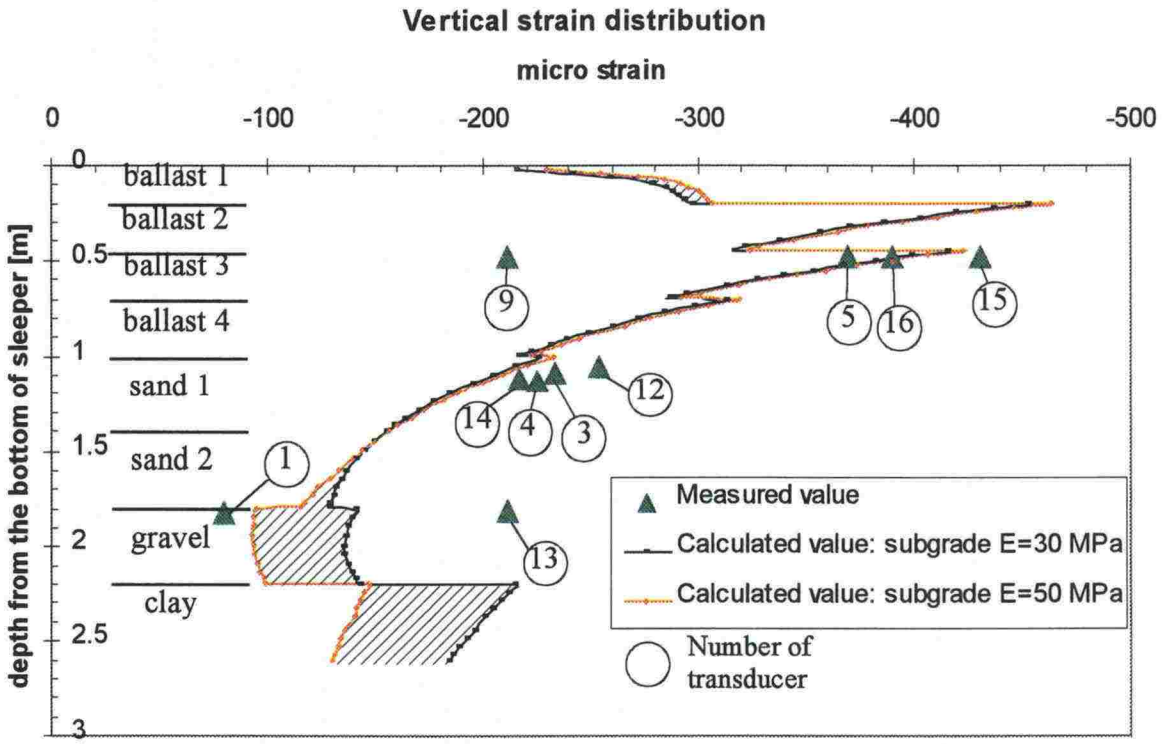

Figure 6.8:1. The range of vertical strain when the subgrade modulus value varies between 30 and 50 MPa.

As shown in Figure 6.8:1, the variation of the modulus value in the subgrade and gravel mainly affects only these layers.

The change in the modulus values of the subgrade and gravel affects the vertical displacement of a sleeper in accordance with Table 6.8:1.

Table 6.8:1 Calculated and measured vertical displacement of the sleeper.

	Measured value (max.)			Calculated value (max.)		
	Outer sleeper end	Middle of the sleeper	Inner sleeper end	Linear interpolation	BISAR calculation	
The maximum vertical displacement of the sleeper [mm]	-1.746	-1.489	-1.935	outer-middle -1.642 inner-middle -1.755	E=30 MPa -1.54	E=50 MPa -1.18

In Table 6.8:1 it can be observed very clearly how the change in the subgrade modulus value affects the calculated sleeper displacement.

The change in subgrade modulus values correspondingly affects the calculated stresses in accordance with Figure 6.8:2.

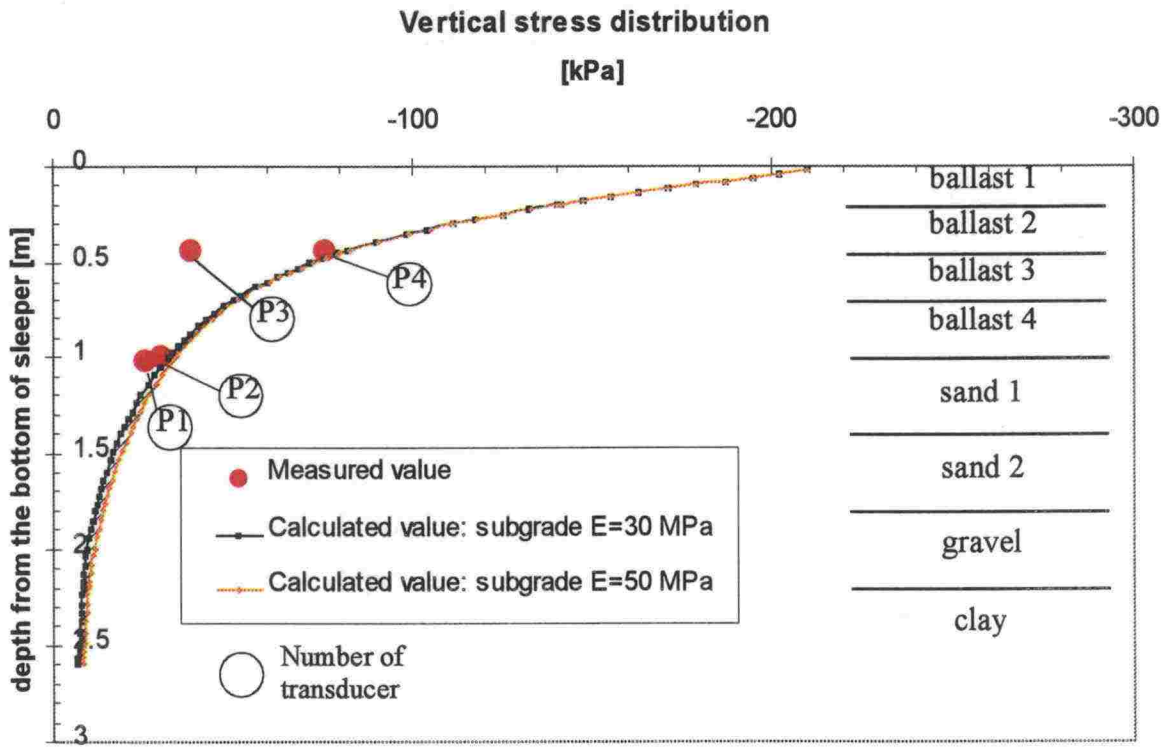

Figure 6.8:2. The effect of the variation in the subgrade modulus value on calculated stresses.

6.9 Sensitivity of the calculation result on the modulus values of embankment materials with an axle load of 250 kN

The sensitivity of the strain values which are obtained as calculation results on the modulus values of embankment materials is examined by reducing and increasing the modulus values shown in Figure 6.5:2 by 20 %. Meantime, the modulus value used for the subgrade clay is 40 MPa and the corresponding value for gravel is 160 MPa. The Poisson's ratio in all cases is again 0.3, apart from that for the subgrade, which is 0.5. Figure 6.9:1 shows the distribution of vertical strain as a function of depth with the reduced and increased modulus values for different embankment layer materials.

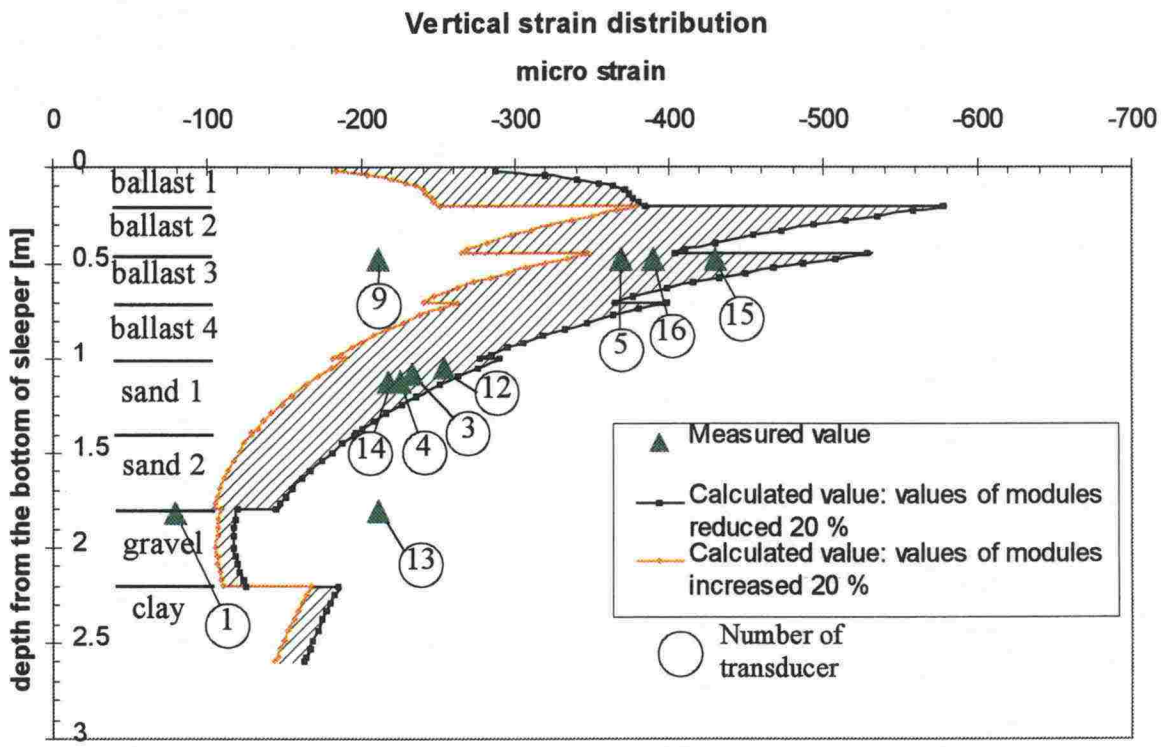

Figure 6.9:1. The range of the vertical strain when the modulus values of structural layers have been changed by –20 % and + 20 % for all other layers except the gravel.

It can be seen in Figure 6.9:1 how all the other transducers except numbers 1, 9 and 13 fit into the modelled area. The change of the modulus values in the upper layers does not affect the vertical strains on the gravel and clay layers very much.

The change in the modulus values of embankment structural layers affects the calculated sleeper displacement in accordance with Table 6.9:1.

Table 6.9:1 Calculated and measured vertical displacement of the sleeper.

	Measured value (max.)			Calculated value (max.)		
	Outer sleeper end	Middle of the sleeper	Inner sleeper end	Linear interpolation	BISAR calculation	
The maximum vertical displacement of the sleeper [mm]	-1.746	-1.489	-1.935	Outer–middle -1.642 inner-middle -1.755	E - 20 % -1.48	E +20 % -1.21

Compared with the basic calculation case, the reduction in the modulus values increases the calculated sleeper settlement relatively more (+12.2 %) than the increase of modulus values decreases the calculated sleeper settlement (-8.3 %). The change in the modulus values affects the vertical stress distribution only nominally and it is not shown graphically in this connection.

6.10 Effect of axle load on the embankment behaviour

The effect of axle load on the behaviour of the embankment can be estimated on the basis of both stresses and strains. This effect is examined for two pressure transducers, i.e. nos. P2 and P4 and for three vertical strain transducers, i.e. nos. 1, 3 and 16. Measurements nos. 11, 64 and 65 are examined in the comparison. Measurement no. 11 is related to a tank train with a wide range of different axle loads. Measurement no. 64 applies to the test train whose average axle load is 250 kN. Measurement no. 65 applies to a maintenance vehicle, whose axle load remains below 100 kN. The positions of the inspected strain and pressure transducers measured from the bottom level of the sleepers are shown in Figure 6.10:1.

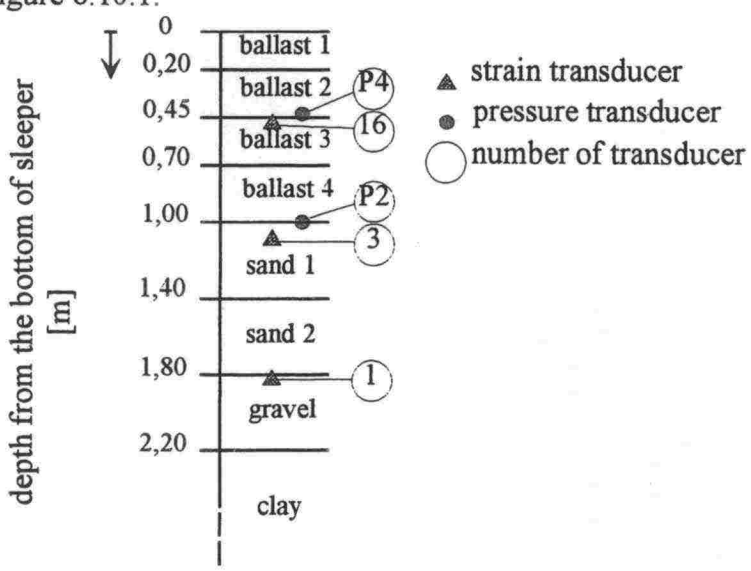

Figure 6.10:1 The depth position of the examined transducers.

Figure 6.10:2 gives a comparison between the stresses measured by the pressure transducer no. P4 and the stresses calculated by the BISAR program with different axle loads. Regarding the effect of the axle load one should be careful not to extrapolate the calculation result obtained using a program which is solely based on elasticity theory, since the soil mass acts more and more elastoplastically with high, i.e. >250 kN, axle loads. Consequently, we did not want to estimate the effect of axle load by extrapolating the calculation result up to an axle load of 300 kN.

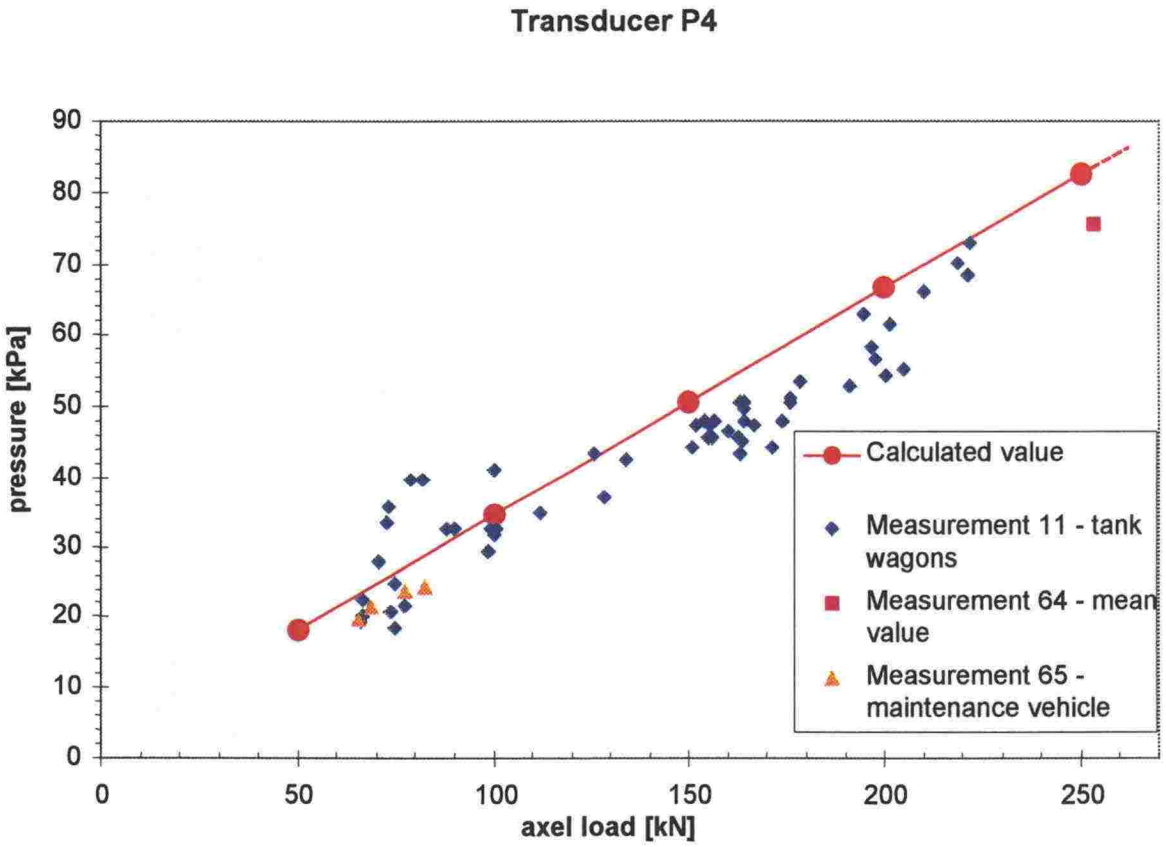

Figure 6.10:2. Comparison of stresses measured by pressure transducer no. P4 and the calculated ones.

In Figure 6.10:2, the measured and calculated values seem to be quite compatible. The relation of the axle load exceeding 250 kN and the corresponding compressive stress has been marked by a dotted line. This dotted line is achieved by extrapolating the line between 200 and 250 kN axle loads, and it is thus only trend-setting.

Strain transducer no. 16 is almost at the same depth as pressure transducer no. P4 (Figure 6.10:1). A comparison between the measured strains and those calculated at the same depth is given in Figure 6.10:3.

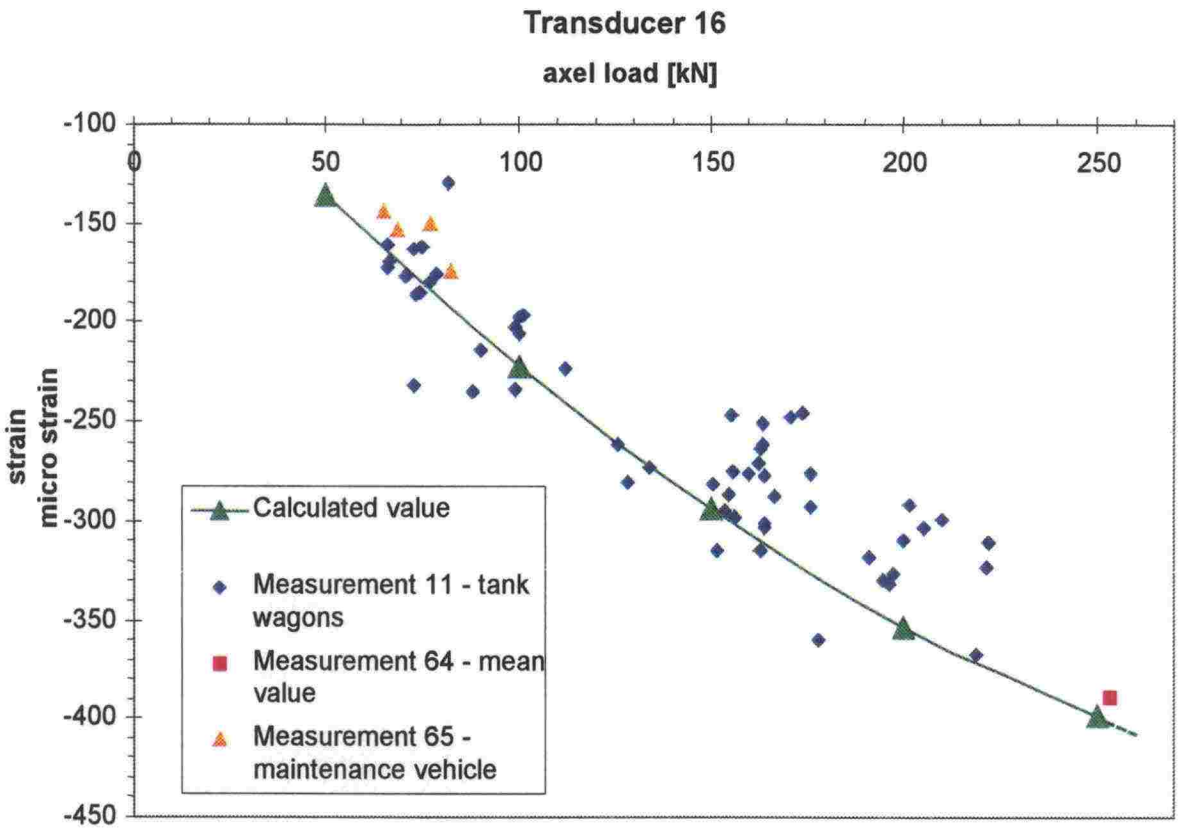

Figure 6.10:3. The comparison between strains measured by pressure transducer no. 16 and those calculated at the same depth.

The measured and calculated values in Figure 6.10:3 correspond very well to each other.

Figure 6.10:4 shows the stress values measured by pressure transducer P2 on the intermediate transducer level and the corresponding calculated stress values under different axle loads.

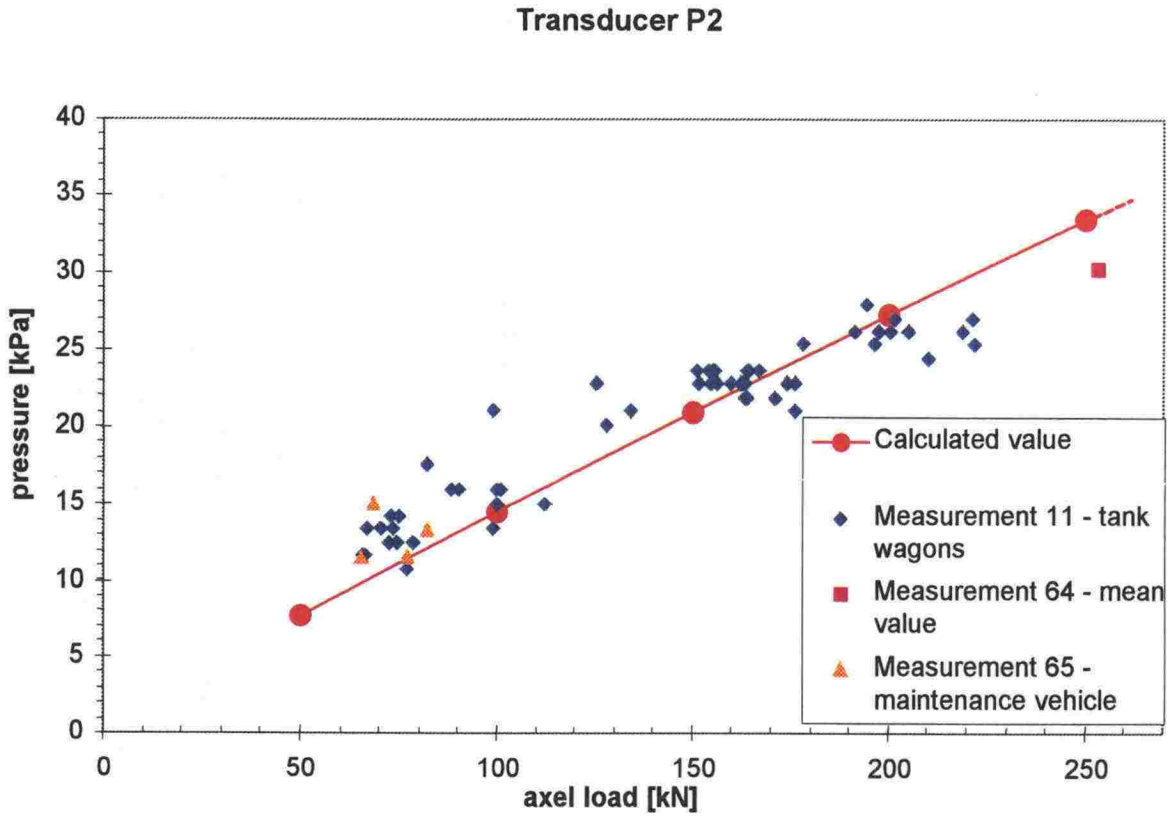

Figure 6.10:4. Comparison of strains measured by pressure transducer no. P2 and those calculated on the same level.

The values measured by pressure transducer no. P2 and those calculated on the same level appear to be also quite compatible. A comparison between the pressure transducer no. 3, which is on the intermediate installation level and the strain transducer no. 1, on the lowest transducer level, and the strains calculated at the same depths are shown in Figure 6.10:5 a and b.

(a)

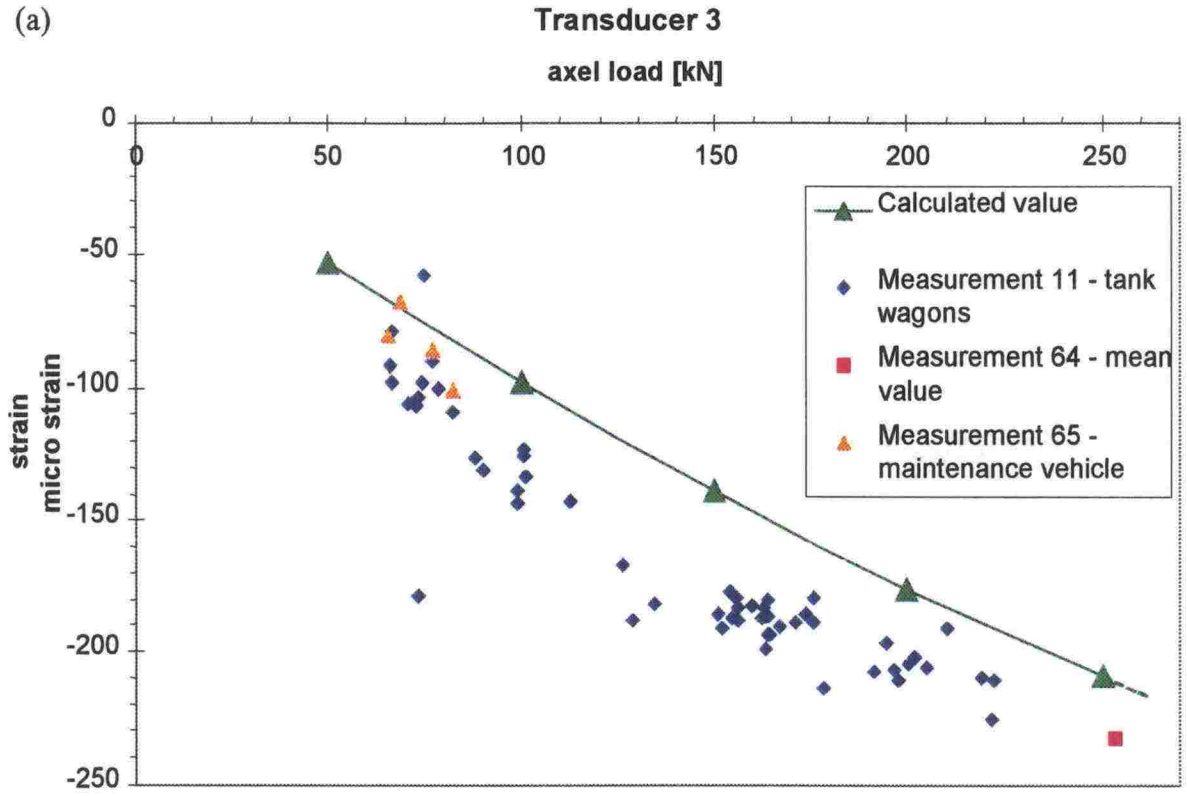

(b)

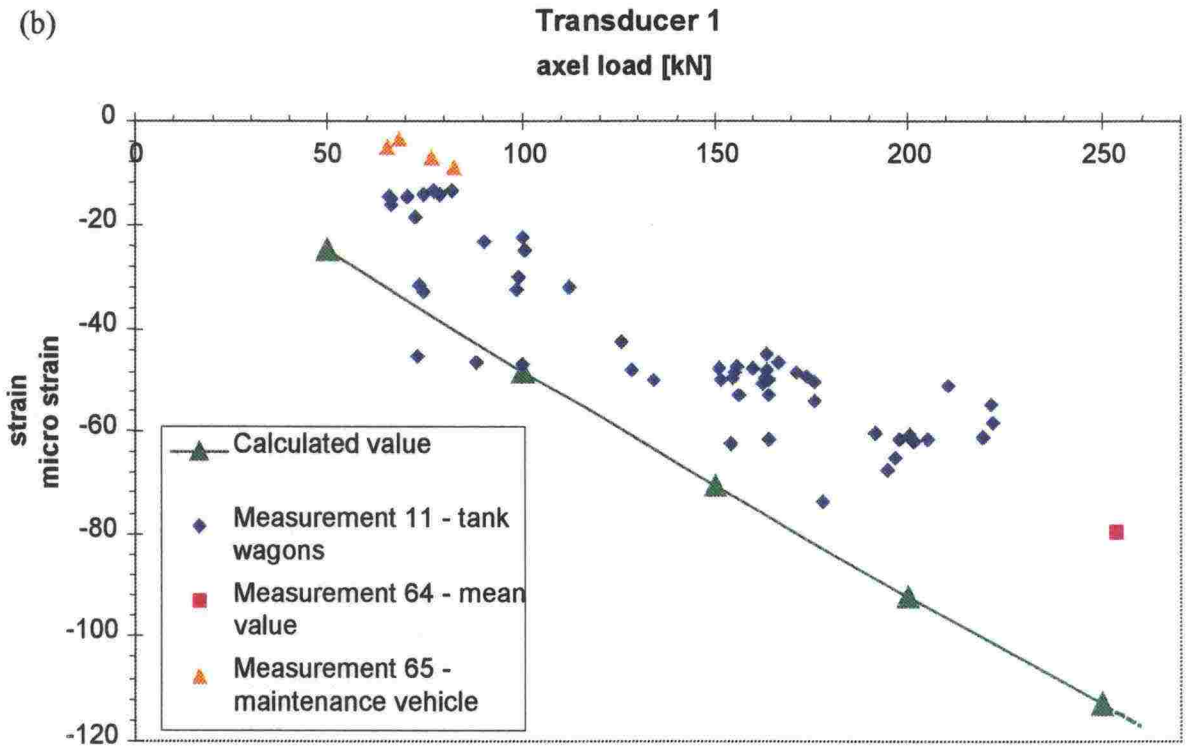

Figure 6.10:5. The comparison of vertical strain values measured by strain transducers 3 (Figure a) and 1 (Figure b) and those calculated at the same depths.

Figures 6.10:5 a and b show a similar tendency in the calculated and measured values. The calculated values of strain transducer no. 3 on the intermediate transducer level are, however, somewhat smaller than the measured ones. Strain transducer no. 1, on the lowest transducer level, gave correspondingly somewhat smaller values than the calculated ones.

6.11 Connection of the multi layer linear elastic modelling and the track modulus

Track modulus of C is defined in this connection by the relation of pressure p affecting at the level of the bottom of a sleeper to the ballast and the vertical displacement of the sleeper in accordance with equation 6.11:1.

$$C = \frac{p}{z} \tag{6.11:1}$$

where C = track modulus
p = pressure at the bottom of the sleeper
z = vertical displacement of the sleeper

According to equation 6.11:1, the track modulus has a unit of N/mm^3. The track modulus corresponding to the multi layer linear elastic modelling made by using the BISAR program can be defined by the relation between the surface pressure distributed evenly on the effective surface of a sleeper and settlement of the top surface of the corresponding structure model. In graphical form, the track appears, in accordance with the coordinate system of Figure 6.11:1, as the slope of the straight line connecting the calculation point corresponding to a certain axle load and the origin.

The assumptions of the load distribution used for the BISAR calculation have been according to those presented in Chapter 6.4 and the observation point of the settlement has been the one under the rail, as shown in Figure 6.4:5. Compared to the basic calculation case of Chapter 6.5, however, the modulus value of the subgrade has been changed in the BISAR calculation so that the settlement corresponding to an axle load of 73.3 kN has been made compatible with the real settlement values in measurement no. 65. This new subgrade modulus value has then been used in the multi layer linear elastic calculations corresponding to 150 and 250 kN axle loads as well.

In Figure 6.11:1, it can be seen that the track modulus C is not constant but is increasing as a function of axle load. This is due to the non-linear behaviour of embankment materials in relation to stress level, which is why the modulus values of the embankment materials, and thus the stiffness of the whole structure, increase as the axle load is increasing.

The reduced value of the track modulus presented in Chapter 5.5, C_R = 0,075 N/mm^3, has been calculated using the results of measurement no. 65. As the average of the measured axle load in that case was 73.3 kN, this can be compared with the track modulus C_1 = 0,11 N/mm^3 corresponding to the 73.3 kN axle load, obtained by the BISAR calculation and shown in Figure 6.11:1. The difference in the values of the track modulus is mainly explained by the effect of the rail pad included in the reduced value

of track modulus according to Chapter 5.5. In addition, differences are caused at least by the different assumptions regarding load distribution made according to this chapter and Chapter 5.5.

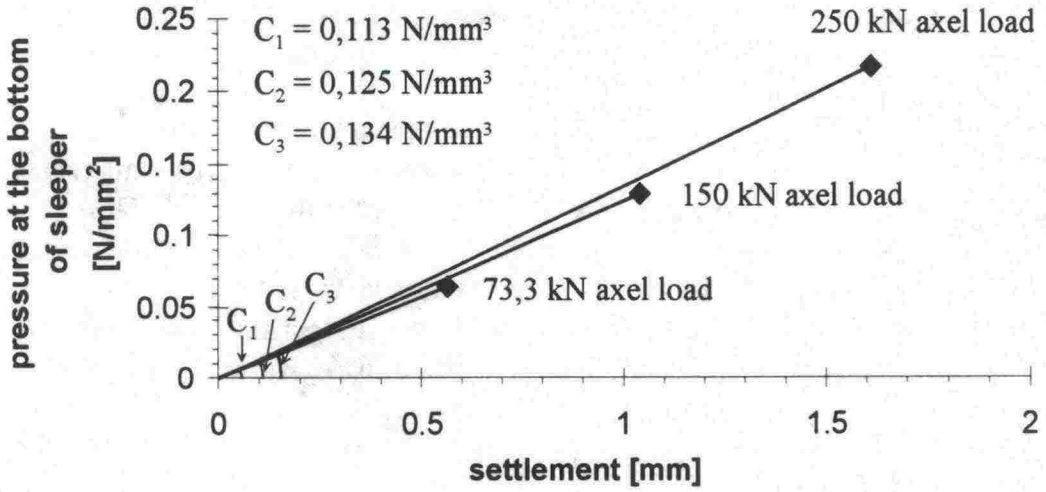

Figure 6.11:1. Determination of track modulus with different axle loads.

6.12 Conclusions

The multi layer linear elastic program enables modelling of the vertical stress-strain response of a railway embankment that corresponds to the measured behaviour, at least up to 250 kN axle loads. However, application of a calculation result based solely on elasticity theory for axle loads of up to 300 kN is not justified without reference measurement, because the embankment materials and the subgrade act increasingly elastoplastically with higher loads.

On the basis of the comparisons between the measured and calculated values the results obtained by strain transducer no. 9 can be assessed as being unreliable. One cannot, however, draw any firm conclusions from the results obtained regarding the strain transducers at the lowest level, if the either of transducers no. 1 and 13 is operating properly or not. The results from strain transducer no. 1 are, however, closer to the calculated results. In regard to the pressure transducers, all the other transducers apart from transducer no. P3, one of the transducers located inside of the ballast layer, seem to give congruent results with the calculations (Figures 6.7:1-6.9:1).

The sensitivity analysis of the calculation results shows that variation in the modulus values of embankment materials directly affects the strain values of the structure, while the effect in the stress distribution is small. Variation in the modulus value of the subgrade is probably the most important factor affecting the vertical movement of sleepers. The effect of the variation in the Poisson's ratio, both on the distribution of stresses and strains of the embankment, is rather small.

7. SUMMARY

7.1 Conclusions on the instrumentation and modelling

The following conclusions can be drawn from the arrangements and practical implementation of the measurements on the railway line between Koria and Kouvola in the summer of 1999:

- Generally, the measurements of the rail and the embankment succeeded at least as well as expected, if not even better. The measurement data for the rail remained slightly vague only with regard to the lateral force affecting the rail. This was not due to the malfunctioning or non-functioning of the instrumentation but to the small absolute values of the measured quantity itself, and to some extent also to the random nature of the variation, which is typical on a straight line. The measurement data for the embankment remained less conclusive in regard to the lateral strains. However, the arrangements for measuring these at the instrumentation site were considered somewhat experimental even from the outset.

- It can be concluded that the careful planning of the instrumentation was very important to the success of the measurements. This was made possible because the commissioner had a realistic view of the necessity for, and usefulness of, thorough preparations.

- In regard to the installation of the measuring instruments in the embankment, it must be said that the short, few hour installation break made the work very stressful. In order to obtain reliable measurement data, the installation work should be carried out extremely carefully. This should be taken into account in any future installation schedules; a longer time should be reserved for the work. In some respects, however, the experiences gained with installing the equipment at the Koria site would make it possible to carry out similar work more quickly in the future.

- Contrary to the expectations, reasonable results were also obtained from inside the ballast layer. The deviations between parallel transducers were, however, greater than what they were with the measuring instruments installed in a more fine grained material.

- The measuring instruments embedded in the embankment stood up well to the stresses resulting from the compaction and rail supporting measures carried out after the installation. By the start of the monitoring period only one strain transducer had become unfit for use. The reason was probably that the transducer had moved outside the measuring area, rather than that it was damaged.

- The measurements were made according to the preliminary plans and no major problems or disturbances occurred. However, it was observed at the instrumentation site that if visibility in the approach direction of trains is much poorer than at the present site, initiation of the measurements should be automated.

- All in all, cooperation with the people at the instrumentation site and the local track upgrading organisation went very well. The same can also be said about the cooperation with all the organisations responsible for the instrumentation and the measurements.

7.2 Conclusions on the modelling of rail function

Based on the measurement results and the inspections and analyses made of them thus far, the following can be said in regard to the rail:

- If one could define the value of the track modulus on a certain line section by knowing the characteristics of the railway embankment and foundation soil (see Chapters 6.11 and 9.3), the rail bending stresses could be defined by using the traditional 'beam-on-elastic-foundation-theory'. On the basis of the track modulus and the characteristics of the track structure and rolling stock, the characteristic rail length can be determined by calculation, after which bending moments and static bending stresses caused by different axle combinations can be calculated. For supporting the measurement results, coefficients from the literature are also needed in order to take into account the extra stresses caused by the dynamic character of loadings, circumstances and other factors. Contact stresses and impact from wheel flats call for a separate inspection.

- Information was obtained on the size of stresses affecting the rail attachment components on a straight line in good condition. The characteristics and function of the rail pad play an important part, as also how worn the rails and wheels are. The running characteristics of rolling stock affect the size of dynamic wheel loads. When the direction and size of loadings are known, the stresses of attachments can be estimated by modelling the rail for a beam on an elastic foundation. However, it is difficult to estimate, for instance, the durability of the rail pad itself without any loading tests in a laboratory.

- Naturally, an FE-model can be developed for a sleeper to estimate stresses. Then, among other things, the effect of the support on the bending stresses of a sleeper could be inspected and compared with the stresses measured on the line. The latter could also be compared to the stresses on sleepers in instructed laboratory tests. For example, a single static bending test to be made in the middle part of a sleeper with the loading and support required in a dynamic test gave a strain of 200 – 300 % of the maximum level measured on the track.

- The load distribution on consecutive sleepers from one axle has been covered in Chapter 5.6. On the basis of the measurement results obtained, it seems that under the instrumented circumstances the distribution in accordance with Figure 6.4:3 is closer to reality than the one in Figure 6.4:4. A more detailed analysis of the distribution would require, among other things, the flexible curve of rail pads used in the rail to be measured.

7.3 Conclusions on the modelling of the railway embankment behaviour

As a whole, the results and the analyses of the measurements can be considered to confirm the conclusions drawn earlier during the literature review on the ballast and substructure (Kolisoja et al. 1999). Thus, the following can be stated on the basis of the preliminary modelling of the measurements and measurement results:

- The quasi-static modelling of the vertical stiffness of a railway embankment based on the multi layer linear elastic model corresponds well to the actual behaviour of the railway embankment measured at the instrumentation site. The mechanical behaviour of layer materials and subgrade should, however, be described by models taking the effects of stress and strain levels into account. Consequently, when aiming for a high level of accuracy, the parameters of the models should be determined in the laboratory with the stress and strain levels corresponding to the real loading condition.

- The Young's modulus values of the subgrade based on the laboratory tests, and found to be of the correct order of magnitude during modelling of the structure, are somewhat higher than generally expected for instance when estimates of the bearing capacity of road structures are made (Kolisoja et al. 1999). The reason for this is most obviously that the modulus values used for the subgrade in those cases mainly represent the frost thawing period, which is the most unfavourable situation for the bearing capacity. As, owing to the thicker frost non-susceptible layers, the track structure offers better frost insulation than a normal road structure, with the subgrade under the track structure it is not necessary to take into account the same kind of seasonal variation. Thus, the real value based on the measured results is directly applicable as the Young's modulus value.

- It is clearly more difficult task to specify the sufficient width of a railway embankment in regard to stability corresponding to different axle loads in long-term repeated loading than modelling of the vertical stiffness of a railway embankment. On the basis of the measured data obtained from single train passages at the instrumentation site and the preliminary modelling work carried out so far, no direct answer to the problem can be given for 250 kN or higher axle loads. The measurement results at the instrumentation site provide, however, a clear indication that in certain parts of the railway embankment there will exist lateral cyclic tensile strains with high axle loads. The higher these tensile strains appear, the greater the proportion of them is which will remain irreversible. Along the whole railway embankment this will be seen as a gradual increase in flatness of the embankment. Thus, with smaller embankment widths the stability of the railway embankment under long-term repeated loading can become a factor which limits the increase in axle loads.

7.4 Suggestions for further investigations

The following can be said regarding the application areas of the preliminary modelling work describing the mechanical behaviour of railway embankments performed thus far and the needs for further investigation:

- As an addition to the measurements made in the instrumentation site in Koria during the summer 1999, another series of measurements could be carried out under winter conditions. The railway embankment should be mostly frozen, so that on the basis of the results it could be evaluated, for instance, how the increasing stiffness due to the freezing of the embankment materials affects the stresses on track components and the magnitude of the vibrations propagating to the track environment. The winter measurements would also give a more reliable basis for separating the deformations that take place in the subgrade from the overall deformations of the track embankment detected during the measurements in the summer 1999. Naturally, this is always provided that the railway embankment is properly frozen and that the measuring instruments inside the embankment remain functioning until the new monitoring period. The instrumentation for the rail should be rebuilt, but the instrumentation can be carried out in a somewhat simpler way than during the summer 1999 measurements.

- On the basis of the modelling work carried out thus far it seems that it would be possible to construct a modelling environment that is able to describe the vertical stiffness of railway embankments. This would enable theoretical anticipation of the vertical stiffness of various types of railway embankments, the structures of which are known, and the stresses and strains to which the components of the track structure are thus exposed. In order to obtain an approximate result regarding a certain type of track embankment one should be at least aware of the layer thicknesses and the material grading curves, as well as the type of subgrade. If necessary, a more accurate estimate can be obtained by testing the properties of the layer materials and subgrade under laboratory conditions. At an early stage, it should also be checked whether the existing modelling programmes (e.g. GEOTRACK) can be used, so that the required software development would not become unreasonably extensive.

- An interesting field of application for the modelling environment of the stiffness of the railway structure would be to combine it with the analysis of the measurement results of the so-called diagnostic train. In that case the modelling environment could in principle act as a tool in the interpretation of measurement results related to extensive investigations of the railway network condition and in analysing the operation and repair alternatives of some single problem areas.

- One possible application area for the results of the multi layer linear elastic modelling performed within this project is to estimate the average stresses affecting the ballast. One could estimate the ballast durability and the speed of degradation under different axle loads on the basis of, for instance, the grain shape and the quality of the rock material with a series of cyclic loading tests on different kinds of

rock material. The magnitude of loading corresponding to the different axle loads can be estimated by calculations based on the layer modelling of the track structure.

- In regard to embankment structures, it is not sensible to compare the stress distribution of the railway embankment, obtained by multi layer linear elastic model, directly with the results of the so-called 2:1 distribution applied in many cases in the estimation of stresses affecting in the subgrade. The primary reason for this is that the result of the approximate 2:1 distribution depends to a large extent on the assumptions of the load distribution at the bottom of the sleeper, among other things.

- On the basis of the very preliminary analysis regarding the sufficiency of the embankment width it is not possible to define what would be a sufficient width for an embankment under long term cyclic loading with an axle load of 250 kN or 300 kN. As a matter of fact, even under the present axle loads there is nothing more substantial available than experimental observations on the stability, and even these have been questioned to some extent. An approximate estimation of the minimum embankment width required for higher axle loads could be obtained, however, from the stability calculations on a static loading condition, by means of which the embankment width could be specified where the safety factor of the railway embankment against failure would be at least as good as it is with the combination of the present axle load, embankment width and allowable train speed.

- In order to achieve a more reliable and accurate result, it is suggested that the studies on the effects of the embankment width would be continued later on by a theoretical modelling based on more sophisticated modelling tools - mainly by the use of finite element calculations enabling a three-dimensional model of the embankment structure to be used. In this way a clear understanding of the physical behaviour of the railway embankment under repeated loading and the location of the critical points in regard to the stability of the railway embankment could be formed. With this method it would be possible to examine the effect not only of the embankment width, but also of the slope of the embankment, on the above-mentioned aspects.

- The results of the theoretical modelling of the railway embankment referred to above would be extremely useful in planning a separate instrumentation site for specifically studying the effect of the embankment width. This could be carried out, for instance, so that the site would be located on a curve on a single track, where the railway embankment width, and possibly also the slope of the embankment, would be varied systematically during the measurements. This cannot be carried out, however, before the summer 2001.

Some further issues, mainly related to the loading assumptions of track structures, have come up during the modelling work. They have not been specifically studied during this investigation, but an examination of the results of the modelling work goes some way towards answering these questions. The following can be said:

- Based on the measurements at the instrumentation site, one cannot directly draw any conclusions as to whether the loading assumption of 120 kN/rail metre is sufficient for subsoil stability calculations with higher axle loads, mentioned in Part 3, "Track Structure" of the Technical Rules and Guidelines for Fixed Installations of Railway (RAMO). This is mainly due to the fact that the sufficiency or correctness of the loading assumption mentioned depends on the rolling stock to be used with higher axle loads. On the other hand, on the test train there were only four axles with a 250 kN load, placed in two bogies rather distant from each other. Thus, the test train did not apparently have the most critical loading combination with regard to higher axle loads, where there are several bogie axles loaded with higher axle loads and these are placed successively closer to each other. If it is assumed, however, that the above-mentioned 2:1 distribution is applied to the stress distribution caused by two successive bogies in the subgrade in the longitudinal direction of the track, the loading assumption of 120 kN/rail metre can be considered suitable for a 250 kN axle load, even when there are single bogies with such a loading in successive wagons. However, without a more precise analysis of the stress distribution, the same conclusion cannot be drawn directly from the measurement results regarding the 8-axle wagon, as shown in Figure 4.5:9, and this applies in particular to an axle load of 300 kN.

- A trend-setting example of the share of the dynamic component in the measured wheel force values is shown in Figure 5.1:3, where the distribution of the measured vertical components of the wheel load of the test train wagon passing the instrumentation site is presented. In the distribution shown in Figure 5.1:3, the majority of the deviations is caused by the passages of the test train from Koria towards Kouvola, thereby approaching the instrumentation site from the direction of a curve. With the train approaching the instrumentation site along a straight line from Kouvola direction, the deviations in the vertical component of the rail force have been much smaller (table 4.4:1). However, on the basis of the above measurement results no general conclusions regarding the share of the dynamic wheel load component can be made, as the measurement results obtained from the instrumentation site represent only the circumstances prevailing in this particular place. Since the track at the instrumentation site was recently upgraded and the wheels in the test train were in very good condition, at least according to visual examination, it is obvious that the share of the dynamic load component on a poorer track, i.e. the extent of the axle load variation around the static axle load, is probably larger than the one shown in Figure 5.1:3.

- In addition to the track characteristics, the type of rolling stock is also presumed to have an effect on the share of the dynamic load component when estimating wheel forces on the rail. In this case it could be evaluated, in principle, based on the passages of other trains, if the static axle loads of the trains were known. Two examples of the distribution of the measured wheel forces in tank trains passing the instrumentation site are shown in Figures 5.1:4 and 5.1:5.

- The assumptions of the vertical and lateral components of the wheel force, 170 kN and 70 kN, according to Technical Specifications for Rolling Stock in Finland (LIMO), Part 1 "General Rules for Rolling stock", can be considered sufficient in

the circumstances of the instrumentation site for the axle load of 250 kN of the test train and also the other trains passing the instrumentation site, which have been analysed in more detail. No extrapolation of the conclusion on an axle load of 300 kN, or on another track with a different condition or geometry, can be made on the basis of the results obtained at the instrumentation site.

REFERENCES

AASHTO T 294-92 I (1992). Interim method of test for resilient modulus of unbound granular base/subbase materials and subgrade soils – SHRP protocol P46. American Association of State Highway and Transportation Officials.

Gåsemyr, H. (1996). Overbygnings komponenter: Sviller. Nordisk baneteknisk ingeniörutdannlse. Ellivuori. 19.11.1996. 45 p. (*In Norwegian*)

Järvenpää, I., Kolisoja, P. & Levomäki, M. (1999). Ratarakenteen instrumentointi- ja mallinnussuunnitelma, 250 kN:n ja 300 kN:n akselipainot. Ratahallintokeskuksen julkaisuja A 4/1999. Ratahallintokeskus, Helsinki. 30 p. (*In Finnish*)

Kolisoja, P. (1997). Resilient deformation characteristics of granular materials. Tampereen teknillinen korkeakoulu, Julkaisu nro 223. 214 p.

Kolisoja, P., Niskanen, P., Mäkelä, E. & Levomäki, M. (1999). Tukikerros ja alusrakennne – kirjallisuusselvitys, 250 kN:n ja 300 kN:n akselipainot. Ratahallintokeskuksen julkaisuja A 6/1999. Ratahallintokeskus, Helsinki. 135 p. (*In Finnish*)

NYNAS (1995). NOAH computer software for pavement design calculations. Part: documentation. Version 1995.

Puikkonen, E. (1989). Ratatekniikka 1989. Suomen maarakentajien keskusliitto ry. 74 p. (*In Finnish*)

Raymond, G. P. (1985). Analysis of track support and subgrade stability. Lecture notes.

Riessberger, K. (1998). Track part of the system 'railway'. Nordic railway seminar 1998. Lecture notes. 46 p.

Selig, E. T. & Waters, J. M. (1994). Track geotechnology and substructure management. London. Thomas Telford. pp. 1.1-16.11

Shell (1995). BISAR-PC user manual. Version 1995, Release 2.0.

Souto, A., Hartikainen, J. & Özüdogru, K. (1994). Measurement of dynamic parameters of road pavement materials by the bender element and resonant column methods. Géotechnique, Vol. 44, No. 3, pp. 519-526.

Table L1:1 List of trains crossing instrumentation site and the train speeds.

Meas. No.	Date	Time	Train No.	Train type	V1 (km/h)	V2 (km/h)	V avg (km/h)	NB
1	6.7.	14:37	P8	P	115	119	117	
2	6.7.	14:56	T6010	F	61	65	63	No video
3	6.7.	16:00	P24	P	118	118	118	No video
4	6.7.	17:04	IC10	P	129	115	122	
5	6.7.	17:12	T2092	F	53	52	52,5	Wheel flat
6	6.7.	18:06	P76	P	131	128	129,5	
7	6.7.	18:13	T2086	F	58	53	55,5	Wheel flat
8	6.7.	18:27	T2838	F	73	76	74,5	Wheel flat
9	6.7.	20:07	P36	P	119	124	121,5	
10	6.7.	20:13	P14	P			113	Mallfunc. of rad.
11	6.7.	20:21	T2030	F	68	68	68	Wheel flat
12	6.7.	21:18	T2038	F	77	77	77	
13	6.7.	22:22	P80	P	133	132	132,5	
14	6.7.	23:24	T2017	F	69	66	67,5	Wheel flat
15	7.7.	01:43	T2850	F	74	74	74	
16	7.7.	01:48	T2806	F	43	44	43,5	Wheel flat
17	7.7.	03:57	T2852	F	70	71	70,5	
18	7.7.	04:05	T2012	F	75	75	75	Wheel flat
19	7.7.	04:32	H9730	P	108	108	108	
20	7.7.	04:36	T2854	F	78	78	78	
21	7.7.	04:48	T2810	F	75	75	75	Wheel flat
22	7.7.	05:36	H9744	P	111	115	113	
23	7.7.	05:43	T2011	F	80	75	77,5	
24	7.7.	06:27	P222	P	126	127	126,5	
25	7.7.	06:34	T2028A	F	60	54	57	Wheel flat
26	7.7.	07:37	IC2	P	117	120	118,5	
27	7.7.	08:31	IC72	P	135	133	134	
28	7.7.	08:35	H9762	P	120	119	119,5	
29	7.7.	09:05	IC4	P	109	113	111	
30	7.7.	09:34	P32	P	113	109	111	

P = passenger train, F = freight train, T = tank train, Te = test train

Table L1: List of trains crossing instrumentation site and the train speeds. (cont.)

Meas. No.	Date	Time	Train No.	Train type	V1 (km/h)	V2 (km/h)	V avg (km/h)	NB
31	7.7.	10:18	P34	P	99	99	99	
32	7.7.	10:36	P6	P	105	109	107	
33	7.7.	11:52	P74	P	127	126	126,5	
34	7.7.	12:03	T2084	F	59	50	54,5	Wheel flat
35	7.7.	13:28	H9792	P	80	80	80	
36	7.7.	14:37	P8	P	124	125	124,5	
37	7.7.	16:01	P24	P	113	113	113	
38	7.7.	16:06	T6010	F	76	75	75,5	2 trains same t
X	7.7.	17:08	IC10	P	136	141	138,5	Narrow emb.
X	7.7.	17:13	T2092	F	60	56	58	Narrow emb.
39	7.7.	17:55	P76	P	131	130	130,5	
40	7.7.	18:03	T2086	F	62	57	59,5	Wheel flat
41	7.7.	18:19	T2034	F	75	73	74	Wheel flat
42	7.7.	20:01	P36	P	88	92	90	
43	7.7.	20:09	P14	P	112	112	112	
44	7.7.	20:18	T2030	F	76	75	75,5	Wheel flat
45	7.7.	21:03	P80	P	137	137	137	
46	7.7.	21:16	T2038	F	77	74	75,5	Wheel flat
47	7.7.	23:44	T2017	F	64	62	63	Wheel flat
48	8.7.	01:36	T2032	F	57	54	55,5	Wheel flat
49	8.7.	01:54	T2850	F	68	66	67	Wheel flat
50	8.7.	03:36	T2012	F	77	79	78	Wheel flat
51	8.7.	03:59	T2852	F	71	67	69	
52	8.7.	04:32	H9730	P	116	115	115,5	
53	8.7.	04:38	T2810	F	80	80	80	
54	8.7.	05:36	H9744	P	112	112	112	
55	8.7.	05:43	T2011	F	60	60	60	
56	8.7.	06:29	P222	P	123	125	124	
57	8.7.	06:36	T2082A	F	58	54	56	Wheel flat
58	8.7.	07:37	IC2	P	124	128	126	

P = passenger train, F = freight train, T = tank train, Te = test train

Table L1: List of trains crossing instrumentation site and the train speeds. (cont.)

Meas. No.	Date	Time	Train No.	Train type	V1 (km/h)	V2 (km/h)	V avg (km/h)	NB
59	8.7.	App. 8	--	Te	0	0	0	Weighting of Te
60	8.7.	08:24	IC72	P	120	119	119,5	
61	8.7.	08:28	H9762	P	101	100	100,5	
62	8.7.	08:35	--	Te	41	41	41	
63	8.7.	09:04	IC4	P	121	123	122	
64	8.7.	09:09	--	Te	50	45	47,5	
65	8.7.	09:18	--		84	84	84	M. V. Ttv 16
66	8.7.	09:29	P32	P	110	113	111,5	
67	8.7.	09:34	--	Te	61	61	61	
68	8.7.	10:08	--	Te	68	68	68	
69	8.7.	10:18	P34	P	110	110	110	
70	8.7.	10:25	--	Te	80	81	80,5	
71	8.7.	10:36	P6	P	131	130	130,5	
72	8.7.	10:43	Kv Pv 2	F	35	33	34	Wheel flat
73	8.7.	10:49	--	Te	89	89	89	
74	8.7.	11:04	--	Te	97	99	98	
75	8.7.	11:29	--	Te	100	100	100	
76	8.7.	11:43	P74	P	126	125	125,5	
77	8.7.	11:52	T2084	F	54	53	53,5	Wheel flat
78	8.7.	11:58	--	Te	95	85	90	Braking of Te

P = passenger train, F = freight train, T = tank train, Te = test train, M. V. = maintenance vehicle

Table L1:2 Weighing report of the test train.

VR Cargo
Lappeenranta jnt.

Juna nro: 2335 Aks.-edellä: 4 Vaunut: 1 Punnitus nro: 100033

Liikkeessä-punnitus aloitus: 07.07.99 17:05 BRUTTO Punnitus

	Vaunu nro	PAINO kg	Nopeus km/h	Akse	Silt	T	Lastaus	A-T-K	Virhe	Punnitus nro
1	75140-4	98000	10.4	4		*	S02/498	A		100067

Liikkeessä-punnitus lopetus: 07.07.99 17:11 Suunta: <-

HUOM:

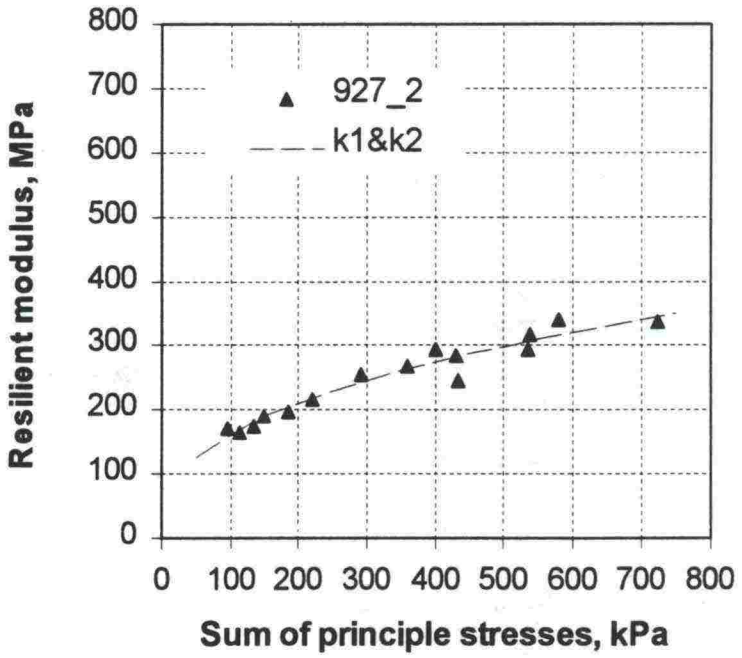

Figure A2:1 The result of cyclic triaxial test for the sand, which is located between depths 1.2 m ... 2.0 m.

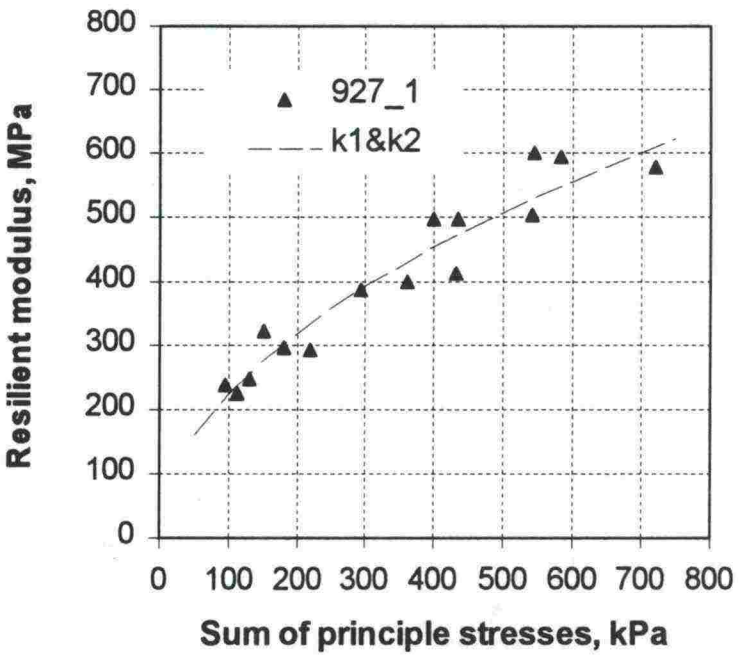

Figure A2:2 The result of cyclic triaxial test for the sand, which is located below the depth 2.0 m.

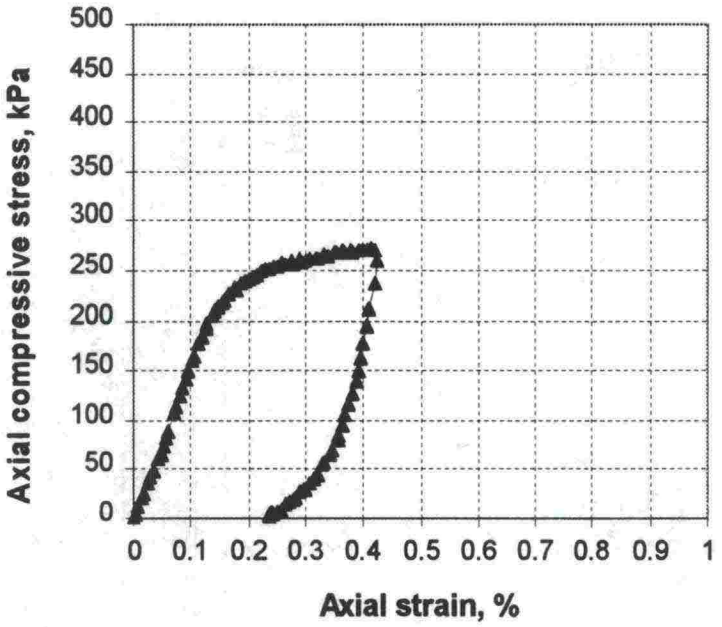

Figure A2:3 The result of static triaxial test for the sand, which is located between depths 1.2 m ... 2.0 m.

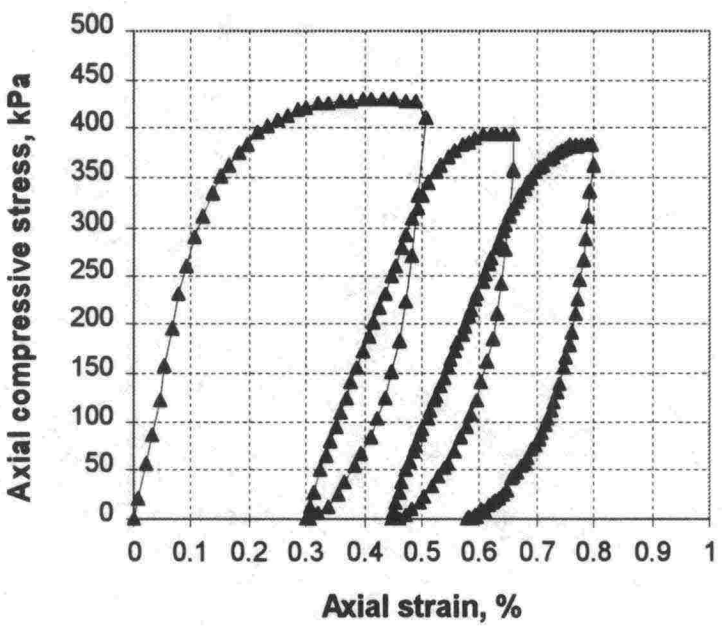

Figure A2:4 The result of cyclic triaxial test for the sand, which is located below the depth 2.0 m.

Painokairauspisteiden sijainti

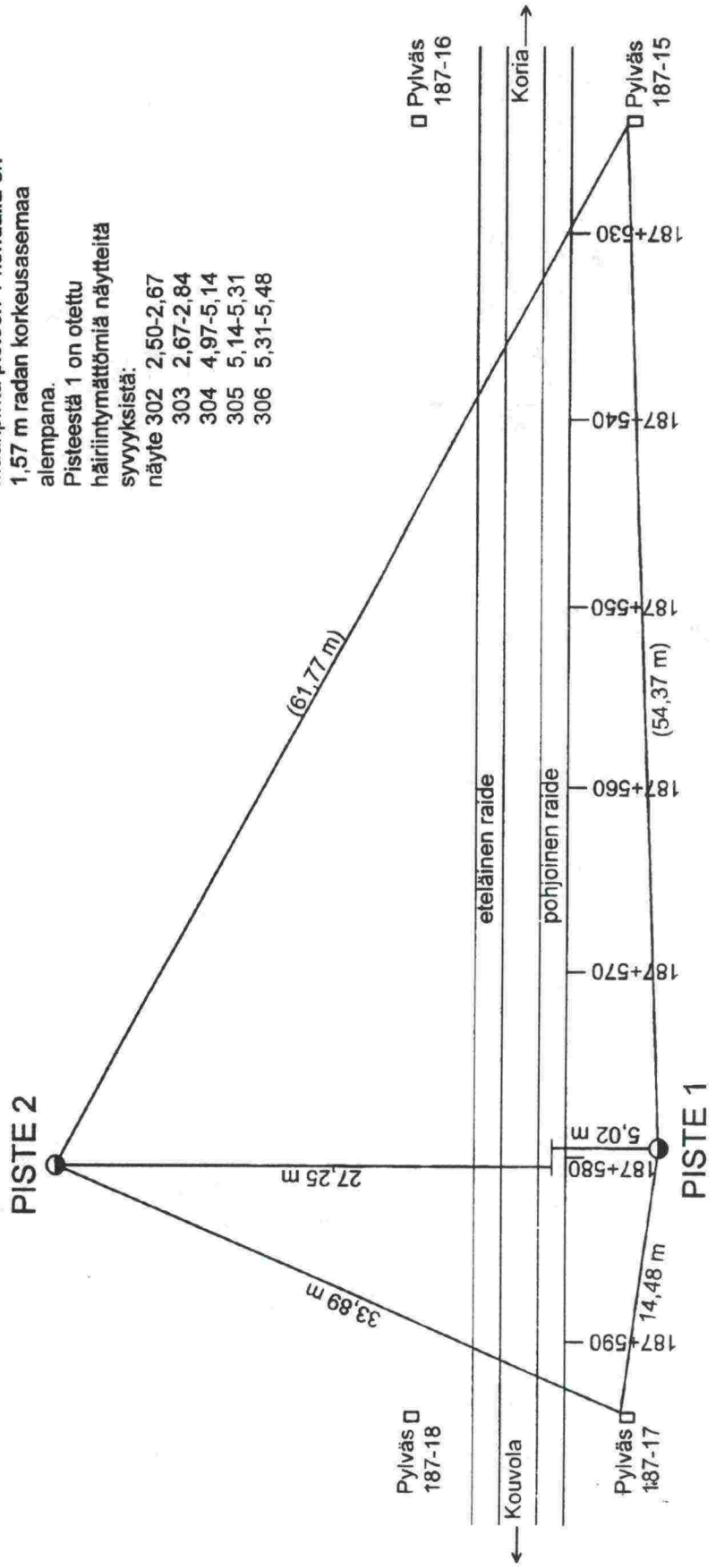

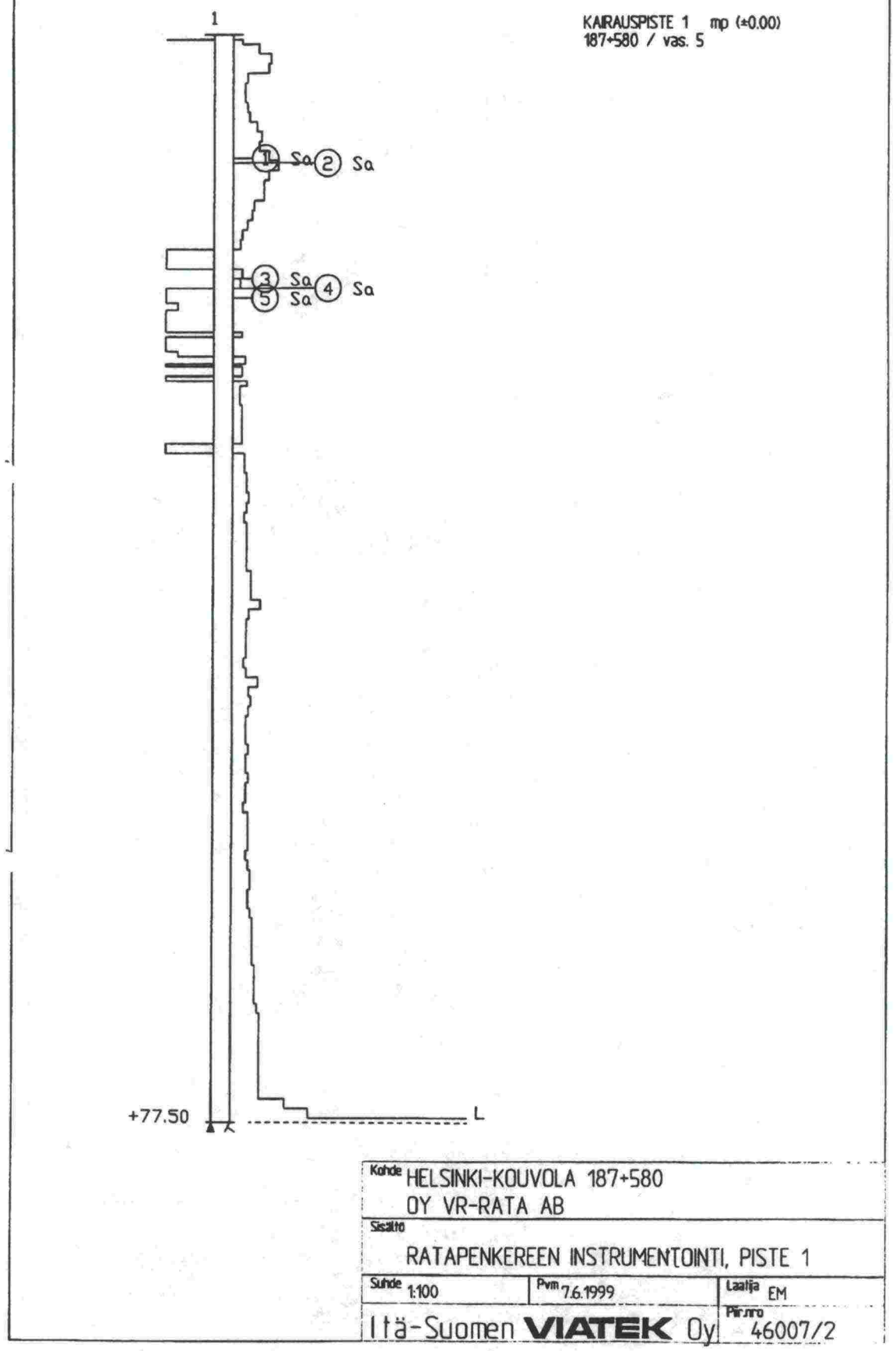
KAIRAUSPISTE 1 mp (±0.00)
187+580 / vas. 5
1
1 Sa
2 Sa
3 Sa
4 Sa
5 Sa
+77.50
L
Kohde HELSINKI-KOUVOLA 187+580
OY VR-RATA AB
Sisältö
RATAPENKEREEN INSTRUMENTOINTI, PISTE 1
Suhde 1:100
Pvm 7.6.1999
Laatija EM
Itä-Suomen VIATEK Oy
Piirros 46007/2

KAIRAUSPISTE 2 mp (±0.00)
187+580 / oik. 27,25

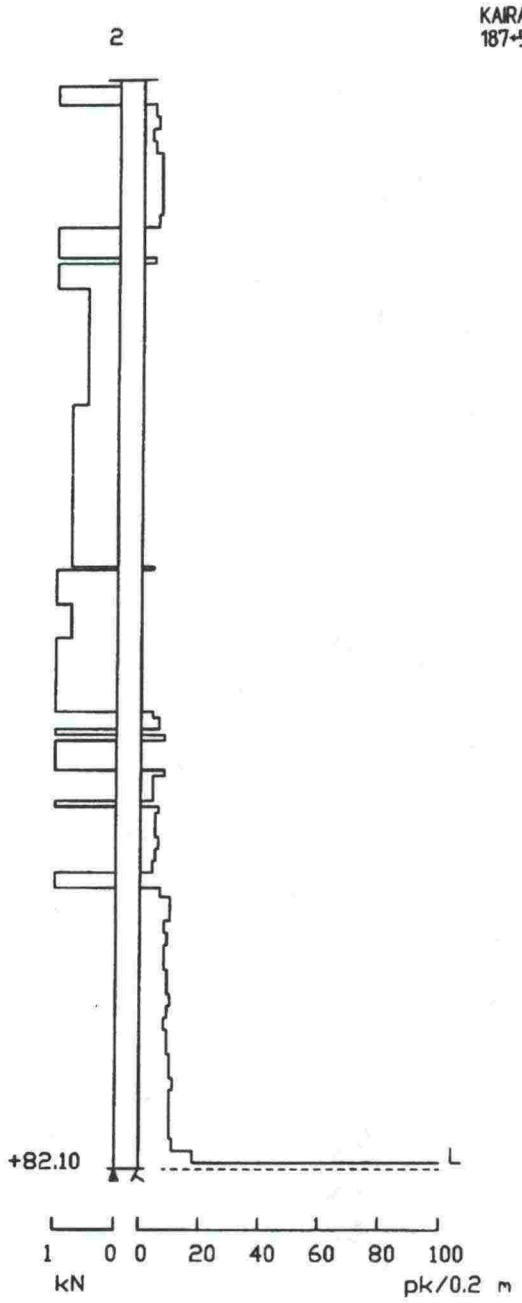

Kohde: HELSINKI-KOUVOLA 187+580 OY VR-RATA AB		
Sisältö: RATAPENKEREEN INSTRUMENTOINTI, PISTE 2		
Suhde 1:100	Pvm 7.6.1999	Laatija EM
Itä-Suomen VIATEK Oy		Piir.nro 46007/3

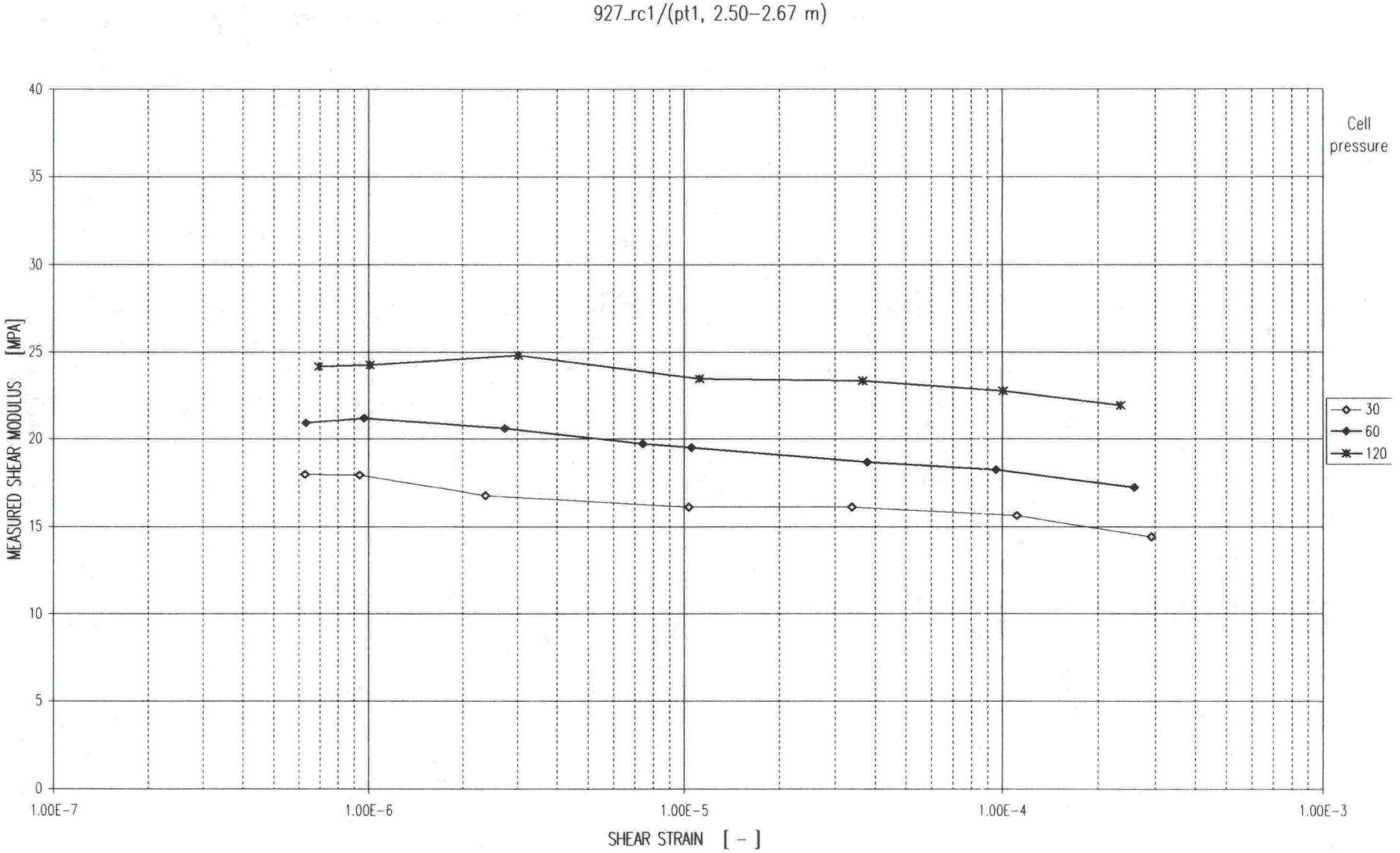

Figure A4:1 Variation of shear modulus of the sample located between depths 2.50 –2.67 m.

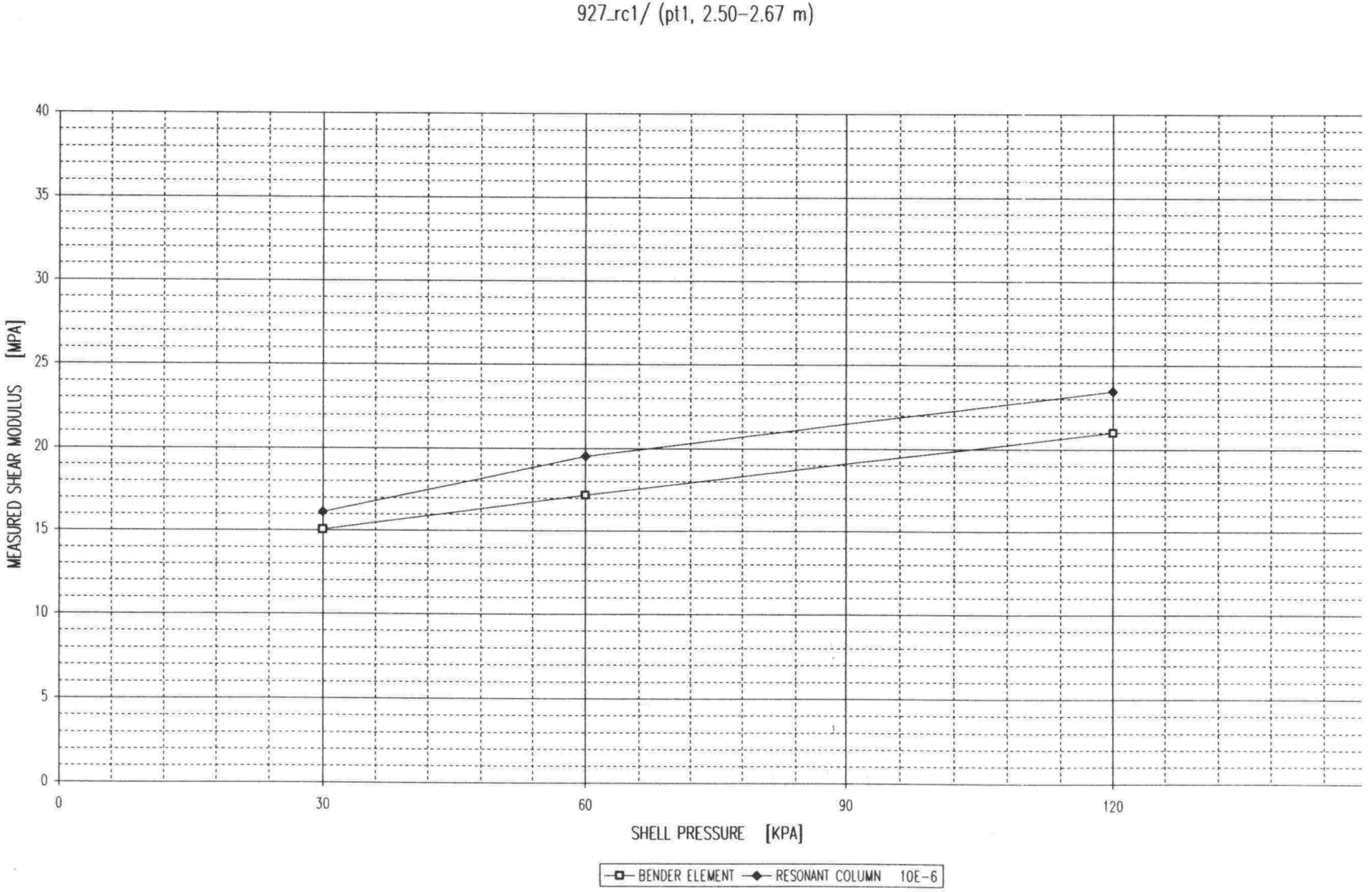

Figure A4:2 Maximum value of the shear modulus located between depths 2.50 – 2.67 m.

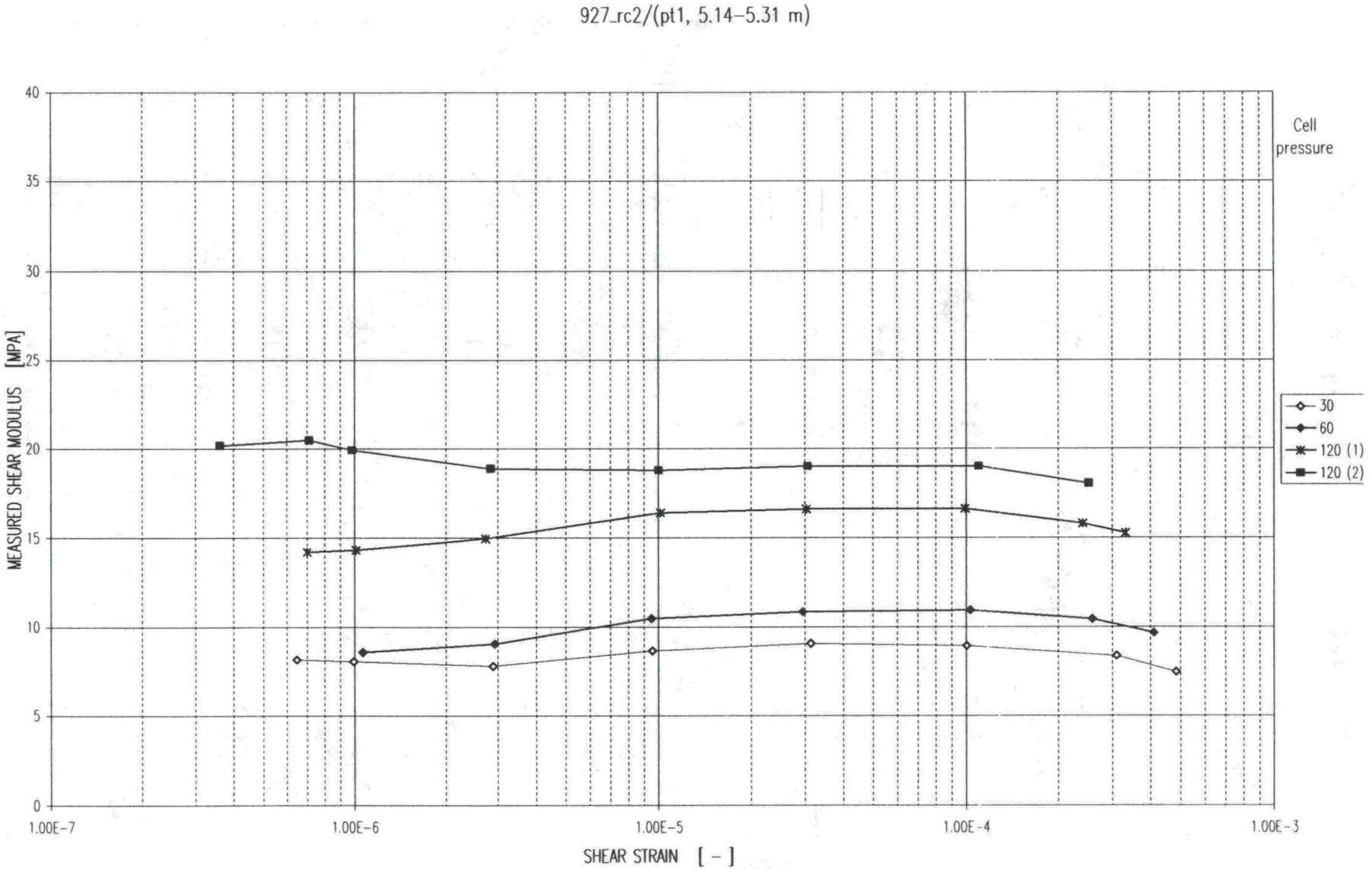

Figure A4:3 Variation of shear modulus of the sample located between depths 5.14 –5.31 m.

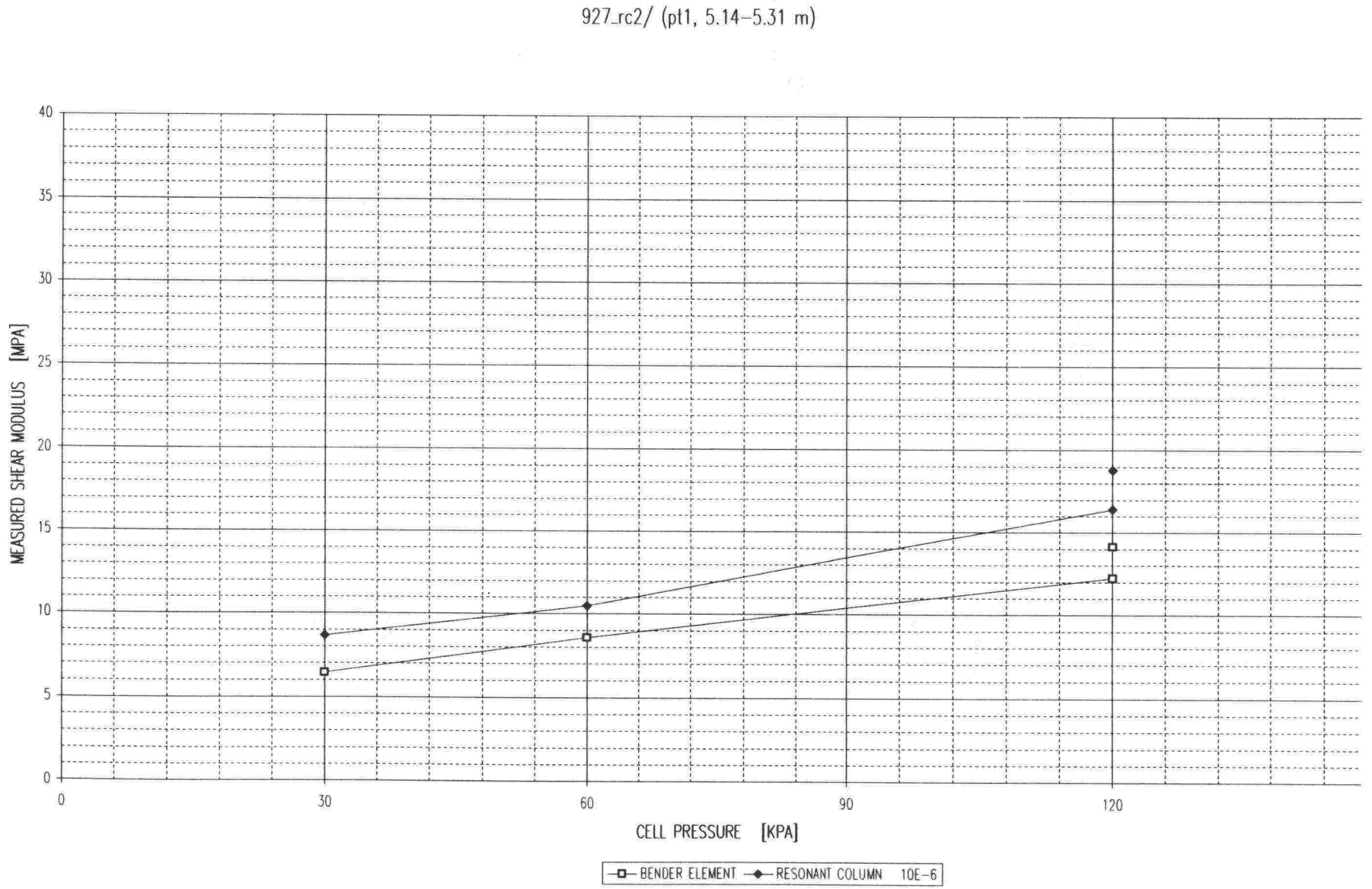

Figure A4:4 Maximum value of the shear modulus located between depths 5.14 – 5.31 m.

Publications of the Finnish Rail Administration **A**

1/1997	Railway Industry Structures and Capital Investment Financing
2/1997	Nopean junaliikenteen aluekehitysvaikutukset
3/1997	Rautateiden henkilöliikenteen ennustemalli (RALVI)
4/1997	Kilpailuedellytykset ja niiden luominen Suomen rataverkolla
5/1997	Rataverkon tavaraliikenne-ennuste 2020
1/1998	Rataverkon jatkosähköistyksen yhteiskuntataloudellinen vaikutusselvitys
2/1998	Suomen rautatieliikenteen päästöjen laskentajärjestelmä (RAILI 96)
3/1998	Rautateiden tavarakuljetusten laatutekijät
4/1998	Ratahallintokeskuksen tutkimus- ja kehittämistoiminta 1997 - 99
5/1998	Rataverkon kehittämisen yhdyskuntarakenteellisten vaikutusten ja menetelmien arviointi
6/1998	Yksityisrahoituksen käyttömahdollisuudet Suomen ratahankkeissa
1/1999	Ratarakenteen instrumentoinnin kirjallisuustutkimus, 250 kN:n ja 300 kN:n akselipainot
2/1999	Rautatieliikenteen polttoaineperäisten päästöjen aiheuttamat ympäristökustannukset
3/1999	Rautatieliikenteen aiheuttama tärinä, 250 kN:n ja 300 kN:n akselipainot
4/1999	Ratarakenteen instrumentointi- ja mallinnussuunnitelma, 250 kN:n ja 300 kN:n akselipainot
5/1999	Rautatietärinän mittauskäytäntö Pohjoismaissa
6/1999	Radan tukikerroksen ja alusrakenteen kirjallisuustutkimus, 250 kN:n ja 300 kN:n akselipainot
7/1999	Rautatiesiltojen luokittelu ja inventointi rataosuudella Rautaruukki–Haaparanta akselipainojen korottamista varten
8/1999	Ratarumpujen maastoselvitys, 250 kN:n ja 300 kN:n akselipainot
1/2000	Rataverkko 2020 -ohjelman väliraportti. Kehittämisvaihtoehtojen vaikutustarkastelut
2/2000	Bantrummor, 250 kN och 300 kN axellaster
3/2000	Liikkuvan kaluston kirjallisuustutkimus
4/2000	Raidesepelin lujuuden vaikutus tukikerroksen ikään
5/2000	Ratarakenteen instrumentointi ja mallinnus, 250 kN:n ja 300 kN:n akselipainot
6/2000	Väliraportti 250 kN:n ja 300 kN:n akselipainojen ratateknisistä tutkimuksista
7/2000	Intermediate Report, 250 kN and 300 kN axle loads
8/2000	Ratatekniset määräykset ja ohjeet -julkaisun käytettävyystutkimus
9/2000	Ratakapasiteetin perusteet

FINNISH RAIL ADMINISTRATION
KAIVOKATU 6, P.O. Box 185
FIN-00101 HELSINKI

TECHNICAL UNIT

For further information, please contact:
Mr.Pasi Leimi, Tel. +358 9 5840 5184, e-mail: pasi.leimi@rhk.fi
Mrs. Sinikka Kiikka, Tel. +358 9 5840 5192, e-mail: sinikka.kiikka@rhk.fi

ISBN 952-445-042-9
ISSN 1455-2604